ADSORPTION AND PHOTOCATALYTIC DEGRADATION OF ACETAMINOPHEN USING $ZnFe_2O_4$-TiO_2 COMPOSITE

BY

AISHA ZUBAIR

DEPARTMENT OF CHEMICAL ENGINEERING

AHMADU BELLO UNIVERSITY

ZARIA NIGERIA

NOVEMBER, 2016

ADSORPTION AND PHOTOCATALYTIC DEGRADATION OF ACETAMINOPHEN USING $ZnFe_2O_4$-TiO_2 COMPOSITE

BY

Aisha ZUBAIR, B. ENG. (ATBU) 2012
P13EGCE8009

A DISSERTATION SUBMITTED TO THE SCHOOL OF POSTGRADUATE STUDIES,
AHMADU BELLO UNIVERSITY, ZARIA

IN PARTIAL FULFILLMENT OF THE REQUIREMENTS FOR THE AWARD OF A MASTER OF SCIENCE DEGREE IN CHEMICAL ENGINEERING

DEPARTMENT OF CHEMICAL ENGINEERING,
FACULTY OF ENGINEERING,
AHMADU BELLO UNIVERSITY,
ZARIA, NIGERIA

NOVEMBER, 2016

DECLARATION

I, Aisha ZUBAIR do solemnly declare that this dissertation entitled "Adsorption and photocatalytic degradation of acetaminophen using $ZnFe_2O_4$-TiO_2 composite" was carried out by me in the Department of Chemical Engineering, Ahmadu Bello University, Zaria. The information derived from the literature has been duly acknowledged in the text and list of references provided. No part of this dissertation was previously presented for another degree or diploma at this or any other institution.

Aisha ZUBAIR _____ _____

Signature Date

CERTIFICATION

This dissertation entitled "ADSORPTION AND PHOTOCATALYTIC DEGRADATION OF ACETAMINOPHEN USING $ZnFe_2O_4$-TiO_2 COMPOSITE" by Aisha ZUBAIR meets the regulation governing the award of Master of Science Degree in Chemical Engineering of the Ahmadu Bello University Zaria and it is therefore approved for its contribution and literary presentation.

Dr. A. Hamza Chairman, Supervisory Committee	_____ Signature	_____ Date
Dr. M. S. Galadima Member, Supervisory Committee	_____ Signature	_____ Date
Dr. S.M. Waziri Head, Department of Chemical Engineering, A.B.U Zaria	_____ Signature	_____ Date
Professor Kabir Bala Dean, Postgraduate School, A.B.U Zaria	_____ Signature	_____ Date

ACKNOWLEDGEMENT

My deepest and greatest gratitude goes to Almighty Allah (S.W.T) in making this dissertation a success.

I sincerely thank my supervisors Dr. A. Hamza and Dr. M.S. Galadima for their continuous support, encouragement, and insightful guidance during the course of my masters studies at this University. I consider myself immensely fortunate and privileged to be able to work with them. I would like to appreciate the constant assistance, support and guidance afforded to me by all teaching and non-teaching staff members of the department of Chemical Engineering, A.B.U Zaria. I am also thankful to Dr. S.M. Waziri, the Head Chemical Engineering, A.B.U Zaria for his insightful comments, academic and moral advice and encouragement throughout my entire study period.

Thanks to my parents, Alh. Zubair Usman and Haj. Aishatu Hammayo for their unconditional love and support, without which I would not have been able to succeed in this endeavor. I am also thankful to my uncle Prof. Idris Abubakar Misau who has been a role model in my life.

I would like to thank my friends and colleagues, Abdullahi, Dikko, Yusuf, Lamido, Suleiman, Shola and Menta, amongst many others.

ABSTRACT

Frequent occurrence of pharmaceutical compounds in aquatic environments and drinking water has raised a concern about their potential effects on environment and human health. Advanced oxidation processes (AOPs) including heterogeneous photocatalysis have proved to be one of the most effective methods for water treatment. The coupling of TiO_2 and $ZnFe_2O_4$ semiconductors results in a composite having high photocatalytic activity under solar and/or visible light irradiation. Thus, $ZnFe_2O_4$-TiO_2 composite was synthesized using microwave assisted combustion method. The $ZnFe_2O_4$-TiO_2 composite was characterized using XRF, XRD and SEM techniques. Adsorption of acetaminophen in the dark onto the $ZnFe_2O_4$-TiO_2 composite nicely fitted pseudo second-order kinetic model and the Langmuir isotherm model. The maximum adsorption capacity of the $ZnFe_2O_4$-TiO_2 composite was 26.88 mgg^{-1}. Control experiments showed that the percentage removal of acetaminophen via adsorption in the dark, photolysis (irradiation with visible light) and photocatalysis were 35%, 4% and 88%, respectively. The kinetics of photocatalytic degradation of acetaminophen under visible light irradiation using the $ZnFe_2O_4$-TiO_2 composite obeys pseudo-first order approximation of the Langmuir-Hinshelwood kinetic model. Quadratic model equations that adequately describe photocatalytic degradation and mineralization of acetaminophen were developed using RSM (response surface methodology). The significant photocatalytic process parameters were: initial concentration of acetaminophen, dosage of $ZnFe_2O_4$-TiO_2 composite (photocatalyst) and irradiation time. Numerical optimization of the process parameters was carried out for photocatalytic degradation and mineralization of acetaminophen. The predicted optimum conditions for photocatalytic degradation of acetaminophen were initial acetaminophen concentration of 11.0 mg/l, photocatalyst dosage of 0.6 g/L and irradiation time of 42.0 min. The predicted optimum conditions for photocatalytic mineralization of acetaminophen were initial acetaminophen concentration of 11.2 mg/l, photocatalyst dosage of 1.0 g/L and irradiation time of 28.7 min. Under the predicted optimum conditions, photocatalytic degradation and mineralization of acetaminophen were 91.5% and 96.3% respectively. The validated experiments for photocatalytic degradation and mineralization of acetaminophen were 90.9% and 95.9 %, respectively.

TABLE OF CONTENTS

List of Figures

List of Tables

List of Plate

List of Appendices

LIST OF ABBREVIATIONS

AC:	Activated Carbon
Ace:	Acetaminophen
ANOVA:	Analysis of variance
AOPs:	Advanced oxidation processes
APIs:	Active pharmaceutical ingredients
AS:	Activated sludge
CCD:	central composite design
COD:	Chemical oxygen demand
$Fe(NO_3)_3.9H_2O$:	Iron(iii) nitrate nonahydrate
HOMO:	highest occupied molecular orbital
LUMO:	lowest unoccupied molecular orbital
MBRs:	Membrane Bioreactors
NaAc:	Sodium acetate
NF:	Nanofiltration
OVAT:	One variable at a time
PPCPs:	Pharmaceuticals and personal care products
RO:	Reverse Osmosis
SBRs:	Sequence Batch Reactors
SEM:	Scanning Electron Microscope
TiO_2:	Titanium dioxide
UASRs:	Up-flow anaerobic stage reactors
USABR:	Up-Flow Anaerobic Sludge Blanket Reactor

wt%: Weight Percentage

XRD: X-Ray Diffraction

XRF: X-Ray Florescence Spectroscopy

$ZnFe_2O_4$: Zinc ferrite

$Zn(NO_3)_2.6H_2O$: Zinc Nitrate Hexahydrate

CHAPTER ONE

INTRODUCTION

1.1 PREAMBLE

Pharmaceutical compounds have recently been detected in sewage effluents (Carballa *et al*., 2004; Rabiet *et al*., 2006; Nikolaou *et al*., 2007), surface and ground water (Rabiet *et al*., 2006; Nikolaou *et al*., 2007), and even drinking water (Stackelberg *et al*., 2004; Rabiet *et al*., 2006). Frequent occurrence of pharmaceuticals in aquatic environments and drinking water has raised a concern about their potential effects on environment and human health. Some of the adverse health effects caused by pharmaceutical pollutants include: aquatic toxicity, resistance development in pathogenic bacteria, genotoxicity and endocrine disruption (Arcand-Hoy *et al*., 1998; Kummerer, 2004). As pharmaceuticals and personal care products (PPCPs) are often not biodegradable, their treatment using conventional technologies does not result in efficient removal. Therefore, PPCPs pose serious threats to public health and aqueous organism.

Among the variety of PPCPs, acetaminophen is a common analgesic and antipyretic drug and represents one of the most widely used prescription and over-the-counter drugs globally (Yang *et al*., 2008). It was found that 58–68% of acetaminophen was excreted from the body after therapeutic use (Muir *et al*., 1997). The pollutant is hardly biodegradable, more toxic than azo-dyes even at low concentration. When acetaminophen was used in excess or with alcohol, it could cause liver failure and death (Corey *et al*., 2007). These compounds make their way to water bodies through various sources, such as direct disposal of surplus drugs in households, excretion by humans and animals, and inadequate treatment of manufacturing effluents (Ikehata *et al*., 2006; Nikolaou *et al*., 2007). To avoid undesired accumulation of drugs in aquatic environments, powerful

oxidation techniques are being developed (Zwiener and Frimmel, 2000; Balcioglu and Otker, 2003; Ikehata *et al*., 2006).

Advanced oxidation processes (AOPs) including heterogeneous photocatalysis have proved to be one of the most effective methods for water treatment (He, 2008). These processes are based on the generation of hydroxyl radicals (·OH) which oxidize a broad range of organic pollutants present in water (Han *et al*., 2004; Qamar *et al.,* 2006). A photocatalytic process using semiconductor particles is an emerging technique for the treatment of toxic pollutants (Alfano *et al.,* 2000; Fujishima *et al.,* 2000). Among various semiconductor photocatalysts, TiO_2 has received a great deal of attention due to its high photocatalytic activity, chemical stability, non-toxicity, and low cost (Carp *et al*., 2004; Kabra *et al*., 2004; Konstantinou and Albanis, 2004). It is very difficult to recover TiO_2 powders after photocatalytic treatment of wastewater due to the high dispersive properties of TiO_2 powders. However, because of its large band gap (3.2 eV); it cannot absorb sunlight efficiently. To reduce the band gap and increase the photoactivity of TiO_2, various strategies have been developed. Some of these strategies include: doping with transition metals, surface modification by noble metals (e.g. Pd, Au, Ag, Pt) and coupling with other semiconductors (Shapovalov *et al*., 2010; Chong *et al*., 2010).

$ZnFe_2O_4$ is a semiconductor with a narrow band gap of about 1.9 eV. $ZnFe_2O_4$ exhibits characteristics of excellent visible-light response, good photochemical stability, as well as favorable magnetism (Li *et al*., 2011; Laokul *et al*., 2011), Although $ZnFe_2O_4$ with such superior properties open up a promising gate for applications in photocatalysis, it is seldom used as photocatalyst due to its lower valence band potential (Xu *et al*., 2009). Coupling $ZnFe_2O_4$ with TiO_2 yields $ZnFe_2O_4$-TiO_2 composite that has a narrow band gap of 2.96 eV (Yao *et al.,* 2015). The photocatalytic activity of the $ZnFe_2O_4$-TiO_2 composite is better than

that of separate TiO_2 and $ZnFe_2O_4$ under visible light irradiation. Due to the magnetic property of $ZnFe_2O_4$, $ZnFe_2O_4$-TiO_2 composite can be easily separated after photocatalytic treatment of wastewater using an external magnet (Li *et al*., 2011). Various techniques such as sol gel method (chen et al., 2012) have been used to prepare $ZnFe_2O_4$-TiO_2 composite. However, to the best of knowledge obtained from literature, $ZnFe_2O_4$-TiO_2 composite has never been prepared via microwave combustion method in spite of the several advantages of the method.

In this research work, $ZnFe_2O_4$-TiO_2 composite was prepared via microwave combustion method. The composite was characterized by determining its chemical and phase compositions, morphology as well as its adsorptive and photocatalytic properties for the removal of acetaminophen from water. The work also involved modelling and optimization of photocatalytic degradation and mineralization of acetaminophen under visible light irradiation using response surface methodology.

1.2 Problem Statement

I. Toxic pharmaceutical pollutants generated during production, distribution and application of drugs have adverse effects on human and aquatic lives.

II. Traditional wastewater treatment methods, such as sedimentation, adsorption and coagulation, cannot destroy active pharmaceutical ingredients in water.

III. High band gap of conventional photocatalysts such as titanium dioxide (TiO_2) limits their applications to UV light.

1.3 Aim and Objectives

The aim of this research work was to synthesize, characterize and apply $ZnFe_2O_4$-TiO_2 composite for the removal of acetaminophen from simulated acetaminophen water

via adsorption and photocatalysis.

The specific objectives are:

I. To synthesize the $ZnFe_2O_4$-TiO_2 composite using microwave combustion method.

II. To characterize the $ZnFe_2O_4$-TiO composite using SEM, XRD and XRF techniques.

III. To study the kinetics and isotherms of acetaminophen adsorption onto the $ZnFe_2O_4$-TiO_2 composite.

IV. To study the effects of parameters (the $ZnFe_2O_4$-TiO_2 composite dose, initial concentration of acetaminophen and irradiation time) on the removal of acetaminophen from simulated acetaminophen water via photocatalysis using design expert version (6.0.6).

V. To optimize photocatalytic degradation and mineralization of acetaminophen under visible light irradiation using response surface methodology.

1.4 JUSTIFICATION OF STUDY

Photocatalysis is an environmentally friendly process and the process can be driven by sunlight which is a renewable energy source. $ZnFe_2O_4$-TiO_2 can easily be separated from simulated acetaminophen water using magnets. In addition there is the need to protect human beings and aquatic lives from the hazardous effects of pharmaceutical effluents containing acetaminophen and related drugs.

1.5 Scope and Limitation

The scope of this work is limited to preparation of $ZnFe_2O_4$-TiO_2 composite through microwave combustion and application of $ZnFe_2O_4$-TiO_2 composite for the adsorption and photocatalytic treatment of acetaminophen in simulated water under visible light

irradiation. The effects of three process variables ($ZnFe_2O_4$-TiO_2 composite dose, initial concentration of acetaminophen) on the photocatalytic degradation and mineralization of acetaminophen were also studied.

CHAPTER TWO

LITERATURE REVIEW

2.1 Pharmaceutical Pollution

Pharmaceutical pollution is the pollution of the environment with pharmaceutical drugs and their metabolites, which reach the marine environment (groundwater, rivers, lakes, and oceans) through wastewater. Drug pollution is therefore mainly a form of water pollution. The ubiquitous use of pharmaceuticals in human and veterinary medical practices, aquaculture and agricultural products has led to the continual release of a wide array of pharmaceutical chemicals into our environment. Pharmaceutical compounds are being used for several beneficial purposes in modern society but simultaneously pharmaceutical industries are releasing very toxic contaminants in the environment directly or after chemical modifications (Halling-Sorensen *et al*., 2002).

Pharmaceutical compounds may enter the environment by different routes such as discharge of treated wastewater, from landfill sites, sewer lines, runoff from animal wastes etc. (Glassmeyer *et al*., 2005; Atchley *et al*., 2009). Even though various physical and biological processes occurring in aquatic ecosystem may cause reduction of many pharmaceutical compounds, trace concentrations of human and veterinary pharmaceutical compounds as well as their metabolites have been detected in different water bodies like surface water, groundwater and drinking water sources (Bruce *et al*., 2010).

It has been found that the pharmaceutical compounds reach the environment and can be considered as environmental pollutants. Several pharmaceutical production facilities were found to be sources of much higher environmental concentrations than those caused by the applications of drugs (Larsson *et al*., 2007). Generally, pharmaceutical industries generate a huge quantity of wastes during manufacturing and maintenance operations.

Pharmaceuticals have been detected in wastewater treatment plant effluents and drinking water sources. Trace amount of pharmaceuticals in drinking water for longer duration may cause considerable adverse effects to human health and aquatic life, though concentrations of pharmaceuticals detected in drinking water (in nano gram per liter range) are several orders of lower magnitude than the minimum therapeutic dose (WHO, 2013).

One of the most common over-the-counter and heavily used pharmaceuticals is acetaminophen. Acetaminophen acts as an inhibitor of prostaglandin synthesis and is thus used as an antipyretic and analgesic drug all over the world.

2.2 Occurrence of Pharmaceuticals in Water

Pharmaceuticals have been found in small amounts in our streams, groundwater and marine waterways. Prescription and over-the-counter medicines used by consumers enter our environment in two ways:

1. Excretion from humans and animals - Humans and animals pass drugs or drug metabolites through their bodies and then these chemicals pass through septic systems or wastewater treatment plants. Wastewater treatment systems cannot effectively remove all medicines, and some are discharged to surface waters or are collected in biosolids that are often applied to land (Bruce *et al*., 2010).

2. Direct disposal to sewers or trash - Medicines can enter the environment when flushed down toilets or sinks because they are not effectively removed or degraded by septic systems or wastewater treatment processes. Medicines thrown in the trash retain their biological and chemical activity, and may eventually end up in the environment. In areas with large amounts of rainfall, leachate from landfills is collected in liners and pumped to wastewater treatment plants, which cannot effectively remove all medicines (Bruce *et al*., 2010).

Thus, pharmaceuticals enter the environment through many routes, including human or animal excreta, wastewater effluent, treated sewage sludge, industrial waste, and medical waste from health-care and veterinary facilities, landfill leachate and biosolids. Figure 2.1 illustrates the various methods of pharmaceutical occurrence in water.

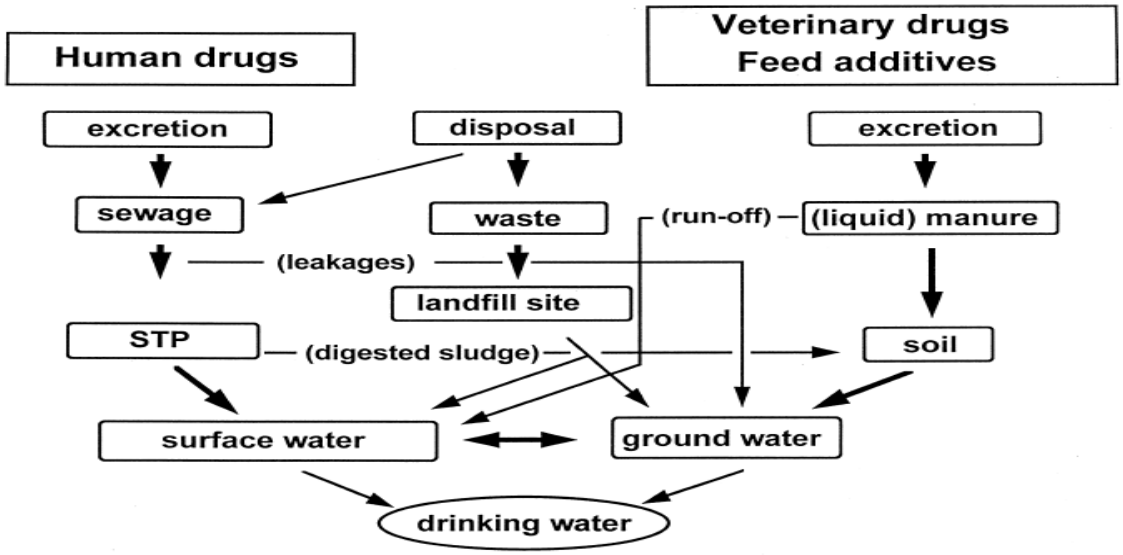

Figure 2.1: Fate and transport of pharmaceuticals in the environment (Ternes, 1998)

2.3 Impacts of Pharmaceutical Waste on Humans and Environment

The long term exposure of lower concentration of complex pharmaceutical mixtures on stream biota may result in acute and chronic damages (Crane *et al*., 2006; Quinn, *et al*., 2008) behavioral changes (Stanley *et al*., 2007), accumulation in tissues, reproductive damage and inhibition of cell proliferation. Several studies have demonstrated that fish exposed to wastewater effluents can exhibit reproductive abnormalities. Moreover, fish exposed to trace levels of birth control pharmaceuticals in the range of concentrations found in the environment show dramatic decreases in reproductive success, suggesting

population level impacts are possible (Sanderson *et al*., 2004). High doses of acetaminophen can cause serious liver damage.

2.4 Biological Treatment Methods for Pharmaceutical Effluents

2.4.1 Conventional biological treatment methods

Biological treatment methods have traditionally been used for the management of pharmaceutical wastewater (Suman Raj and Anjaneyulu, 2005). They may be subdivided into aerobic and anaerobic processes. Aerobic applications include activated sludge, membrane batch reactors and sequence batch reactors (LaPara *et al*., 2002; Noble, 2006; Chang *et al*., 2008 and Chen *et al*., 2008). Anaerobic methods include anaerobic sludge reactors, anaerobic film reactors and anaerobic filters (Gangagni *et al*., 2005; Enright *et al*., 2005; Chelliapan *et al*., 2006; Oktem *et al*., 2007; Sreekanth *et al*., 2009). The advantages of anaerobic treatment over aerobic processes is its ability to deal with high strength wastewater, with lower energy inputs, sludge yield, nutrient requirements, operating cost, space requirement and improved biogas recovery. However, because a wide range of natural and xenobiotic organic chemicals in pharmaceutical wastewaters are recalcitrant and nonbiodegradable to the microbial mass within the conventional treatment system, anaerobic processes are not always effective in removing these substances. One way around this is to use anaerobic microorganisms such as methanogenic archaea, which can adapt to levels many times those that inhibit unadapted methanogens (Fountoulakis *et al*., 2008) as well as incorporating different configurations including biomembrane reactors, stirred tank reactors, up-flow anaerobic filters and fluidized bed reactors (Gangagni *et al*., 2005; Chelliapan *et al*., 2006; Oktem *et al*., 2007).

2.4.2 Activated sludge (AS) treatment

Activated sludge (AS) treatment is unsuitable for the treatment of wastewater where the chemical oxygen demand (COD) levels are greater than 4000 mg/L (Suman Raj and Anjaneyulu, 2005). Conventional activated sludge with a long hydraulic retention time (HRT) has historically been the method of choice for the treatment of pharmaceutical industry wastewater (El-Gohary and Abou-Elea, 1995; Oz *et al*., 2004). It has a lower capital cost than more advanced treatment methods and a limited operational requirement; it is generally more environmentally friendly than chlorination. However, high energy consumption, the production of large amounts of sludge (Sreekanth *et al*., 2009) and operational problems including color, foaming and bulking in secondary clarifiers are associated with activated sludge plants (Oz *et al*., 2004). Activated sludge is an efficient method for the removal of some active pharmaceutical ingredients (APIs), but not all from municipal facilities (Zwiener and Frimmel, 2003; Castiglioni *et al.,* 2006; Watkinson *et al.*, 2007).

2.4.3 Sequence batch reactors (SBRs)

SBR is an activated sludge method of treatment in which separate tanks for aeration and sedimentation are not required and there is no sludge return. This type of process is ideal for use in small systems or when land is limited (Ileri *et al*., 2003).

2.4.4 Membrane bioreactors (MBRs)

MBRs are known to be effective for the removal of bulk organics and can replace traditional methods or operate in combination with conventional activated sludge systems or as hybrid systems (Noble, 2006). The main advantages of MBRs over activated sludge is that they require less space for operation (Yang *et al*., 2006), and can also treat variable wastewater compositions (Chang *et al*., 2008).

2.4.5 Up-flow anaerobic stage reactors (UASRs)

Up-flow anaerobic stage reactors (UASRs) used as a pre-treatment to activated sludge for industrial effluent have been shown to be efficient for the removal of pharmaceuticals even at high concentrations (Chelliapan *et al*., 2006; Oktem *et al*., 2007). A UASR fed with real pharmaceutical wastewater containing the antibiotics tylosin and avilamycin showed a high degree of COD and drug removal (Chelliapan *et al*., 2006).

2.4.6 Up-Flow anaerobic sludge blanket reactor (USABR)

A hybrid which combines a UASR and anaerobic filter technology showed significant removal of COD at a much higher OLR from pharmaceutical wastewater (Oktem *et al*., 2007).

2.5 Physico-Chemical Treatment Methods

These technologies include membrane separation, chemical removal, activated carbon, chlorination, ultraviolet irradiation and other novel approaches. The efficiency of these methods for the treatment of pharmaceutical wastewater varies significantly (Gangagni *et al*., 2005; Chelliapan *et al*., 2006; Oktem *et al*., 2007).

2.5.1 Membrane processes

Several membrane types and applications were evaluated for the removal of APIs at pilot and fullscale, including microfiltration, ultra filtration, nanofiltration, reverse osmosis, electro dialysis reversal, membrane bioreactors and combinations of membranes in series (Bellona and Drewes, 2007; Snyder *et al*., 2007).

2.5.2 Nanofiltration (NF) and reverse osmosis (RO)

The pressure-driven membrane processes have been the focus of attention of many researchers for the treatment of drinking water (Watkinson *et al*., 2007). Reverse osmosis in

different configurations showed efficient removal of thirty-six personal care products and endocrine disrupting chemicals including antibiotics, lipid regulators, hormones and oral contraceptives, antiepileptics and analgesics (Snyder *et al*., 2007; Watkinson *et al*., 2007). Some studies reported higher removal efficiencies of polar and charged compounds in NF/RO processes due to interactions with membrane surfaces (Ozaki and Li, 2002; Braeken *et al*., 2005). Though both NF and RO treatment shows potential as an efficient method for removing pharmaceuticals from the wastewater, the disposal of the sludge which could contain the pollutant in a more concentrated form remains.

2.5.3 Adsorption using activated carbon

Activated carbon (AC) is a recognized conventional technology for the removal of both natural and synthetic organic contaminants (Hrubec *et al*., 1983; Annesini *et al*., 1987). Snyder *et al*. (2007) found that both powdered activated carbon (PAC) (5mg/L) and granular activated carbon (GAC) removed greater than 90% of estrogens (100–200 ng/L initial concentrations). However, dissolved organic compounds, surfactants and humic acids compete with binding sites and can block pores within the AC structure (Zhang and Zhou, 2005; Snyder *et al*., 2007).

2.5.4 Oxidation reactions

Oxidation reactions have primarily been used to supplement rather than replace conventional systems and to enhance the treatment of refractory organic pollutants (Balcioglu and Otker, 2003). This technology has been successfully applied to the treatment of pharmaceuticals (Khetan and Collins, 2007). A chemical agent such as hydrogen peroxide, ozone, transition metals and metal oxides are required for advanced oxidation processes (AOPs). In addition, an energy source such as ultraviolet-visible radiation, electric current, gamma-radiation and ultrasound is required (Ikehata *et al*., 2006). AOPs

are based on the production of free radicals, in particular the hydroxyl radical and facilitate the conversion of pollutants to less harmful and more biodegradable compounds (Ikehata *et al*., 2006).

Ozone has been applied to the treatment of waters primarily due to its strong disinfection and sterilization properties (Araña *et al*., 2002). Its application for the treatment of waters containing pharmaceutical residues is now a broad area of research (Balcioglu and Okter, 2003; Ternes *et al*., 2003; Andreozzi *et al*., 2005; Andreozzi *et al*., 2006; Nakada *et al*., 2007; Dantes *et al*., 2008). The main mode of action in the ozonation process is the formation of OH- radicals due to ozone decay in the water, but there are also ozone molecules present for chemical attack. This increases the oxidation capacity (Ternes *et al*. 2003).

2.6 Photocatalysis

Photocatalysis implies photon-assisted generation of catalytically active species (Suppan, 1994). It is widely used to describe the process in which the acceleration of a reaction occurs when a material, usually a semiconductor, interacts with light of sufficient energy (or of a certain wavelength) to produce reactive oxidizing species (ROS) which can lead to the photocatalytic generation of H_2 and transformation of a wide variety of molecules (Pelaez *et al.*, 2012) as shown in Figure 2.2. It must be noted that during the photocatalytic reaction, at least two events must occur simultaneously in order for the successful production of reactive oxidizing species to occur. Typically, the first involves the oxidation of dissociatively adsorbed H_2O by photogenerated holes, the second involves reduction of an electron acceptor by photoexcited electrons; these reactions lead to the production of a hydroxyl and superoxide radical anion (Pelaez *et al.*, 2012).

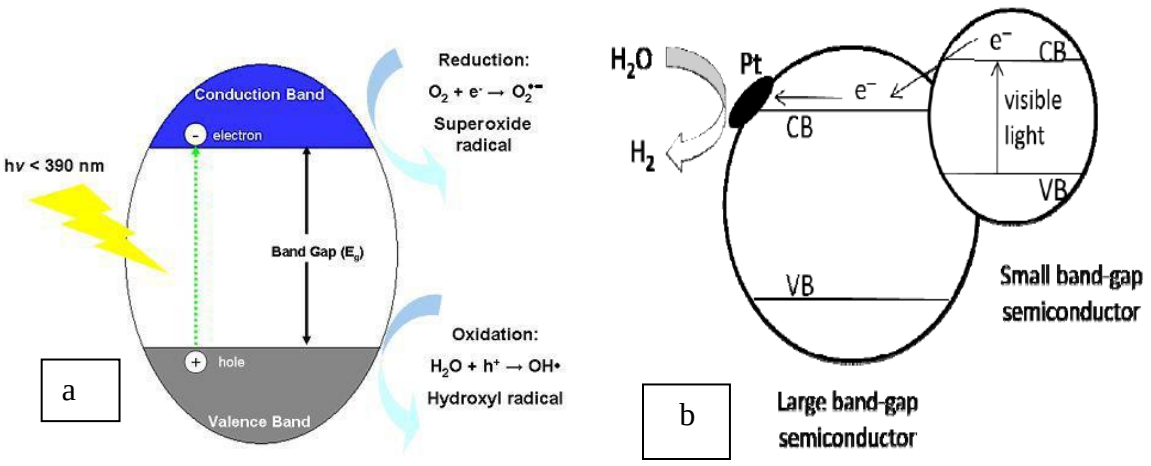

Figure 2.2: Simplified mechanism of (a) semiconductor photocatalytic process, (b) visible-light induced photocatalyst sensitized with small Band-Gap semiconductor called Hybrid or Composite photocatalysts (Pelaez, *et al.*, 2012).

It is clear that photocatalysis implies photon-assisted generation of catalytically active species rather than the action of light as a catalyst in a reaction (Suppan, 1994). If the initial photoexcitation process occurs in an adsorbate molecule, which then interacts with the ground state of the catalyst substrate, the process is referred to as a "catalyzed photoreaction", if, on the other hand, the initial photoexcitation takes place in the catalyst substrate and the photoexcited catalyst then interacts with the ground state adsorbate molecule, the process is a "sensitized photoreaction" (Pelaez *et al.*, 2012).

When a photocatalyst is illuminated by light with energy equal to or greater than the band-gap energy, the valence band electrons can be excited to the conduction band, leaving a positive hole in the valence band. In the case of anatase TiO_2, the band gap is 3.2 eV, therefore UV light ($\lambda \leq 387$ nm) is required. The absorption of a photon of this energy will excite an electron to the conduction band (e^-_{CB}) generating a positive hole in the valence band (h^+_{VB}) (Equation 2.1) (Ohtani, 2011).

$$TiO_2 + h\nu \rightarrow h^+_{VB} + e^-_{CB} \qquad (2.1)$$

Charge carriers can be trapped as Ti^{3+} and O^- defect sites in the TiO_2 lattice, or they can

recombine, dissipating energy. Alternatively, the charge carriers can migrate to the catalyst surface and initiate redox reactions with adsorbates. Positive holes can oxidize OH^- or water at the surface to produce •OH radicals (Equation 2.3) which, are extremely powerful oxidants. The hydroxyl radicals can subsequently oxidize organic species with mineralization producing mineral salts, CO_2 and H_2O (Equation 2.5) (Ohtani, 2011).

$$e^-_{CB} + h^+_{VB} \rightarrow \text{energy} \quad (2.2)$$

$$H_2O + h^+_{VB} \rightarrow {}^{\bullet}OH + H^+ \quad (2.3)$$

$$O_2 + e^-_{CB} \rightarrow O_2\bullet^- \quad (2.4)$$

$$\bullet OH + \text{pollutant} \rightarrow H_2O + CO_2 \quad (2.5)$$

$$O_2\bullet^- + H^+ \rightarrow \bullet OOH \quad (2.6)$$

$$\bullet OOH + \bullet OOH \rightarrow H_2O_2 + O_2 \quad (2.7)$$

$$O_2^{\bullet-} + \text{pollutant} \rightarrow CO_2 + H_2O \quad (2.8)$$

$$\bullet OOH + \text{pollutant} \rightarrow CO_2 + H_2O \quad (2.9)$$

Electrons in the conduction band can be rapidly trapped by molecular oxygen adsorbed on the titania particle, which is reduced to form superoxide radical anion ($O_2^{\bullet-}$) (Equation 2.4) that may further react with H^+ to generate hydroperoxyl radical (${}^{\bullet}OOH$) (Equation 2.6) and further electrochemical reduction yields H_2O_2 (Equation 2.7). These reactive oxygen species may also contribute to the oxidative pathways such as the degradation of a pollutant (Equation 2.8 and 2.9) (Choi *et al.,* 1994).

2.7 Types of Photocatalysis

2.7.1 Homogeneous photocatalysis

In homogeneous photocatalysis, the reactants and the photocatalysts exist in the same phase. The most commonly used homogeneous photocatalysts include, ozone, transition metal oxide and photo-Fenton systems (Fe^+ and Fe^+/H_2O_2). The reactive species is the •OH

which is used for different purposes. According to Pankaj, (2012), the mechanism of hydroxyl radical production by ozone can follow two paths as follows:

$O_3 + h\nu \rightarrow O_2 + O(1D)$ (2.10)

$O(1D) + H_2O \rightarrow \bullet OH + \bullet OH$ (2.11)

$O(1D) + H_2O \rightarrow H_2O_2$ (2.12)

$H_2O_2 + h\nu \rightarrow \bullet OH + \bullet OH$ (2.13)

Similarly, the photo-Fenton system produces hydroxyl radicals by the following mechanism

$Fe^{2+} + H_2O_2 \rightarrow HO\bullet + Fe^{3+} + OH^-$ (2.14)

$Fe^{3+} + H_2O_2 \rightarrow Fe^{2+} + HO\bullet 2 + H^+$ (2.15)

$Fe^{2+} + HO\bullet \rightarrow Fe^{3+} + OH^-$ (2.16)

In photo-Fenton type processes, additional sources of OH radicals should be considered: through photolysis of H_2O_2, and through reduction of Fe^{3+} ions under UV light:

$H_2O_2 + h\nu \rightarrow HO\bullet + HO\bullet$ (2.17)

$Fe^{3+} + H_2O + h\nu \rightarrow Fe^{2+} + HO\bullet + H^+$ (2.18)

The efficiency of Fenton type processes is influenced by several operating parameters like concentration of hydrogen peroxide, pH and intensity of UV. The main advantage of this process is the ability of using sunlight with wavelength up to 450 nm, thus avoiding the high costs of UV lamps and electrical energy (Suresh *et al.*, 2012).The disadvantages of the Fenton type process are the low pH values which are required, since iron precipitates at higher pH values and the fact that iron has to be removed after treatment (Suresh *et al.*, 2012).

2.7.2 Heterogeneous Photocatalysis

Heterogeneous catalysis has the catalyst in a different phase from the reactants. Heterogeneous photocatalysis is a discipline which includes a large variety of reactions:

mild or total oxidations, dehydrogenation, hydrogen transfer, $^{18}O_2$–$^{16}O_2$ and deuterium-alkane isotopic exchange, metal deposition, water detoxification, gaseous pollutant removal. Most common heterogeneous photocatalysts are semiconductors, which have unique characteristics. Unlike the metals which have a continuum of electronic states, semiconductors possess a void energy region where no energy levels are available to promote recombination of an electron and hole produced by photoactivation in the solid (Jina, 2010). The void region, which extends from the top of the filled valence band to the bottom of the vacant conduction band, is called the band gap. When light falls on these semiconductors, the electron present in the valence band jumps to the conduction band, a result of which is the generation of a positive hole. The recombination of the electron and the hole must be prevented as much as possible if a photocatalyzed reaction is to be favoured (Pelaez *et al.*, 2012). The ultimate goal of the process is to have a reaction between the activated electrons with an oxidant to produce a reduced product, and also a reaction between the generated holes with a reductant to produce an oxidized product. Due to the generation of positive holes and electrons, oxidation-reduction reactions take place at the surface of semiconductors. In the oxidative reaction, the positive holes react with the moisture present on the surface and produce a hydroxyl radical. Oxidative reactions due to photocatalytic effect are illustrated as follows:

$$UV + MO \rightarrow MO\ (h + e^{-}) \quad (2.19)$$

Here MO stands for metal oxide

$$h^{+} + H_2O \rightarrow H^{+} + \bullet OH \quad (2.20)$$

$$2\ h^{+} + 2\ H_2O \rightarrow 2\ H^{+} + H_2O_2 \quad (2.21)$$

$$H_2O_2 \rightarrow HO\bullet + \bullet OH \quad (2.22)$$

The reductive reaction due to photocatalytic effect is illustrated as follows:

$e^- + O_2 \rightarrow \bullet O_2$ (2.23)

$\bullet O_2 - + HO\bullet 2 + H^+ \rightarrow H_2O_2 + O_2$ (2.24)

$HOOH \rightarrow HO\bullet + \bullet OH$ (2.25)

Ultimately, the hydroxyl radicals are generated in both the reactions. These hydroxyl radicals are very oxidative in nature and non-selective with redox potential of (E_0 = +3.06 V).

2.9 Photocatalysts

Photocatalysts are often inorganic solid materials (Fujishima and Rao, 1997). They are usually crystals and the crystallinity is often determined by an X-ray diffraction (XRD) pattern. A photocatalytic material is also a substance that generates catalyst activity energy from light. It alters the rate of a chemical reaction when exposed to sunlight (Suresh, 2012). The band gap of a material decides whether it can function as a photocatalyst or not. The bands that are filled with electrons are called the valence band and the empty bands are called the conduction band. The energy difference between the conduction band and the valence band is called the band gap. If the valence band cannot be completely filled with electrons, no band gap will be present and the material is called a metal. If the valence band is completely filled with electrons and a band gap greater than zero and less than 5eV, it will be called a semiconductor. A material with a band gap higher than 5eV is called an insulator (Suresh, 2012).

There are several materials known for their photocatalytic activity of which most of them are metal oxides. Table 2.1 lists the band-gap energies of some common semiconductor materials. Since the discovery of its photocatalytic effect by Honda and Fujishima in 1972, titanium dioxide has become the most popular photocatalytic material due to its abundance; low cost, chemical stability, biocompatibility and high efficiency under UV light. Though

not as popular as titanium dioxide, zinc oxide has been getting increasing attention as a photocatalytic material due to its similar electronic structure and catalytic efficiency with TiO_2. While zinc oxide can be a more efficient photocatalyst in near UV excitations compared to titanium dioxide, it has the problem of photo-corroding itself. This limits its wide use (Suresh, 2012).

Table 2.1: Band-gap energies of some common semiconductor materials

Semiconductor	Band Gap (eV)	Semiconductor	Band Gap (eV)
Fe_2O_3	2.2	CdS	2.4
TiO_2	3.0~3.2	ZnS	3.7
WO_3	2.7	CdSe	1.7
ZnO	3.2	GaP	2.3
SnO_2	3.5	GaAs	1.4
$SrTiO_3$	3.4	SiC	3.0

Source: (Carp *et al.*, 2005).

2.9 Basic Physical Properties of TiO_2

Titanium dioxide has many polymorphs. The well-known phases of titanium dioxide are naturally occurred rutile (discovered in 1803), anatase (discovered in 1801) and brookite (discovered in 1825), named after their reddish color, extended crystallographic shape, and a mineralogist, respectively (Carp *et al*., 2004). The metastable anatase and brookite phases an irreversibly convert to stable rutile upon heating (Hanaor *et al*., 2011) as shown in

Figure 2.3.

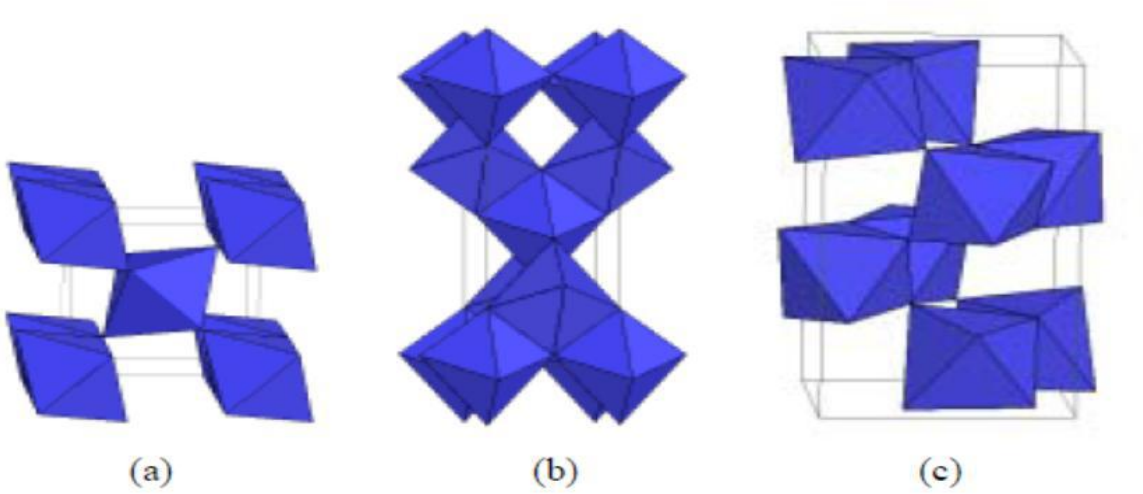

Figure 2.3. Different crystal structures of TiO_2: (a) Rutile ; (b) Anatase ; (c) Brookite (Burdett *et al*., 2012).

Anatase possesses an energy band gap of 3.2 eV with an absorption edge at 386nm which lies in the near UV range. It is generally accepted (Hanaor *et al*., 2011) that the photocatalytic performance of anatase is superior to that of rutile although both forms possess significant photocatalytic activity. First anatase has higher Fermi level over rutile by 0.1 eV, resulting in a lower oxygen affinity and a higher level of hydroxyl groups on TiO_2 surfaces. These hydroxyl groups contribute to the higher photocatalytic activity of anatase. Second anatase possesses an indirect bandgap while rutile has a direct bandgap. The minimum in the conduction band of anatase is away from the maximum in the valence band, enabling the excited electrons to stabilize at the lower level in the conduction and leading to a longer life (slower charge carrier recombination) and higher mobility than that of rutile with a direct bandgap. Third anatase possesses a wider absorption gap. It is generally proposed that excitation electron mass of the outershell electrons of anatase is lower than that of rutile, leading to a higher mobility of electrons in anatase.

2.10 TiO_2 as a Photocatalyst

Titanium dioxide is a wide band-gap semiconductor that can be excited to produce electron–hole pairs when irradiated with light. Such photo-induced electron–hole pairs have been utilized to generate electricity in solar cells, to split water into hydrogen and oxygen, to oxidize and degrade inorganic/organic/biological compounds in environments as well as to create superhydrophilicity (Ahmed *et al*., 2010).

.

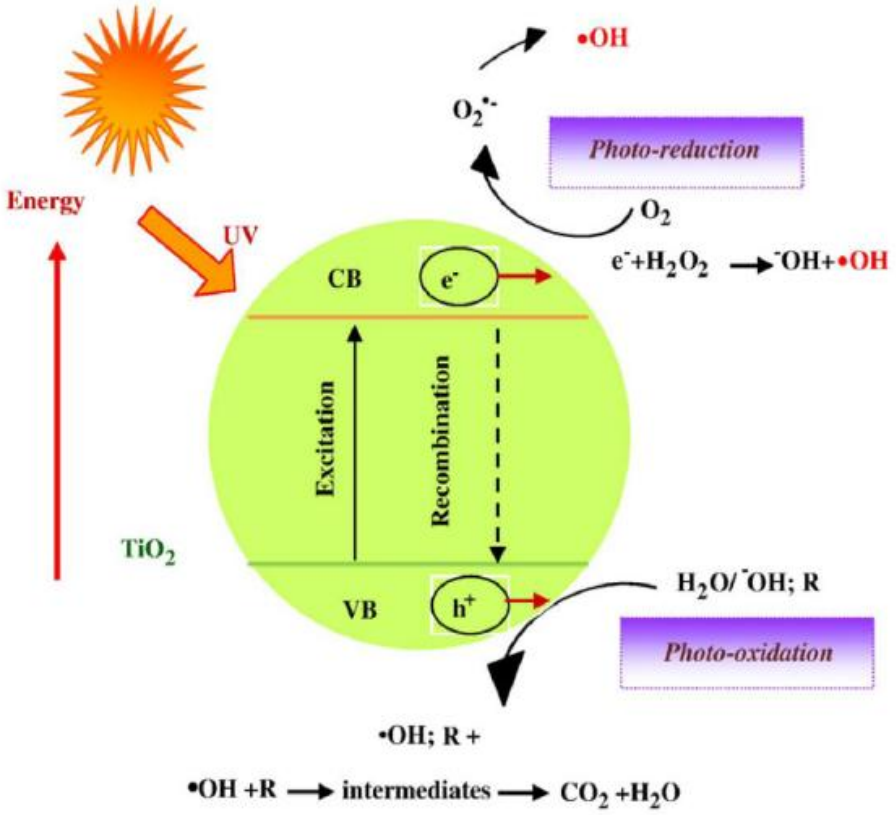

Figure 2.4: Schematic diagram illustrating the principle of TiO_2 photocatalysis (Ahmed *et al*., 2010).

When TiO_2 is exposed to an UV light with a wavelength of 280–400nm (3.10–4.43eV), the UV light will be absorbed by TiO_2 and an electron is elevated from the valence band to the conduction band of TiO_2, leaving behind a hole in the valence band, as shown in Figure 2.4,

to form electron–hole pairs. The fundamental processes of TiO_2 photoelectro-chemistry have been reviewed recently (Fujishima *et al.*, 1997). Generally it is accepted that

$$TiO_2 + h\nu \rightarrow e^- + h^{+-} \quad (2.26)$$

This excited electrons and holes can either be used directly to create electricity in photovoltaic solar cells or drive a chemical reaction, which is called photocatalysis.

As shown in Equation 2.26, under an UV irradiation, electrons in the valence band of TiO_2 will be activated to the conduction band, forming electrons (e−) with high activity. At the same time, holes (h+) will be created in the valence band. The oxidation potential of the photo-induced holes is up to 3.0eV (based on the standard hydrogen electrode, SHE), much higher than that of hydrogen (1.36eV) and ozone (2.07 eV). Therefore the formed electron–hole pairs are strong redox systems. The photo-produced holes h^+ on TiO_2 nanoparticle surfaces can oxidize OH− and H_2O molecules absorbed on TiO_2 surfaces into hydroxyl radicals ($^{\bullet}OH$)

$$h^+ + OH^- \rightarrow \bullet OH \quad (2.27)$$

The holes can also facilitate oxidation through the presence of absorbed water on TiO_2 surfaces

$$h^+ + H_2O \rightarrow \bullet OH + H^+ \quad (2.28)$$

At the same time, the electrons in the conduction band can facilitate reduction of electron acceptors through the presence of absorbed air on TiO_2 surfaces to form adsorbed radicals

$$e^- + O_2 \rightarrow \bullet O_2^- \quad (2.29)$$

The formed hydroxy and peroxy radicals are atomic species with a free unpaired electrons, possessing strong ability to degrade organic pollutants and to split water. These photo-activities occur on Ti atom surfaces. In order to emphasize the location of the photo-activities, the chemical formation of the high-active radicals at Ti surfaces are also

expressed as;

Ti^{4+} ...OH^- + *hv* → Ti^{3+} + •OH

(2.30)

Ti^{3+} + O_2 → Ti^{4+} + •O_2^-

(2.31)

Ti^{4+} ...O_2^- + H_2O → Ti^{4+} + •OH

(2.32)

By combining these equations, the net reaction is given by:

H_2O + O_2 + *hv* → •OH + •O_2

(2.32)

These photo-produced hydroxyl and peroxyl radicals, expressed in Equations 2.27–2.32, in turn oxidize and degrade organic/ inorganic materials. Among various photocatalysts, TiO_2 has the most efficient photo-activity, the highest stability, guaranteed safety to humans and environment, and the lowest cost. Therefore, TiO_2 photocatalysts are almost the only photocatalyst suitable for industrial applications at present and also probably in the future (Fujishima *et al*., 1997).

2.11 Applications of Photocatalysis

2.11.1 Photovoltaics

The photo-produced electrons (e−) and holes (h+) can be separated under electric fields, moving to different regions of TiO_2 nanoparticles. Based on the phenomenon, various TiO_2 photovoltaic solar cells have been designed since 1972. The first photo electrochemical cell of TiO_2 was reported by Fujishima and Honda in 1972 using a rutileTiO_2 photo-anode and a Pt counter electrode. When the surface of the rutile TiO_2 electrode was irradiated with a Xenon lamp that emitted UV light of wavelengths shorter than TiO_2 band gap, about

415nm (3.0eV), photocurrent flowed from the platinum counter electrode to the TiO_2 electrode through an external circuit.

2.11.2 Water-splitting

The idea of photocatalytic water splitting is based on a photocatalyst powder in solution plus sunlight for clean hydrogen/energy production. The water splitting of TiO_2 photocatalytic crystals was first reported in 1972 (Fujishima *et al*., 1972). Later, the water splitting has been intensively studied with TiO_2 nanoparticles as cathodic catalysts since 1980s. TiO_2 photocatalysis has attracted much attention as one promising method to produce hydrogen.

2.11.3 Soil and water purification

The removal of harmful matters from wastewater and detoxification of pollutants in surface water and groundwater is a key issue in the world. Secondary treatment helps in organic matter decomposition to some extent, but major oxidation process occurs in tertiary treatment where wastewater is disinfected by Cl_2, O_3 or UV light. TiO_2 nano-materials have been considered as a promising photocatalyst in the degradation of organic or inorganic pollutants in wastewater. The photo-induced hydroxyl radicals (-OH) are generated at a standard potential of ∼2:8 eV (vs SHE) at the valence band of TiO_2. The produced strong oxidizing radicals OH oxidize these suspended organisms in water to purify the wastewater. Tamoxifen and Gemfibrozil drugs were also photo-degradated by TiO_2 nanoparticle catalysts under near-UV light (Yurdakal *et al*., 2007). Besides organic pollutants, inorganic pollutants can be decontaminated under UV irradiations. TiO_2 photocatalysts offer a great potential as an industrial technology for detoxification or remediation of wastewater and soils due to several important factors: (1) only natural oxygen and sunlight are utilized

during the TiO_2 photocatalytic decontamination. The decontamination procedure occurs under ambient conditions. (2) The TiO_2 photocatalytic decontamination is wavelength selective and can be accelerated by UV light. (3) TiO_2 photo-catalysts are inexpensive, readily available, non-toxic and chemically stable. TiO_2 photocatalysts have strong oxidation ability. (4) There are no any photo-induced intermediate compounds produced during the TiO_2 photo-catalytic decontaminations. TiO_2 photocatalytic nanoparticles can be freely suspended in wastewater or deposited on substrates (Konstantinou *et al*., 2004) to purify wastewater or soils during the decontaminations.

2.11.4 Air purification

Photocatalytic surfaces have the potential to act against a variety of air pollutants and odours such as microbes, volatile organic carbons (VOC), formaldehyde, ammonia and inorganic gaseous substances such as nitrogen or sulphur-oxides (NOX, SOX). TiO_2 catalysts have been incorporated into outdoor building materials, such as paving stones or paints, to substantially reduce concentrations of airborne pollutants such as carbon dioxide, nitrogen oxides and volatile organic compounds. The photo-generated hole–electron pairs produce hydroxyl (-OH) radicals and $-O^{-2}$ radicals to decontaminate the air pollutants. Catalytic TiO_2 nanoparticles oxidizes hydrocarbons, alcohols, carbon monoxide, and ammonia, SO_2 as well as bacteria in air under UV irradiations or solar light (Yurdakal *et al*., 2007).

2.11.5 Self-cleaning of surfaces

Cleanliness and maintenance issues are the key drivers for applications of self-cleaning surfaces (Bräuer *et al*., 2009). Self-Cleaning Photocatalytic Surfaces**:** support the light induced destruction of adherent organic molecules and is of particular importance for antibacterial, anti-virus and fungicidal applications. Particular relevance is given to surface

sterilization in areas such as biomedical engineering and food preparation. The initial process of self-cleaning of organic compounds is the generation of electron–hole (e−/h+) pairs on the TiO_2 nanoparticle surfaces. The produced holes react with absorbed water to produce hydroxyl radicals OH. The produced hydroxyl radicals have enough oxidizing power to convert any organic compounds to CO_2 and water: Self-cleaning effect by photocatalytic titanium dioxide coating can be applied on a glass window. When titanium dioxide is illuminated by UV light (solar illumination), it starts decomposing contaminants to minerals and carbon dioxide. At the same time, titanium dioxide becomes superhydrophillic and it retains this property for a while after illumination ceases. This enables the easy washing (typically by rain) of stains adsorbed on the titanium dioxide surface as water penetrates to the molecular level space between the stain and titanium dioxide surface (Jina, 2010).

Photo-induced hydrophilicity is generated by the exposure of a TiO_2- treated surface to intense UV light. Water is prevented from forming droplets and instead covers the surface with a homogeneous thin wetting layer, which penetrates below dirt particles. Fujishima *et al*. (1997) discovered the Photoinduced superhydrophilicity of titanium dioxide in 1997. This discovery resulted in the development of anti-fogging glasses. It is generally accepted that trapping of holes at TiO_2 surfaces causes the high wettability and photoinduced super-hydrophilicity. The hydrophilicity is affected by many parameters, such as surface roughness of TiO_2 crystals, surface defects, residual tensile stress in TiO_2, crystallographic facets of TiO_2 and others (Fujishima *et al*., 1997).

2.11.6 Antibacterial and sterilization

As early as 1985, it was reported that platinum-loaded titanium dioxide particles sterilized some microbial cells (Nguyen *et al*., 2008) (such as Coenzyme A, Lactobacillus

acidophilus, Sac-charomyces cerevisiae, and Escherichia coli) completely under metal halide lamp or Xenon lamp irradiation for 120 min. Uptonow, *Escherichia coli bacteria*, *Streptococcus sobrinus* AHT bacteria, *Pseudomonas aeruginosa* protein and *Candida albicans* fungi , even cancer cells (such as HeLa tumor cells and Legionella pneumophila) were photo-killed using TiO_2 catalysts. These viruses, bacteria, fungi, algae, and cancer cells have been completely decomposed to CO_2, H_2O, and harmless inorganic anions under UV irradiation. TiO_2 photocatalysts have been added to paints, cements, windows, tiles, or other building products for its sterilizing and anti-fouling properties. TiO_2 nanoparticles can destroy various organic species directly under light irradiation and have been employed to kill germs in operating rooms and kill cancer cells in photocatalytic cancer therapy (Nguyen *et al*., 2008).

2.12 Characterization of Photocatalysts

2.12.1 X-ray diffraction

X-ray diffraction (XRD) is used to examine the crystal structures of photocatalysts particles. It is a method of determining the arrangement of atoms within a crystal, in which a beam of X-rays strikes a crystal and diffracts into many specific directions using a diffractometer. It provides detailed information on the crystallographic structure and physical properties of materials and thin films (Ohtani, 2011).

2.12.2 X-ray florescence spectroscopy

X-ray fluorescence (XRF) is the emission of characteristic “secondary” (or fluorescent) X-rays from a material that has been excited by bombarding with high energy X-rays or gamma rays. The phenomenon is widely used for elemental and chemical analysis of minerals (Ohtani, 2011).

2.12.3 UV-vis diffuse reflectance spectroscopy

Diffuse Reflectance Spectroscopy provides an indication of the visible light activity of the photocatalysts. Diffuse reflectance spectra are obtained with UV-vis spectrometer and can be converted from reflection to absorption spectra by the Kubelka-Munk method (Ohtani, 2011).

2.13 Factors Affecting Phocatalytic Activity

2.13.1 Band structure

The general understanding of the mechanism of photocatalysis is that photoabsorption of a semiconducting material occurs to excite electrons from the valence band (VB) to the conduction band (CB) leaving positive holes in the VB, i.e., electron–hole pair (e^-h^+) generation (Pelaez *et a.,l* 2012). An important point is that photoabsorption and (e^-h^+) generation are inextricably linked; a VB electron is not excited after photoabsorption. This inter-band (band-to-band) excitation is often illustrated by three bands, CB, forbidden band (band gap) and VB, in which an electron moves vertically from the VB to CB, i.e., no spatial change in the position of an electron, though sometimes an electron migrates from the VB to CB spatially (Ohtani, 2011). Anyway, the above-mentioned interpretation seems to be a little strange considering the meaning of band structure and band-to-band transition, in which electrons are not localized and therefore electrons and positive holes can migrate within a crystal; an unlocalized excitation state may be described as "photoexcited crystal", e.g., an excited state of titania, without showing localized e^-,h^+. Do e^- and h^+ migrate in the CB and VB, respectively, after photoabsorption, i.e., photoexcitation. To illustrate the electronic structure of a molecule, lines are drawn to show the electronic state; the length of these lines does not mean spatial distribution of electrons in those states. This should also be the case for semiconducting (or insulating) materials, and band-to-band transition just means that an electron in the VB is excited to the CB without clarifying the location of e^-

and h^+ (Suresh *et al.*, 2012).

A possible interpretation of a better understanding for e^- h^+ location is that there are sites trapping e^- or h^+ in the crystal lattice and that e^- and h^+ are trapped by these sites immediately after the band-to-band transition, i.e., photoabsorption (Suresh *et al.*, 2012). Location of e^- and h^+ in the initial stage of photocatalysis as well as the rate should be controlled by the density and spatial distribution of these traps in a photocatalyst. However, there is little information on the density and spatial distribution of traps, since the structure of traps has not been fully clarified. The possible surface traps may be reaction sites, but not "active sites". It is thought that Fermi level is located just below the CB bottom and above the VB top for n-type and p-type semiconducting materials (Suppan *et al.*, 1994), respectively (Fermi level is a kind of measure of equilibrium electrochemical potential of a solid material). Most metal oxides are categorized as n-type semiconductors with Fermi levels more cathodic (higher) than the standard electrode potential of an electrolyte in contact with the metal oxide, and thereby electrons in donor levels slightly below the CB are injected into the electrolyte to form a space charge (depletion) layer with an electric field, i.e., Schottky barrier. In the 1980's, it was thought that this inner electric field separates e^- h^+ effectively; i.e., e^- and h^+ migrate to the bulk and surfaces of semiconductor electrodes and particles, but it seems that this is not the case for untreated photocatalyst particles because of the expected large thickness of this layer due to very low density of donor levels in ordinary photocatalyst particles (Suresh *et al.*, 2012).

2.13.2 Band gap

Since the ability of a photocatalyst is essentially governed by its band position, i.e., conduction-band (CB) bottom and valence-band (VB) top, as described in “Band structure”, estimation of the potential of the CB bottom and VB top is important to predict

the possibility for driving a photocatalytic reaction from the thermodynamic point of view. A general way for such estimation involves measurements of flat-band potential and band gap corresponding to the potential of the CB bottom and difference in potential between the CB bottom and VB top, respectively, enabling estimation of the potential of the VB top from them. Optical band gap can be estimated using the following equation (Ohtani, 2011).

$$(\alpha\nu)^{\frac{1}{n}} \propto h\nu - E_g \qquad (2.33)$$

Where α, *h*, ν, E_g and *n* are absorption coefficient, Planck constant, oscillation frequency, optical band gap and constant relating to a mode of transition. The constant *n* is ½, $\frac{3}{2}$, or 2 for allowed direct transition, forbidden direct transition or indirect transition, respectively, but the second forbidden direct transition has often been neglected. It is described in textbooks of semiconductor physics (or electronics) that by checking linearity of plots of $(\alpha\nu)^{\frac{1}{n}}$ against *h*ν using *n* as 2 or ½, the mode of transition of a given crystal and optical band gap are estimated, the latter of which is estimated by an x-intercept of the straight line (Suresh *et al.*, 2012).

Another problem in the band-gap energy estimation is the influence of impurity or surface electronic states on absorption spectra; spectral curves at the absorption edge region may be markedly modified to give smaller band-gap energy, and it is very difficult to extract a part of the absorption due to band-gap excitation from that by impurities (dopants) or surface states. Therefore, especially for doped samples, discrimination of narrowing of the band gap and overlapping of absorption by bulk or surface modification from shift of absorption to longer wavelengths is difficult (Suresh *et al.*, 2012).

2.13.3 Crystallinity

Photocatalysts are often inorganic solid materials. They are usually crystals and the

crystalline form is often determined by an X-ray diffraction (XRD) pattern. One of the problems in XRD analyses is that only crystals are detected, while an amorphous part, if present in samples, exhibits no diffraction peaks. Hallow may appear for amorphous parts, but there has been no report showing quantitative determination of amorphous content. Thus, amorphous content must be determined as a test of crystalline part and therefore precise determination of crystalline content is necessary. It is believed that, in principle, XRD peak intensity is proportional to content of corresponding crystallites, but a problem is how a global standard can be obtained for samples of each crystal, because smaller crystallites may exhibit lower peak intensity (Ohtani, 2011). A possible interpretation of this problem is that the outermost surface of particles cannot be involved in a crystal, which can be defined only for bulk, and the ratio of surface/bulk becomes appreciable when the size of crystallites becomes small. Thus, precise analysis of crystalline content can be guaranteed when pure crystalline particles included in a sample are extracted and used for making an XRD calibration curve based on the assumption that crystallites and amorphous particles are separated, but not in the form of, for example, a core-shell structure. In other words, if a sample particle is of a core-shell structure, precise determination of crystalline content may be very difficult (Ohtani, 2011).

Confusion regarding the term "crystallinity" arises because the term is discussed on the basis of sharpness of an XRD peak, e.g., "Sharpness of the peak indicated higher crystallinity of a photocatalyst." Since the width of an XRD peak reflects the size of a particle, i.e., the depth of crystallites measured in the direction vertical to a corresponding lattice plane (Scherer equation) (Suresh *et al.*, 2012), peak sharpness shows the size of crystallites. In this sense, "crystallinity" is used to show how crystallites grow to be larger-sized particles. Another usage of the term "crystallinity" is to show perfectness of crystals,

i.e., higher crystallinity means lesser density of crystalline defects. As mentioned above, sharpness of XRD peaks might be a measure of crystallite size. Assuming that larger crystallites possess smaller density of crystalline defects, sharpness of XRD peaks can also be a relative measure of "crystallinity" (Suresh *et al.*, 2012).

2.13.4 Surface area

The photocatalytic activity of a semiconductor photocatalyst depends on adsorption of the compound (to be oxidized) and trapping of holes and electrons on the catalyst surface. Number of trap centers is important and strongly influences the recombination rate. It is indeed, the competition between charge-carrier recombination and trapping that determines the overall quantum efficiency of a photocatalyst. The surface area of a photocatalysts determines the number of adsorption sites (Ohtani, 2011).

2.13.5 pH

The oxide/electrolyte interface has an electrical surface charge, which strongly depends on the pH of the medium (Jina, 2010). The electrokinetically mobilized charge is a determining parameter in the colloidal stability of the oxide particle suspensions. This involves the study of particle sizing depending on the pH; if the pH is equal to the Point of Zero Charge (PZC), the particles aggregate and ensembles are larger. The pH of the aqueous solution significantly affects the photocatalysts, including the charge of the particle and the size of the aggregates it forms. 300nm sizes increases to 2-4μm when dispersion reaches PZC. The zero surface charge yields zero electrostatic surface potentials that cannot produce the interactive rejection necessary to separate the particles within the liquid. This induces a phenomenon of aggregation and the photocatalysts clusters become larger. This effect is clearly related to the capability of the suspension for transmitting and/or absorbing light. Furthermore, larger clusters sediment more quickly than small particles, thus the

agitation necessary to maintain perfect homogeneity must be more vigorous. The PZC for TiO_2 is around 7. Above and below this value, the catalyst is negatively or positively charged according to (Jina, 2010):

$-TiOH \leftrightarrow -TiO- + H^+$

(2.34)

$-TiOH_2^+ \leftrightarrow TiOH + H^+$

(2.35)

The abundance of all the species as a function of pH: TiOH≥80% when 3□ pH□ 10; TiO ≥20% if pH□ 10; $TiOH_2^+$ ≥20% when pH□ 3. Under these conditions, the photocatalytic degradation of the ionisable organic compounds is affected by the pH. At first sight a very acidic solution appears to be detrimental and a very basic solution to be favourable, since the variations are modest or non-existent around neutrality. In many cases, a very important feature of photocatalysis is not taken into account when it is to be used for decontamination of water, as such, during photocatalytic reaction, a multitude of intermediate products are produced that may behave differently depending on the pH of the solution. To use only the rate of decomposition of the original substrate could yield an erroneous pH as the best for contaminant degradation. Therefore, a detailed analysis of the best pH conditions should include not only the initial substrate, but also the rest of the compounds produced during the process (Jina, 2010).

2.13.6 Photocatalyst dosage

There are number of studies in the literature on the influence of catalyst concentration on process efficiency. Although the results are quite different, it may be deduced from all of them that incident radiation on the reactor and length of path inside the reactor are fundamental in determining optimum concentration. This summarizes the conclusions if the

radiation comes from a source placed outside the photoreactor (as in a reactor illuminated by solar radiation).If the path length is short (1-2 cm maximum), reaction rate is obtained with 1-2 mg/L of TiO_2. If the path length is several centimetres long, the appropriate catalyst concentration is several hundred milligrams per litre (Ohtani, 2011).

In all the cases described above, a "screening" effect is produced when TiO_2 concentration is very high. The reaction rate diminishes due to the excessive opacity of the solution, which prevents the catalyst farthest from being illuminated. Approximately, 1mg/l of catalyst reduces transmissivity to zero in a 1-cm-inner-diameter cylinder. For the solar reactors, it is therefore necessary to find out the optimum catalyst concentration experimentally. That is, the minimum concentration at which the maximum reaction rate is obtained. When catalysts concentration is very high, after travelling a certain distance on an optical path length, turbidity impedes further penetration of light in the reactor (Pankaj, 2012). The percentage of photons absorbed by the suspension and the percentage of photons scattered by the TiO_2 particles is a very complex problem that cannot be solved experimentally, but must be experimentally estimated (Pankaj, 2012).

2.13.7 Substrate concentration

Photocatalytic activity of semiconductor photocatalysts is strongly dependent on the underlying substrate due to the possible chemical interaction between the photocatalysts and the substrate material. The substrate molecules react with the photo-generated hole and/or hydroxyl radical and degrade to different compounds, thus, the concentration of the substrate continuously changes as the reaction progresses. The rate varied as a function of the substrate concentration according to Langmuir-type equation shown in Equation 2.36 (Ohtani, 2011).

$$r = \frac{dC_{H_2}}{dt} = \frac{kKC_o}{1 + KC_o}$$

(2.36)

where, **r** is the initial reaction rate, ***k*** the reaction rate constant, **K** the adsorption constant of substrate on the photocatalyst, and $\mathbf{C_o}$ is the initial concentration of substrate.

2.13.8 Charge recombination

Recombination of photogenerated charge carriers is the major limitation in semiconductor photocatalysis as it reduces the overall quantum efficiency. When recombination occurs, the excited electron reverts to the valence band without reacting with adsorbed species non-radiatively or radiatively, dissipating the energy as light or heat (Ohtani, 2011).

Recombination may occur either on the surface or in the bulk and is in general facilitated by impurities, defects, or all factors which introduce bulk or surface imperfections into the crystal. Ohtani, 2011 found that trapping excited electrons as Ti^{3+} species for example, occurred on a time scale of ~ 30 ps and that about 90% or more of the photogenerated electrons recombine within 10 ns. Doping with ions, heterojunction coupling and nanosized crystals (Ohtani, 2011) have all been reported to promote separation of the electron-hole pair, reducing recombination and therefore improve the photocatalytic activity. For example, the TiO_2 crystallites of Evonik (Degussa) P25 contain a combination of anatase (~80%) and rutile (~20%). The conduction band potential of rutile is more positive than that of anatase which means that the rutile phase may act as an electron sink for photogenerated electrons from the conduction band of the anatase phase. Many researchers attribute the high photocatalytic activity of this preparation to the intimate contact between two phases, enhancing separation of photogenerated electrons and holes, and resulting in reduced recombination (Ohtani, 2011).

2.14 Methods of Improving the Activity of TiO_2 Photocatalyst

Ultraviolet light makes up only 4–5% of the solar spectrum, whereas over 40% of solar photons are in the visible region. A major drawback of pure TiO_2 is the large band gap meaning it can only be activated upon irradiation with photons of light in the UV domain (≤ 387 nm for anatase), limiting the practical efficiency for solar applications (Morikawa *et al*., 2001; Ilrie *et al*., 2003). Therefore, in order to enhance the solar efficiency of TiO_2 under solar irradiation, it is necessary to modify the nanomaterial to facilitate visible light absorption. The development of different strategies to modify TiO_2 for the utilization of visible light, including non-metal and/or metal doping, dye sensitization and coupling semiconductors (Ohtani, 2011).

2.14.1 Nonmetal doping

Non-metal doping of TiO_2 has shown great promise in achieving visible light active (VLA) photocatalysis, with nitrogen being the most promising dopant. Compared with the UV activity of undoped TiO_2, the visible light activity of N–TiO_2 is rather low. Independently of the origin of visible light absorption in substitutional or interstitial nitrogen discrete energy states, the low photocatalytic efficiency is mainly attributed to the limited photo-excitation of electrons in such narrow states, the very low mobility of the corresponding photo-generated holes and the concomitant increase of the recombination rate due to the creation of oxygen vacancies by doping (Ohtani, 2011).

2.14.2 Metal deposition

Modifications of TiO_2 with transition metals such as Cr, Co, V and Fe have extended the spectral response of TiO_2 well into the visible region also improving photocatalytic activity. However, transition metals may also act as recombination sites for the photo induced charge carriers thus, lowering the quantum efficiency. Transition metals have also been found to cause thermal instability to the anatase phase of TiO_2 (Ohtani, 2011).

2.14.3 Ion implantation

Ion implantation is a process in which high energy ions bombard and penetrate a surface, interacting with the substrate atoms below the surface. The most common application of ion implantation is the doping of semiconductors to create charge carriers within the lattice and therefore altering the semiconductor's electronic properties. The key advantage of this experimentally repeatable method, when working with nanoparticles substrates such as TiO_2, the catalysts bulk can be selectively modified and not merely the surface properties as with chemical synthesis techniques. In spite of the promising results that have been reported on ion-implanted TiO_2, the feasibility of cost-effective applications of any considerable size is still disputed (Ohtani, 2011).

2.14.4 Dye sensitization in photocatalysis

Dye photosensitization has been reported by different groups and to be one of the most effective ways to extend the photoresponse of TiO_2 into the visible region. Indeed these types of reactions are exploited in the well known dye sensitized solar cells. The mechanism of the dye sensitized photo-degradation of pollutants is based on the absorption of visible light for exciting an electron from the highest occupied molecular orbital (HOMO) to the lowest unoccupied molecular orbital (LUMO) of a dye. The excited dye molecule subsequently transfers electrons into the conduction band of TiO_2, while the dye itself is converted to its cationic radical. The TiO_2 acts only as a mediator for transferring electrons from the sensitizer to the substrate on the TiO_2 surface as electron acceptors, and the valence band of TiO_2 remains unaffected (Ohtani, 2011).

2.14.5 Coupled semiconductors

Many efforts have been made in the synthesis of different coupled semiconductors such as ZnO/TiO_2 (Marci *et al*., 2001), CdS/TiO_2 (Ghows *et al*., 2011), and Bi_2S_3/TiO_2 (Brahimi *et al*., 2007). The synthesized couples significantly enhance the photocatalytic efficiency by decreasing the recombination rate of the photogenerated electron–hole pairs and present potential applications in water splitting, organic decomposition and photovoltaic devices. These composites were also considered as promising materials to develop a high efficiency photocatalyst activated with visible light. They can also compensate the disadvantages of the individual components, and induce a synergistic effect such as an efficient charge separation and improvement of photostability (Marci *et al*., 2001). The coupling of a large band gap semiconductor with a smaller one, which can be activated with visible light, is of great interest for the degradation of organic pollutants using solar radiation. Blocking trap states by coating the particles with thin layers of a wide band gap material can lead to a drastic enhancement of the photostability (Marci *et al*., 2001).

2.15 Kinetics of Photocatalysis

It is well known that first-order kinetics is commonly observed for reactions occurring in homogeneous phases, i.e., reactions in homogeneous solutions or in gas phase. Ideally, the rate of a monomolecular reaction obeys a first-order rate expression that is explained by that proportion (number) of molecules having kinetic energy larger than the activation energy which is determined only by temperature of the reaction, and that the actual number of molecules with energy for activation is proportional to the concentration (or pressure) of molecules. For these reactions, kinetic data are analyzed by plotting the logarithm of concentration of a substrate or a product against time of the reaction (Suresh, 2012) to obtain a linear line, and absolute value of the slope of the line is a rate constant, *k*. The rate (*r*) of consumption of a substrate (A) is shown by Equation 2.37

$$r = -\frac{d[A]}{dt} = k[A] \quad (2.37)$$

On the other hand, kinetics of reactions occurring on a solid surface, i.e., catalysis or photocatalysis, must be significantly different. There are two representative extreme cases. One is the so-called "*diffusion controlled*" process, in which surface reactions and the following detachment process occur very rapidly to give a negligible surface concentration of adsorbed molecules, and the overall rate coincides with the rate of adsorption of substrate molecules. In this case, the overall rate is proportional to concentration of the substrate in a solution or gas phase (bulk), i.e., first-order kinetics is observed (Ohtani, 2011). The other extreme case is the so-called "*surface-reaction limited*" process; in which surface adsorption is kept in equilibrium during the reaction and the overall rate coincides with the rate of reaction occurring on the surface, i.e., reaction of e^- and h^+ with surface-adsorbed substrate. Under these conditions, the overall rate is not proportional to concentration of the substrate in the bulk unless the adsorption isotherm obeys a Henry-type equation, in which the amount of adsorption is proportional to concentration in the bulk. In the former case, the rate of photocatalytic reaction obeys the first-order rate law, but this is only formal and does not mean the mechanism of monomolecular reaction with activation energy (Ohtani, 2011).

One of the most significant points that we must consider in scientific studies, not limited to studies on photocatalysis, is discrimination of "evidence" and "consistency". In other words, it is necessary to recognize every fact to be a "necessary condition" but not a "sufficient condition" in a strict scientific sense. For example, the fact that reaction rate obeys the first-order rate law giving a linear relation in a plot of data is only a necessary condition for a monomolecular reaction in homogeneous phase and also a necessary

condition for heterogeneous photocatalytic reaction in diffusion-limited conditions or that in surface-reaction limited conditions with a Henry-type adsorption or a Langmuir-type adsorption in the lower concentration region (Ohtani, 2011).

For a heterogeneous system, when the pollutant substrate is in the millimolar levels, reactant oxidation closed to the catalyst surface is believed to generally follow the Langmuir–Hinshelwood model (Equation 2.38). In this equation, υ is the reaction rate, K is the reaction rate constant, b is the adsorption coefficient of the reactant which can be obtained from the Langmuir model in equation 2.40, C is the reactant concentration. When C is very small, the product bC is negligible compared to 1, and the equation below can be described as pseudo first-order reaction kinetics (Equation 2.39):

$$\upsilon = -\frac{dc}{dt} = \frac{Kbc}{1+Kbc} \tag{2.38}$$

$$-\ln\left(\frac{c_t}{c_o}\right) = k_{app}\, t \tag{2.39}$$

where C_0 and C_t are the reactant concentrations at times t = 0 and t, respectively, and $k_{app}(min^{-1})$ is the apparent reaction rate constant determined by plotting $\ln(C_t/C_0)$ vs. the reaction time (t).

Assuming that a certain reaction proceeds through a series of steps without any branching reactions, the rate may be the same as the rate of the slowest step, the rate-determining step, i.e., the overall activation energy is that of the rate-determining step. This original definition cannot be directly applied to photocatalysis. A plausible reason is that reactions by photoexcited electrons and positive holes occur in parallel, not in series (Ohtani, 2011). Considering the requirement of photocatalysis for the same numbers of electrons and positive holes to be used, it seems possible to compare the rates of electron and positive-hole reactions (Ohtani, 2011).

However, it seems that overall reaction rate must also be influenced by the rate of recombination of $e^{-}h^{+}$ included in the process. In ordinary photochemistry in homogeneous phase, steady (stationary)-state approximation is used to analyze kinetics, (Ohtani, 2011) assuming a forward reaction to give products and a backward reaction, i.e., deexcitation. In such analyses, there may not be a rate-determining step (Ohtani, 2011).

On the other hand, it seems reasonable to consider that, under limited reaction conditions, non-chemical processes, i.e., physical processes, may govern the overall rate of photocatalytic reactions. Two possible representative examples are as follows. In the case in which a surface reaction of adsorbed substrates with photoexcited electrons and positive holes is much faster than adsorption from a solution or gas phase, the reaction rate should be the same as that of diffusion of the substrate, i.e., a diffusion-controlled process (assuming a very thin diffusion layer on the surface of a photocatalyst, the rate of diffusion may be proportional to surface area of the photocatalyst). Another example is a light intensity-controlled process. If surface reactions by photoexcited electrons and positive holes proceeds slower than the adsorption of substrates, the surface concentration is always in equilibrium, and the overall rate should be the same as the rate of surface reaction, which is ideally proportional to the light intensity, a "light-intensity limited" process (Ohtani, 2011).

2.16 Adsorption Isotherms

Langmuir Adsorption Isotherm describes quantitatively the formation of a monolayer adsorbate on the outer surface of the adsorbent, and after that no further adsorption takes place. The Langmuir isotherm is valid for monolayer adsorption onto a surface containing a finite number of identical sites. The model assumes uniform energies of adsorption onto the surface and no transmigration of adsorbate in the plane of the surface. Based upon these

assumptions, Langmuir represented the following Equation (Langmuir, 1918):

$$\frac{C_e}{Q_e} = \frac{1}{Q_o b} + \frac{1}{Q_o} C_e \quad (2.40)$$

Where, $Q_e = \frac{(Co - Ce)V}{M}$ (2.41)

Langmuir adsorption parameters were determined by transforming the Langmuir equation (2.40) into linear form Langmuir Equation (1918).

$$\frac{1}{Q_e} = \frac{1}{Q_{max}} + \left(\frac{1}{Q_{max} k_L}\right) \frac{1}{C_e}$$

(2.42)

where C_e is the equilibrium concentration of the adsorbate (milligrams per litre), Q_{max} is the maximum adsorption capacity, (mgg^{-1}), Q_e is the amount of the adsorbate adsorbed per unit mass of the adsorbate (milligrams per gram), V is the volume of substrate solution, M is the mass of adsorbent, Q_o and k_L are Langmuir constants related to adsorption capacity and rate of adsorption, respectively. When $\frac{C_e}{Q_e}$ is plotted against C_e, a straight line with slope of $1/Q_o$ is derived. The essential characteristics of the Langmuir isotherm can be expressed in terms of a dimensionless constant separation factor R_L that is given by:

$$R_L = \frac{1}{1 + b c_o} \quad (2.43)$$

The value of R_L indicates the type of the isotherm to be either favorable ($0<R_L<1$), unfavorable ($R_L>1$), linear ($R_L = 1$), or reversible ($R_L=0$). If the values of R_L were found to be 0 to 1 suggesting the isotherm to be favorable at the condition studied.

Freundlich isotherm model considers a heterogeneous adsorption surface that has unequal available sites with different energies of adsorption is represented by (Monal *et al.*, 2015):

$$\ln q_e = \ln K_f + \frac{1}{n} (\ln C_e)$$

(2.44)

Linearizing equation (2.44), we have:

$$\text{Log } Qe = \log K_f + 1/n \log Ce \quad (2.45)$$

where C_e is the equilibrium concentration of the adsorbate (milligrams per liter), q_e is the amount of adsorbate adsorbed per unit mass of the adsorbent (milligrams per gram), K_f and n are Freundlich constants with *n,* giving an indication of how favorable the adsorption process is and K_F is the adsorption capacity of the adsorbate. K_F can be defined as the adsorption or distribution coefficient. The slope 1/n ranging between 0 and 1 is a measure of the adsorption intensity or surface heterogeneity, becoming more heterogeneous as its value gets closer to 0. The Freundlich isotherm describes the heterogeneous system and reversible adsorption. Theoretically, adsorbent has finite number of sites, and once all these sites are occupied by the adsorbed molecules, further adsorption cannot take place (Monal *et al.,* 2015).

2.17 Adsorption Kinetics

The contact time is evaluated as an important parameter affecting adsorption capacity of a photocalyst. In order to determine the controlling mechanism and dynamics of adsorption process, the largergen pseudo-first-order, the pseudo-second order, intraparticle diffusion, and Elovich kinetic models are applied to the experimental data (Oladoja *et al.,* 2008).

Pseudo-first-order kinetic model is represented by the following equation (Lagergen et al., 1898):

$$\ln(qe - qt) = \ln qe - k_1 t \quad (2.46)$$

The plot of ln(qe-qt) against t provides a linear relationship from which $k_{1,}$ constant of pseudo-first-order adsorption (min^{-1}) and qe, adsorption capacity at equilibrium are determined from the slope and the intercept of the plot, respectively, given q_t is the

adsorption capacity at time t (mg g^{-1}).

Pseudo-second-order kinetic model is represented by the following equation (HO et al., 1998):

$$\frac{t}{q_t} = \frac{1}{k_2 q_e^2} + \frac{1}{q_e} t \quad (2.47)$$

The initial adsorption rate, h (mg g^{-1} min^{-1}), is represented by:

$$h = k_2 q_e^2 \quad (2.48)$$

where k_2 is the equilibrium rate constant of pseudo-second-order adsorption (g mg^{-1} min^{-1}). Values of k_2 and qe are calculated from the plot $\frac{t}{q_t}$ against t.

The simplified Elovich kinetic equation is generally expressed as follows (Chein *et al.*, 1980):

$$q_e = \frac{1}{\beta} \ln(\alpha\beta) + \frac{1}{\beta} \ln t \quad (2.49)$$

where α is the initial adsorption rate (mg g^{-1} min^{-1}), the parameter β is related to the extent of surface coverage and activation energy for chemisorptions (g mg^{-1}).

Several steps are involved in the sorption of sorbate by a sorbent. These involve transport of the solute molecules from the aqueous phase to the surface of the solid particulates and diffusion of the solute molecules into the interior of the pores, which is usually a slow process. When intra-particle diffusion plays a significant role in controlling the kinetics of the sorption process, the plots of qt versus $t^{0.5}$ yield straight lines passing through the origin and the slope gives the rate constant k_p. The intra-particle diffusion rate constant (k_p) is given by the following equation (Weber *et al.,* 1963):

$$q_t = k_p t^{1/2} + C \quad (2.50)$$

Where C is the intercept (mg g^{-1}) and k_p is the intraparticle diffusion rate constant (mg g^{-1} min^{-1}).

However, when the transport of the solute molecules from the liquid phase up to the solid phase, boundary plays the most significant role in adsorption, the liquid film diffusion model may be applied.

$$\ln(1 - F) = - k_{fd}\, t \qquad (2.51)$$

where F is the fractional attainment of equilibrium F = qt/qe and k_{fd} is the adsorption rate constant. A linear plot of –ln (1-F) vs. t with zero intercept would suggest that the kinetics of the sorption process is controlled by diffusion through the liquid film surrounding the solid sorbent (Oladoja *et al.,* 2008).

2.18 Design of Experiments

Interaction of the variables involved in photocatalytic process is often strong, thus, the use of one variable at a time (OVAT) approach to study and interpret responses in a multivariate system such as the photocatalytic process can be grossly inadequate. The OVAT refers to the approach of investigating several process parameters by keeping one variable constant and others varied. In this method, interactive effects are not accounted for and optimal conditions obtained are not representative of the whole process condition. Responses from processes involving several variables cannot be studied without taking account of the strong interaction between the variables; an effective approach to such processes involve conducting a well-planned and predetermined set of chosen experiments based on a multivariate design of experiments. A multivariate approach that utilizes a second-degree quadratic polynomial is thus, necessary in order to obtain unbiased responses that would adequately describe the process with a minimum number of experiments (Montgomery *et al*., 2002).

2.19 Photocatalytic Degradation and Mineralization of Acetaminophen Using the Synthesized $ZnFe_2O_4$-TiO_2 Composite

Unlike adsorption which merely transfers acetaminophen molecules from the aqueous phase onto the surface of the $ZnFe_2O_4$-TiO_2 composite, photocatalytic oxidation of acetaminophen leads to the mineralization of acetaminophen to form less harmful inorganic species such as CO_2, H_2O and ammonium salts (Yang *et al.*, 2008). The main goal of photocatalytic treatment of water pollutants is not just mere destruction of the organic pollutants because some of the intermediates generated during photocatalysis can be more toxic than the pollutants themselves. In addition is to chemically convert the organic pollutants into less harmful inorganic species such as water, carbon dioxide and mineral salts. In this work, photocatalytic degradation of acetaminophen was investigated by determining the residual concentration of acetaminophen in the treated acetaminophen solutions using UV-Vis spectroscopy. Photocatalytic mineralization of acetaminophen is studied by measuring the change in Chemical Oxygen Demand (COD) of the treated acetaminophen solutions.

CHAPTER THREE

MATERIALS AND METHODS

3.1 Materials

The main materials used in this work include:

1. Ferric nitrate; $Fe(NO_3)_3.9H_2O$; (analytical grade)
2. Zinc nitrate; $Zn(NO_3)_2.6H_2O$; (analytical grade)
3. Titanium dioxide; (TiO_2); (analytical grade)
4. Polyethylene glycol; (analytical grade)

5. Sodium acetate (NaAc) (analytical grade)
6. Distilled water (Chemical Engineering Department, A.B.U Zaria).
7. Ethanol; (analytical grade)
8. Acetaminophen

3.2 Apparatus

The apparatus used in this work were:

1. Conical flasks (250, 500ml)
2. Measuring cylinders (100ml, 200ml)
3. Plastic funnels
4. Retort stand and G-Clamp
5. Halogen Lamp (500W), Star Gold.
6. Plastic spoons
7. Rubber gloves
8. Syringe (20ml)
9. 45 Sample bottles (glass and plastic)
10. 1 Burette (50ml)
11. 1 Pipette (25ml)
12. Crucibles
13. Mortar and pestle
14. Timer

3.3 Equipment

The major equipment employed in this work are:

1. Electronic Weighting scale (0-600g) at Chemical Engineering Department, A.B.U Zaria.

2. Domestic Microwave oven (Sainsbury's microwave oven with 800 watt output) at Chemical Engineering Department, A.B.U Zaria.
3. X-Ray Diffractometer at National Geological Research Laboratory (NGRL), Barnawa, Kaduna
4. X-Ray Florescence spectrometer, PANalytical, England at National Geological Research Laboratory (NGRL), Barnawa, Kaduna
5. Hot Plate with Magnetic Stirrer (0-300^{o}C), Stuart, England at Chemical Engineering Department, A.B.U, Zaria.
6. UV-Vis Spectroscopy Equipment, JENWAY 6405 at Pharmaceutical and Medicinal Chemistry Department, A.B.U, Zaria.
7. Scanning Electron Microscope, Phenome Pro-x at Chemical Engineering Department, A.B.U Zaria.

3.4 Experimental Methodology

Figure 3.1 shows the block diagram of the experimental procedure used in this work. The details are given in the subsections 3.4.1 - 3.4.4.

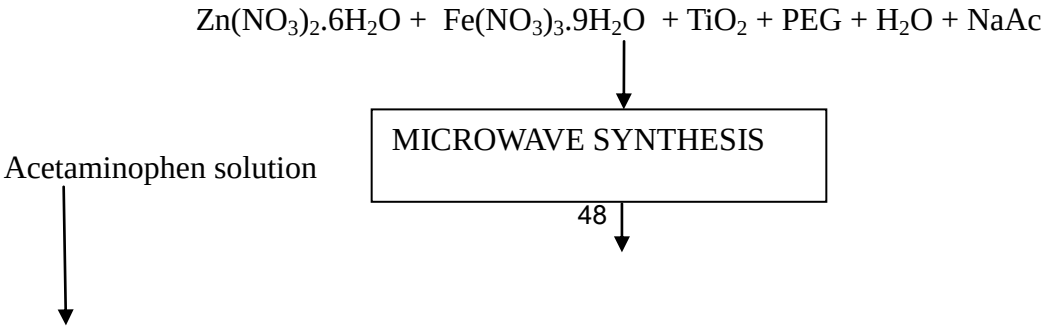

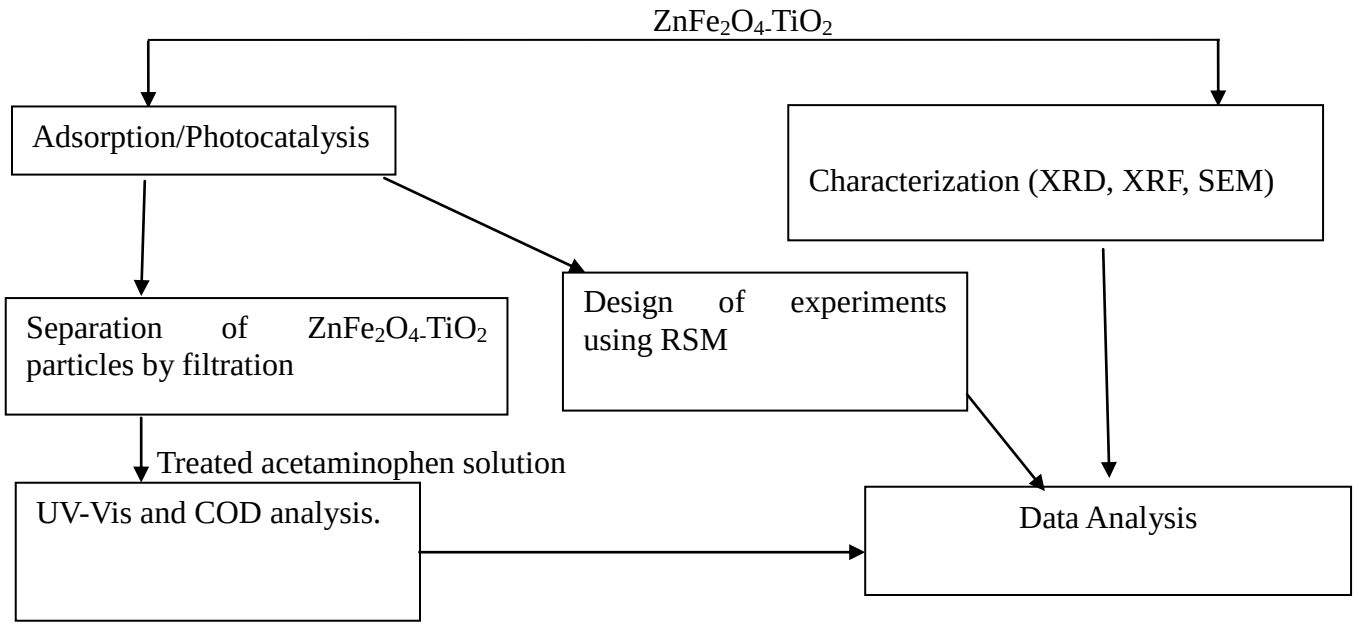

Figure 3.1: Block diagram of the experimental methodology

3.4.1 Microwave assisted synthesis and characterization of $ZnFe_2O_4$-TiO_2

The procedure reported by Feng *et al.* (2014) for the synthesis of $ZnFe_2O_4$-ZnO was adopted and modified for the synthesis of $ZnFe_2O_4$-TiO_2 in this work. Thus the optimum molar ratio for the synthesis of $ZnFe_2O_4$-TiO_2, 0.15:1 reported by (li *et al.*, 1996) was adopted in this work.

The modification done to the microwave combustion synthesis method involved the synthesis of the catalyst in batches due to excessive combustion reaction which took place as such resulted to damages in the domestic microwave oven used. Thus the photocatalyst was prepared in 10 batches. For each batch 0.297g of $Zn(NO_3)_2{\cdot}6H_2O$, 0.807 $Fe(NO_3)_3{\cdot}9H_2O$, 0.094g polyethylene glycol and 2.65g of titanium dioxide were mixed with 1.8 ml distilled water under vigorous stirring manually. Then 2.8ml of sodium acetate solution (0.05 g/l) was dripped into the solution. The mix solution was heated in a domestic microwave oven at 120 W for 5 min, and then at 700 W for 10 min. The solid powder was

washed with water and ethanol for several times. $ZnFe_2O_4$-TiO_2 powder was obtained after drying.

X-Ray Diffraction (XRD) patterns of the $ZnFe_2O_4$-TiO_2 was recorded using an X-ray diffractometer at an accelerating voltage of 40kV with 30-mA flux. The X-ray source was CuKα1 with a wavelength of 1.5406A°. The chemical composition of the $ZnFe_2O_4$-TiO_2 was obtained with a 15kV acceleration voltage and 10nA beam current.

Scanning Electron microscopic (SEM) image of the $ZnFe_2O_4$-TiO_2 was taken using Scanning Electron Microscope (Phenom Pro-X) working at accelerating voltage of 15 kV.

3.4.2 Adsorption of acetaminophen onto $ZnFe_2O_4$-TiO_2

Adsorption experiments were conducted at room temperature (30±2 °C) in the dark. The initial concentration of the aqueous solution of acetaminophen was in the range of 5- 25 mg/L at 5mg/L interval. The adsorbent ($ZnFe_2O_4$-TiO_2) dosage was fixed at 0.1 g/L. The adsorbent was dispersed in acetaminophen solution and stirred using a magnetic stirrer at 200 rpm for one hour in the dark. Aliquots were withdrawn from the suspension at 5min intervals of time and filtered to completely remove the particles of $ZnFe_2O_4$-TiO_2. The obtained filtrates were then analysed for the residual concentration of acetaminophen using a UV-Vis spectrophotometer (Jenway 6405 model). The percentage removal of acetaminophen was calculated using Equation 3.1.

$$\text{Removal} = \frac{(A_0 - A_t)}{A_0} \times 100\% \qquad (3.1)$$

where A_t is the absorbance of acetaminophen remaining in the solution at contact time, t, and A_0 is the initial absorbance of acetaminophen.

3.4.3 Photocatalytic treatment of acetaminophen using $ZnFe_2O_4$-TiO_2

Chang *et al.* (2008) reported the optimum range for catalyst dosage and initial concentration of acetaminophen to be (0.1 g-1.0 g) and (4.8 mg/L- 8 mg/L) respectively which was adopted in this work. For the photocatalytic experiments, the range of 0.1 g - 1.0 g of the photocatalyst ($ZnFe_2O_4$-TiO_2) obtained from the central composite design (CCD) was added to the aqueous solution of acetaminophen with the range of 4.8 mg/L-18 mg/L for low and high points respectively stirred for 60 minutes in the dark to reach the adsorption equilibrium. The suspension was then exposed to visible light (500W Halogen lamp). To minimize the influence of temperature emanating from the lamp, the photoreactor was placed under a fan. Photocatalytically treated samples of acetaminophen at various irradiation times were taken and analysed using a UV-Vis spectrophotometer at maximum absorption peak of acetaminophen at 242 nm in order to determine photocatalytic degradation of acetaminophen calculated using Equation 3.2

$$\text{D}egradation = \frac{(A_0 - A_t)}{A_0} \times 100\% \tag{3.2}$$

where A_t is the absorbance of acetaminophen remaining in the solution at irradiation time, t, and A_0 is the initial absorbance of acetaminophen.

It shall be noted that adsorption merely transfers acetaminophen molecules from the aqueous phase onto the surface of the adsorbent; hence, removal is used in Equation 3.1. On the other hand, photocatalysis involves chemical oxidation of the acetaminophen molecules thus degradation is used in Equation 3.2. Photocatalytic degradation of acetaminophen generates several intermediates which may be more toxic than the acetaminophen. Hence, the best way to assess the performance of the photocatalyst is by measuring the organic loading of the raw and treated water using lump parameters such as the Chemical Oxygen Demand (COD). Thus, each sample of the photocatalytically treated

samples of acetaminophen was subjected to UV-Vis spectrophotometric and COD analyses. Mineralization of acetaminophen was calculated using equation 3.3.

$$Mineralization = \frac{(COD_0 - COD_t)}{COD_0} \times 100\% \quad (3.3)$$

where, COD_t is the COD of acetaminophen remaining in the solution at irradiation time, t, and COD_0 is the initial COD of acetaminophen.

3.4.4 Experimental design and modeling of photocatalytic treatment of acetaminophen using $ZnFe_2O_4$-TiO_2

The effects of three independent variables, namely initial acetaminophen concentration, the catalyst dosage, and reaction time, on the photocatalytic treatment of acetaminophen using $ZnFe_2O_4$-TiO_2 were investigated using the central composite design (CCD) as implemented in Design Expert 6.06 software package. However, pH was not considered as a specific variable due to the several reported literature that established the optimal pH of about 6.9 close to neutral (Gotostos *et al*., 2014) for the photocatalytic reaction. Thus, in this study, the initial reaction pH of acetaminophen was fixed at 6.9. Central composite design (CCD) with two level factorial design with additional experimental referred to as the star point; the latter experiments are introduced for determining the quadratic response surface. Six repetitions at the centre points were done to allow for better prediction of the reproducibility (Kiril *et al*., 2010). The choice of CCD out of the numerous available designs was informed by its popularity, reliability and its general acceptance as a standard second-order design (Tarley *et al*., 2009; Virkutyte *et al*., 2010). Table 3.1 shows the design matrix for photocatalytic treatment of acetaminophen solution in water. A total of 20 experimental runs were carried out with their various responses. From the experimental runs performed, mathematical relationship of the response function (y) and influence of the

independent variables is express as a general quadratic polynomial model (Equation 3.4). The regression coefficients obtained by response surface regression analysis were achieved by fitting experimental data to the quadratic model.

$$y = \beta_o + \beta_i X_i + \Sigma\ \beta_{ij} X_i X_j + \Sigma\ \beta_{ii} x_i^2 + \varepsilon \quad (3.4)$$

The regression coefficients for intercept, linear, quadratic and interaction terms are represented by β_0, β_i, β_{ii} and β_{ij}, respectively, while the independent variables that affect the response y are denoted by x_i, x_{ii} and x_{ij} and ε is the random error or noise to the response. Data generated was analyzed, coefficients in the mathematical model predicting the response estimated, and analysis of variance (ANOVA) was used for gaining insight into the interaction between the variables affecting the process and the response. Adequacy check was also performed to ascertain the quality of the fit of polynomial expressed in equation 3.4 using the coefficient of determination R^2 and $R^2_{adj.}$

Table 3.1: Design matrix for photocatalytic degradation and mineralization of acetaminophen

Run	Independent variables			Response 1	Response 2
	A	B	C	Photocatalytic degradation (%)	Photocatalytic mineralization (%)
1	11.40	0.55	37.50		
2	0.3	0.55	37.5		
3	4.8	1.0	15		
4	11.40	0.55	-0.34		
5	4.8	0.1	60		
6	18.0	0.1	15		
7	18.0	1.0	15		
8	11.4	0.55	75		
9	4.8	1.0	60		
10	11.4	1.31	37.5		
11	11.4	0.55	37.5		
12	18.0	0.1	60		
13	18.00	1.00	60		
14	11.4	-0.21	37.5		
15	22.5	0.55	37.5		
16	11.4	0.55	37.5		

17	11.4	0.55	37.5
18	11.4	0.55	37.5
19	11.4	0.55	37.5
20	4.80	0.1	15

3.4.5 Optimization of photocatalytic degradation and mineralization of acetaminophen

Optimization was performed on the basis of desirability function in order to find the optimum conditions for the photocatalytic degradation and mineralization of acetaminophen. Numerical optimization was used to locate the specific point that maximizes the desirability function for photocatalytic degradation and mineralization of acetaminophen under the constraints listed in Tables 3.2 and 3.3.

Table 3.2: Constraints for the numerical optimization of photocatalytic degradation acetaminophen

Name	Goal	Lower Limit	Upper Limit	Lower Weight	Upper Weight	Importance
Initial conc of Ace (mg/L)	is in range	4.8	18	1	1	3
Photocatalyst dosage (g/L)	is in range	0.1	1	1	1	3
Irradiation time (min)	is in range	15	60	1	1	3
Degradation (%)	maximize	18.98	91.5	1	1	3

Table 3.3: Constraints for the numerical optimization of photocatalytic and mineralization of acetaminophen

Name	Goal	Lower Limit	Upper Limit	Lower Weight	Upper Weight

Importance						
Initial Conc. of Ace (mg/L)	is in range	4.8	18	1	1	3
Photocatalyst dosage (g/L)	is in range	0.1	1	1	1	3
Irradiation time (min)	is in range	15	60	1	1	3
Mineralization (%)	maximize	23.65	96.29	1	1	3

The desired goal was selected by adjusting the weight or importance that might alter the characteristics of a goal. The goal fields for response have five options: none, maximum, minimum, target and within range. The criteria for optimization of all studied factors in correspondence with percentage degradation and mineralization were shown in Table 3.2 and 3.3. From ANOVA, it has shown that the main effects of catalyst dosage and time were significant, therefore these factors were assigned ‘within range’ with corresponding ‘importance 3’ as higher percentage degradation and mineralization is usually preferred for this study also ‘importance 3’ was assigned as the maximum goal respectively. The lower limits and upper limits responses are taken from the CCD design levels, in order to maximize the percentage degradation and mineralization with recalculating all responsible factors by using desirability functions. By using all of the above described settings and boundaries, the software optimized 91.5% and 96.4% respectively, for photocatalytic degradation and mineralization of acetaminophen. For photocatalytic degradation, the optimized values of the initial acetaminophen concentration were 11.0 mg/L, catalyst dosage was 0.6g/L and irradiation time was 42.0 min. For mineralization, the optimized values were: of initial concentration of 11.2 mg/L, catalyst dosage of 1.0 g/L and irradiation time of 28.7min. To validate the theoretical results, duplicate confirmatory experiments were conducted using the optimized parameters.

CHAPTER FOUR

RESULTS AND DISCUSSION

4.1 Characterization of the Synthesized $ZnFe_2O_4$-TiO_2 Composite

4.1.1 Chemical composition of the $ZnFe_2O_4$-TiO_2 composite

The X-Ray Florescence (XRF) result of the synthesized $ZnFe_2O_4$-TiO_2 Composite indicates that the main constituents are titanium dioxide (78.68%) followed by Iron (III) oxide (10.22%) and Zinc Oxide (5.27%) as shown in Table 4.1. The mole fraction of the composite was calculated by dividing the mass fraction of ZnO, Fe_2O_3 and TiO_2 by their corresponding molecular weights. The mole fractions of ZnO and Fe_2O_3 were 0.064 and 0.065, respectively; hence, the mole fraction of $ZnFe_2O_4$ in the composite was 0.0065. The mole fraction of TiO_2 was 0.985. Therefore, the mole ratio of $ZnFe_2O_4$ to TiO_2 in the composite is 0.15:1.

Table 4.1: Chemical composition of the synthesized $ZnFe_2O_4$-TiO_2 composite

Component	Concentration (wt. %)	Component	Concentration (wt. %)
Al_2O_3	1.8	MnO	0.027
SiO_3	1.0	**Fe_2O_3**	**10.22**
P_2O_5	0.38	**ZnO**	**5.27**
SO_3	0.20	CdO	0.35
CaO	0.88	Ta_2O_5	0.14
TiO_2	**78.68**	BiO_4	0.57
V_2O_5	0.52		

4.1.2 XRD analysis of the $ZnFe_2O_4$-TiO_2 composite

The XRD pattern of the synthesized $ZnFe_2O_4$-TiO_2 composite is shown in Figure 4.1. The

XRD peaks of the anatase phase of TiO_2 are observed at Bragg angles of 24.9°, 37.8°, 48.0°, 53.9° and 57.4° (JCPDS card No 78 – 2486). The peaks at 18.36^{o}, $34.03^{o,}$ $^{42.8o,}$ $^{56.5o}$ and $^{62.14o}$ correspond to $ZnFe_2O_4$ (JCPD card No 74-2397). The broad peaks 63.5°,32.6° are due to the low crystallinity of the prepared $ZnFe_2O_4$ (Cheng *et al.,* 2012). Cheng et al. (2004) synthesized zinc ferrite -doped TiO_2 nanopowders with various amount of zinc ferrite by sol-gel method. They reported the X-ray diffraction results which showed that the anatase TiO_2 main peaks are 25.3°, 37.8°, 48.0°, 53.9° and 55.8° in XRD were similar to the The XRD peaks of the anatase phase of TiO_2 shown this research. In addition the $ZnFe_2O_4$ main peaks were 29.9°, 35.2°, 42.8°, 56.8° and 62.1° in XRD which corresponds to the $ZnFe_2O_4$ (JCPD card No 74-2397) as shown in this research.

.

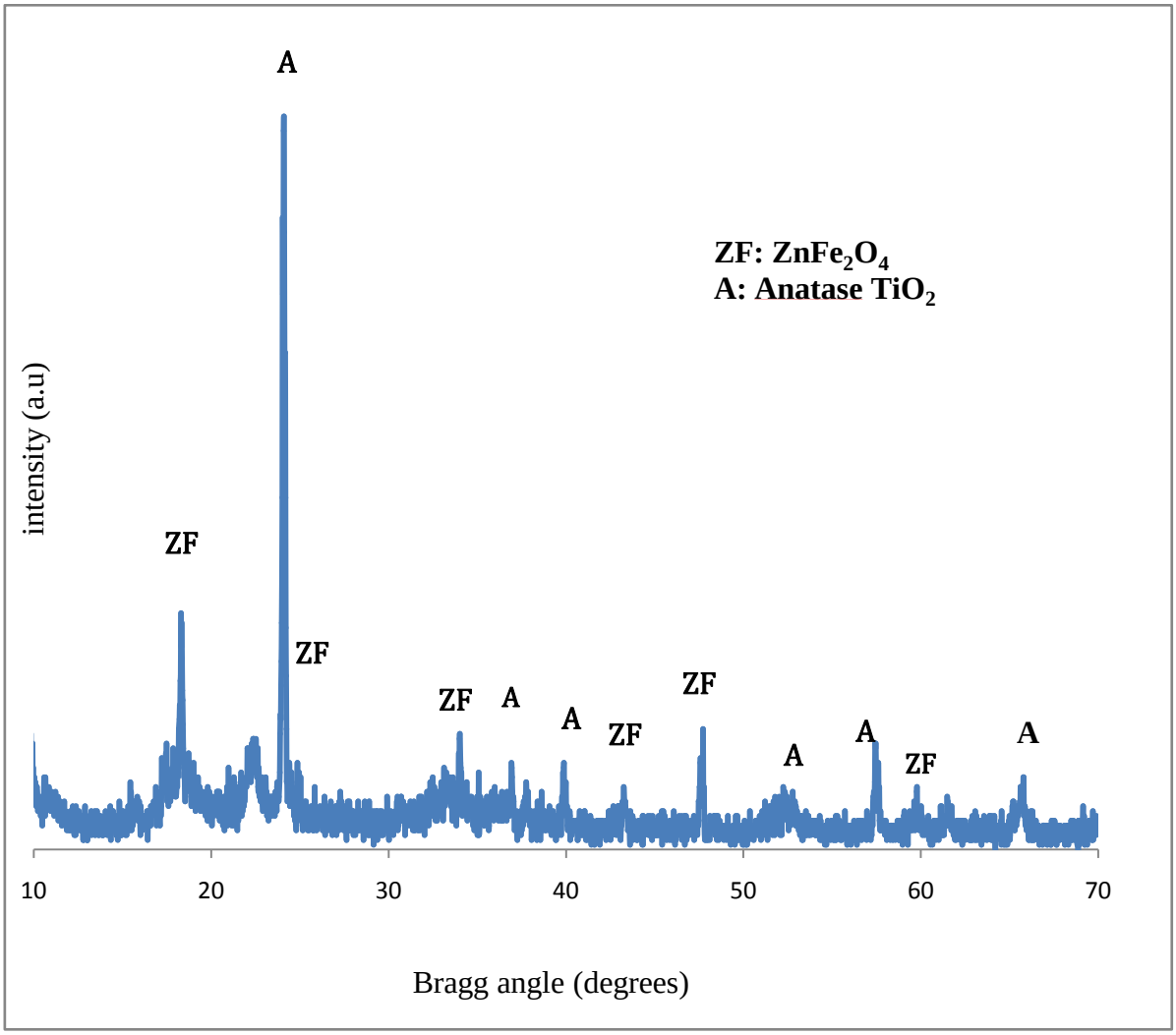

Figure 4.1: XRD pattern of the $ZnFe_2O_4$-TiO_2 composite

4.1.3 Scanning Electron Microscopy of the $ZnFe_2O_4$-TiO_2 composite

The morphological characteristics of the synthesized $ZnFe_2O_4$-TiO_2 composite were investigated by SEM analysis. The SEM image of $ZnFe_2O_4$ sample displayed in Plate 1 shows that $ZnFe_2O_4$-TiO_2 exhibits a compact arrangement of particles with roughly irregular shape. Most of the particles are aggregated which makes it difficult to determine the exact size and shape of the particle.

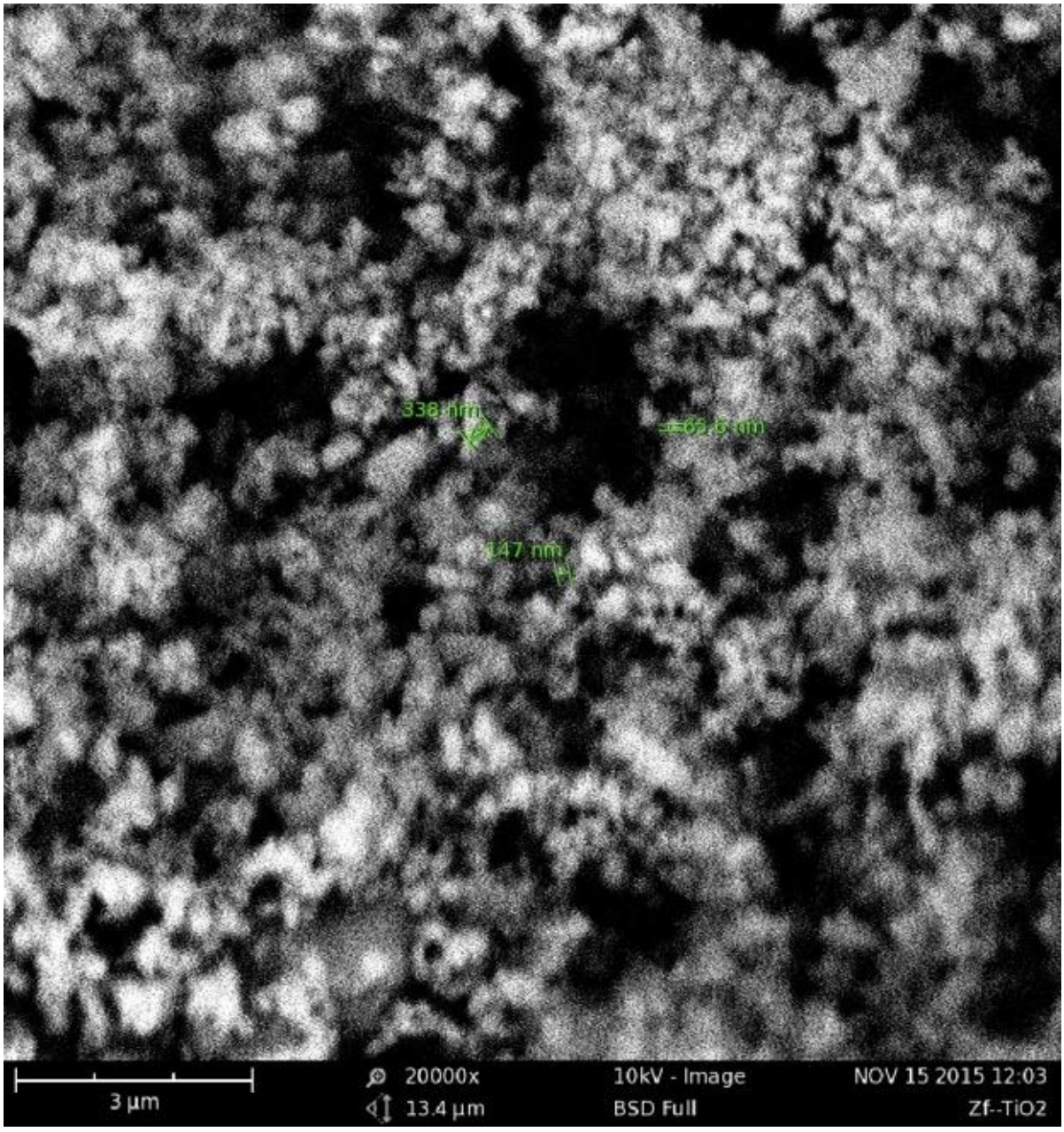

Plate 1: Scanning Electron Microscopic image of the $ZnFe_2O_4$-TiO_2 composite

4.2 Adsorption of Acetaminophen onto $ZnFe_2O_4$-TiO_2

4.2.1 Effect of the initial concentration of acetaminophen and contact time on the adsorption of acetaminophen onto $ZnFe_2O_4$-TiO_2

Figure 4.2 shows the effect of contact time on the adsorption of acetaminophen on

$ZnFe_2O_4$-TiO_2 using five different initial concentrations of acetaminophen (5, 10, 15, 20 and 25 mg/L) at room temperature (30±2°C) under dark conditions. The adsorption process could be divided into two steps, a quick step and a slow step. Adsorption of acetaminophen onto $ZnFe_2O_4$-TiO_2 increased with increase in the initial concentration of acetaminophen. The adsorption was fast within the first 20 min (quick step) due to the large driving force of the process (concentration gradient between the acetaminophen solution and the surface of $ZnFe_2O_4$-TiO_2). In other words, relatively strong interactions between adsorbate and adsorbent gave rise to higher adsorption efficiency in a shorter contact time (Zhang *et al*., 2007). After 20 min the adsorption decreases until it reaches equilibrium at 50 min (slow step). Equilibrium adsorption was achieved within 50 min regardless of the initial concentration of acetaminophen. In the slow step, the adsorption was slow and reached equilibrium at 60 min (Figure 4.2). This observation is in line with the published report on the adsorption Adsorption and photocatalytic degradation of pharmaceuticals by BiOClxIynanospheres Wang *et al.* (2015). From Figure 4.2 q_t (mgg^{-1}) stands for the equilibrium adsorption capacity of the adsorbent ($ZnFe_2O_4$-TiO_2 composite) which was plotted against the contact time t (min). The corresponding values for absorbance with conversions to adsorption of acetaminophen unto $ZnFe_2O_4$-TiO_2 composite were shown at the Appendix (Table A2).

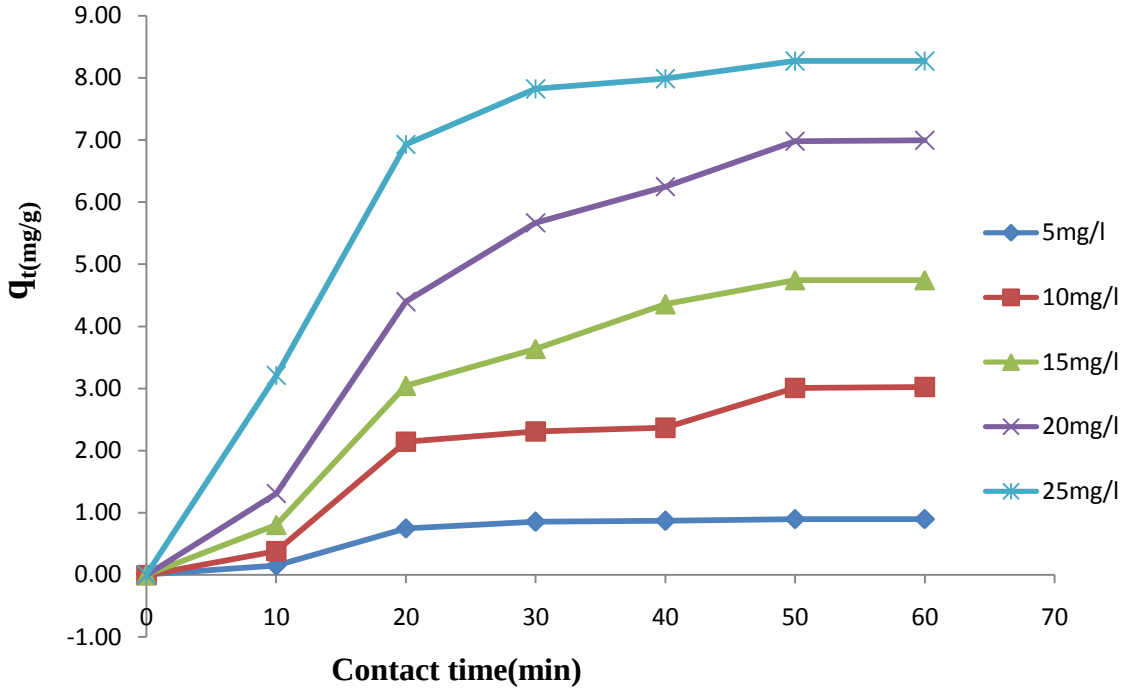

Figure 4.2: Effect of the initial concentration of acetaminophen and contact time on the adsorption of acetaminophen onto $ZnFe_2O_4$-TiO_2

4.2.2 Isotherms for the adsorption of acetaminophen onto $ZnFe_2O_4$-TiO_2

The Langmuir and Freundlich isotherms were selected in this study. The linear forms of the Langmuir and Freundlich isotherms were given by Equations (2.42) and (2.45), respectively. The linear plots of the Langmuir and Freundlich isotherms for the adsorption of acetaminophen onto $ZnFe_2O_4$-TiO_2 were shown in Figures (4.3) and (4.4), respectively. After plotting a graph of $1/q_e$ against $1/c_e$ for the Langmuir isotherm model with the corresponding values shown in Appendix A (Table A3). The plot of $1/q_e$ versus $1/c_e$ yielded a slope of $1/q_{max}k_L$ and an intercept $=1/q_{max}$ from which the values for the langmuir adsorption constant were calculated as shown in Appendix A. The R^2 value of 0.979 obtained for the Langmuir Isotherm model was higher than the R^2 value of 0.962 obtained for the Freundlich Isotherm model. Hence, the adsorption data was best described by the

Langmuir Isotherm model. Likewise for the Freundlich isotherm model after plotting a graph of lnq_e against lnc_e for the Langmuir isotherm model with the corresponding values shown in Appendix A (Table A4). The plot of lnq_e versus lnc_e yielded a slope of n and an intercept = k_F from which the values for the Freundlich adsorption constant were calculated as shown in appendix A.

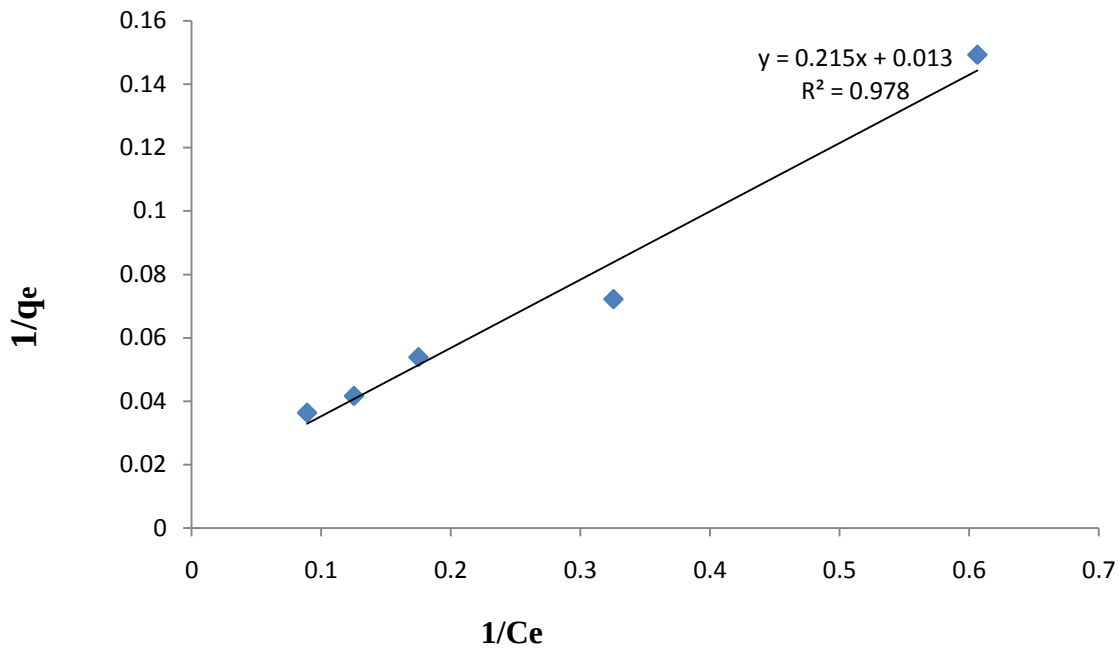

Figure 4.3: Linear plot of the Langmuir isotherm for the adsorption of acetaminophen onto $ZnFe_2O_4$-TiO_2

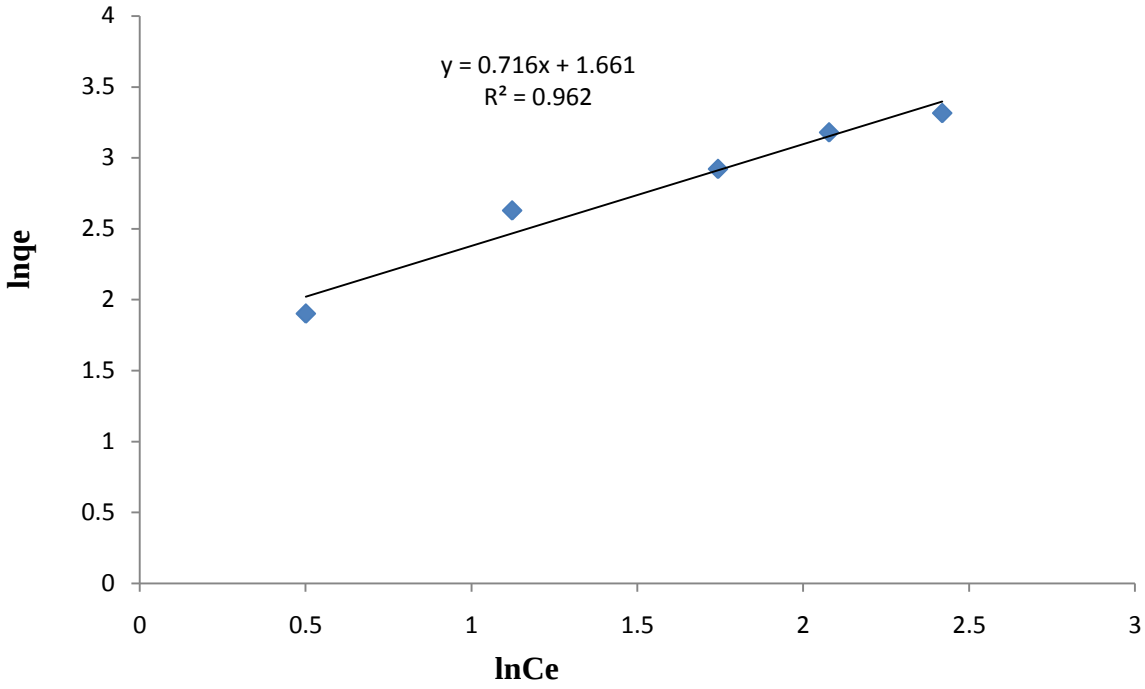

Figure 4.4: Linear plot of the Freundlich isotherm for the adsorption of acetaminophen onto $ZnFe_2O_4$-TiO_2

The derived values of q_{max}, K_L, K_F, n and the correlation coefficients (R^2) for the two isotherm models are listed in Table 4.2, from where it is apparent that the maximum monolayer coverage capacity of $ZnFe_2O_4$-TiO_2 (q_{max}) for acetaminophen is 26.88 mg/g. The Langmuir equilibrium adsorption constant (K_L) is 0.0963 Lmg^{-1}. The essential characteristics of the Langmuir isotherm are often expressed using a dimensionless constant called dimensionless separation factor (R_L) which is expressed by equation 2.43.

The adsorption process can be unfavourable if $R_L > 1$, linear if $R_L = 1$, favourable if $0 < R_L < 1$ or irreversible if $R_L = 0$. In this work, the calculated R_L value is 0.41. Therefore, adsorption of acetaminophen onto $ZnFe_2O_4$-TiO_2 is favourable.

Table 4.2: Derived Langmuir and Freundlich Isotherm constants for the adsorption of acetaminophen onto $ZnFe_2O_4$-TiO_2 composite

Isotherm	Parameters			
Langmuir	q_m = 26.88 mg/g	K_L= 0.0963 L/mg	R_L = 0.41	R^2 = 0.979
Freundlich	K_F = 2.6343	n = 0.7169		R^2 = 0.96

4.2.3 Kinetics of acetaminophen adsorption onto $ZnFe_2O_4$-TiO_2

The experimental adsorption kinetic data were fitted with the pseudo first-order and the pseudo second-order models (Equations 2.46 and 2.47). Figures 4.5 and 4.6 featured pseudo first order and pseudo second-order kinetic plots for the adsorption of acetaminophen onto $ZnFe_2O_4$-TiO_2, respectively. The derived kinetic data are presented in Table 4.3, from where it can be seen that the correlation coefficients for the pseudo-second-order model were higher than those of the pseudo-first-order kinetic model especially at higher initial concentrations of acetaminophen. In addition the values of the equilibrium adsorption capacity (q_e) yielded by the pseudo-second-order model were closer to the values of the experimental adsorption capacity (q_e experimental) listed in the last column of Table 4.3. Therefore pseudo-second order kinetics best describes the process. As the initial acetaminophen concentration was increased from 5 to 20 mg/L, the rate constant of pseudo-second-order decreased from 0.573 min^{-1} to 0.02 min^{-1} likewise for the pseudo-first-order rate constant decreases from 0.085g/mgmin to 0.055g/mgmin at 5 to 20 mg/L initial concentrations whereas the values of q_{1e} and q_{2e} increased with increase in the initial concentration of acetaminophen.

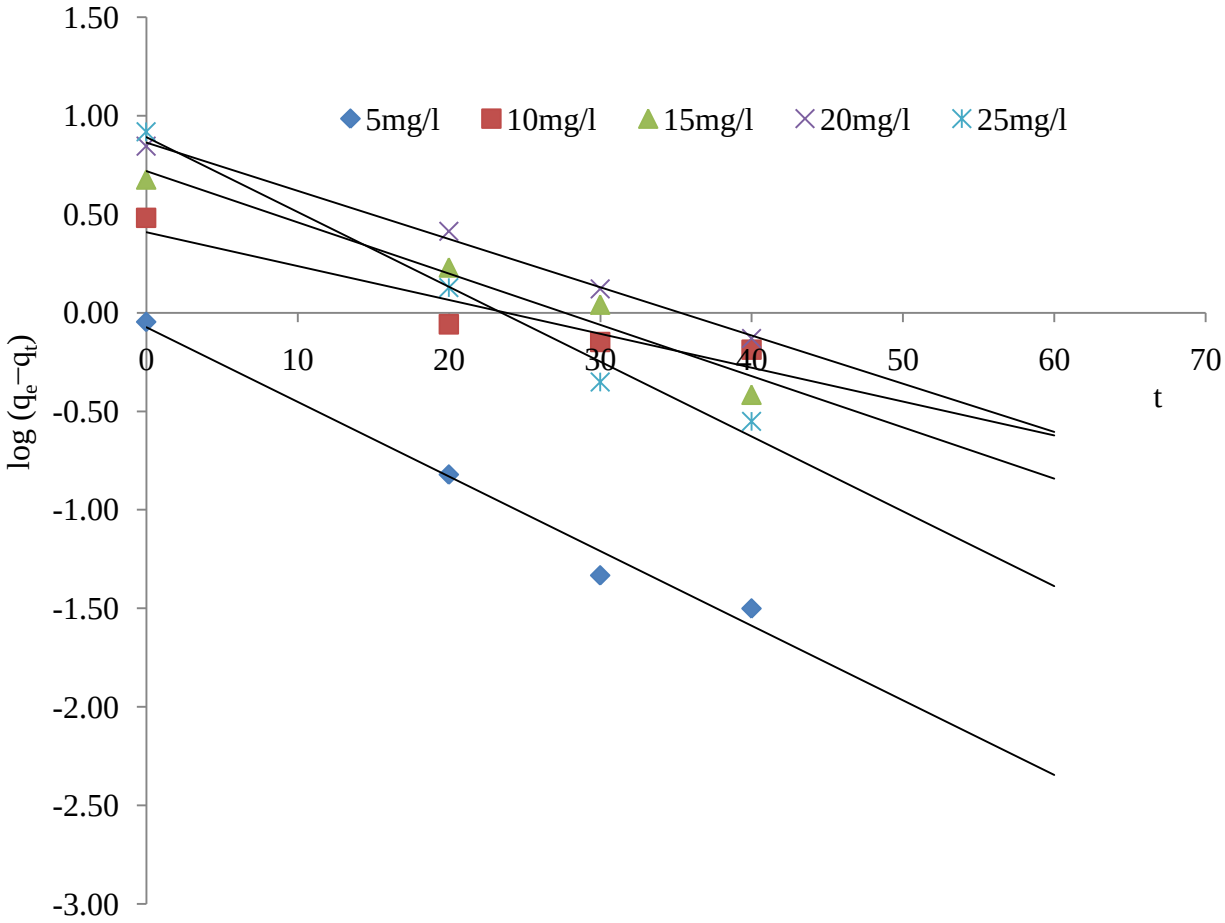

Figure 4.5: Pseudo first order kinetic plot for the adsorption of acetaminophen onto $ZnFe_2O_4$-TiO_2

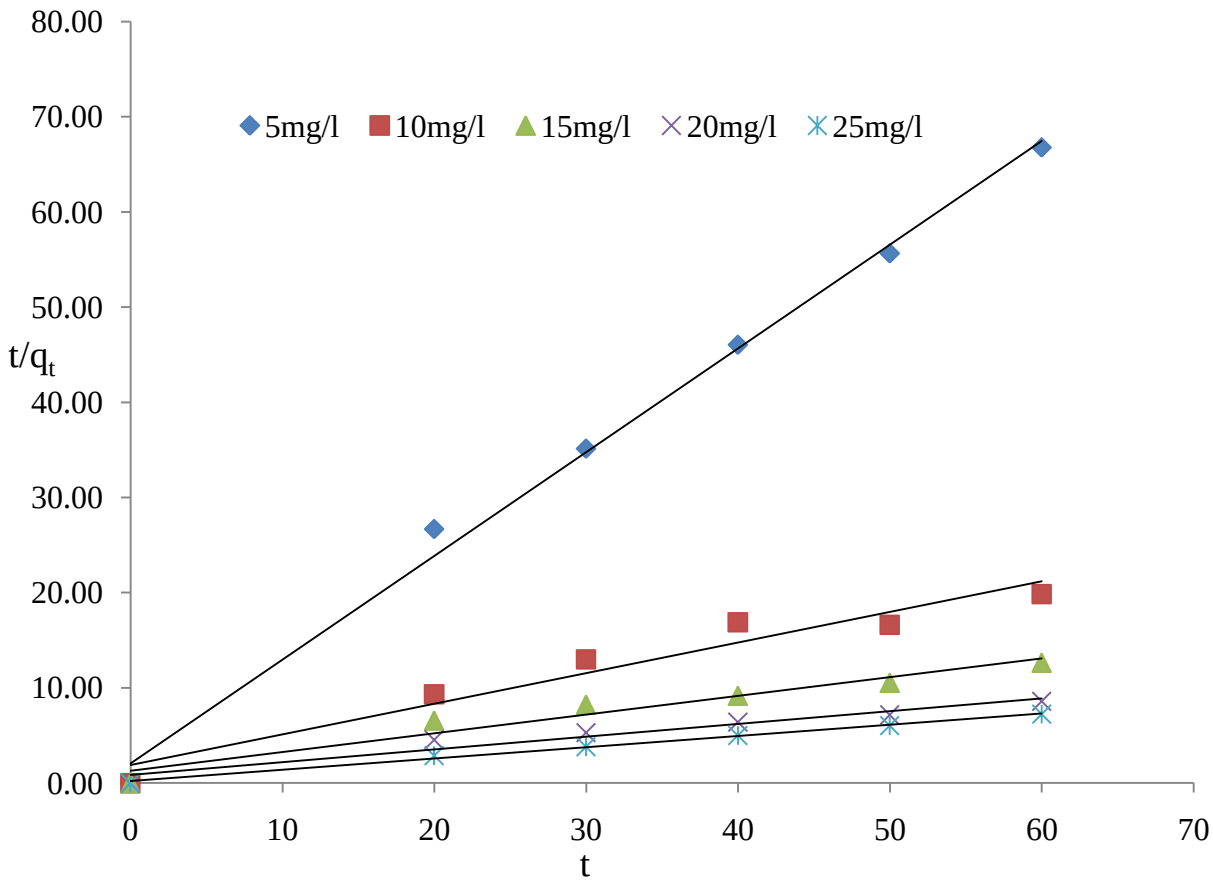

Figure 4.6: Pseudo second order kinetic plot for the adsorption of acetaminophen onto $ZnFe_2O_4$-TiO_2

Table 4.3: Kinetic model parameters for the adsorption of acetaminophen onto $ZnFe_2O_4$-TiO_2

C_0 (mg/l)	Pseudo-first-order kinetic model			Pseudo-second-order kinetic model			Experimental q_e (mg/g)
	q_{1e} (mg/g)	k_1 (min^{-1})	R^2	q_{2e} (mg/g)	k_2 (gm/gmin)	R^2	
5	0.85	0.085	0.981	0.92	0.573	0.995	0.90
10	2.56	0.039	0.894	3.12	0.055	0.941	3.02
15	5.22	0.060	0.963	5.10	0.0293	0.946	4.74
20	7.29	0.055	0.995	7.52	0.020	0.949	6.99

25	7.76	0.088	0.986	8.48	0.062	0.995	8.27	

4.3 Control experiments

Control experiments were performed in order to determine the effects of light and $ZnFe_2O_4$-TiO_2 on the removal/degradation of acetaminophen in water. The removal of acetaminophen from its aqueous solution was carried out via dark adsorption at 0.1g/L of $ZnFe_2O_4$-TiO_2 in the absence of light, photolysis (under illumination of 500W halogen lamp, in the absence of $ZnFe_2O_4$-TiO_2), and photocatalysis at 0.1g/L of $ZnFe_2O_4$-TiO_2 under illumination of 500W halogen lamp. In all cases the initial concentration of acetaminophen is 10 mg/L.

The experimental results displayed in Figure 4.7 show that only 4% of acetaminophen was degraded via photolysis (photochemical decomposition) under simulated solar illumination (provided by a halogen lamp) for one hour. Hence, acetaminophen is fairly stable to light. Indeed, Aguilar *et al*. (2011) showed that purely photochemical decomposition of acetaminophen is less than 10%. Yang *et al*. (2008) found that photolysis of acetaminophen was negligible under UVA irradiation. Adsorption of acetaminophen onto $ZnFe_2O_4$-TiO_2 in the absence of light resulted in 35% removal of acetaminophen from its aqueous solution (Figure 4.7). This result implied that, under the experimental conditions employed, at equilibrium only 35% of acetaminophen was adsorbed on the surface of $ZnFe_2O_4$-TiO_2. As shown in Figure 4.7, 88% of acetaminophen was degraded by $ZnFe_2O_4$-TiO_2 under visible light illumination. Therefore, photocatalytic degradation of acetaminophen under visible light illumination is an efficient process.

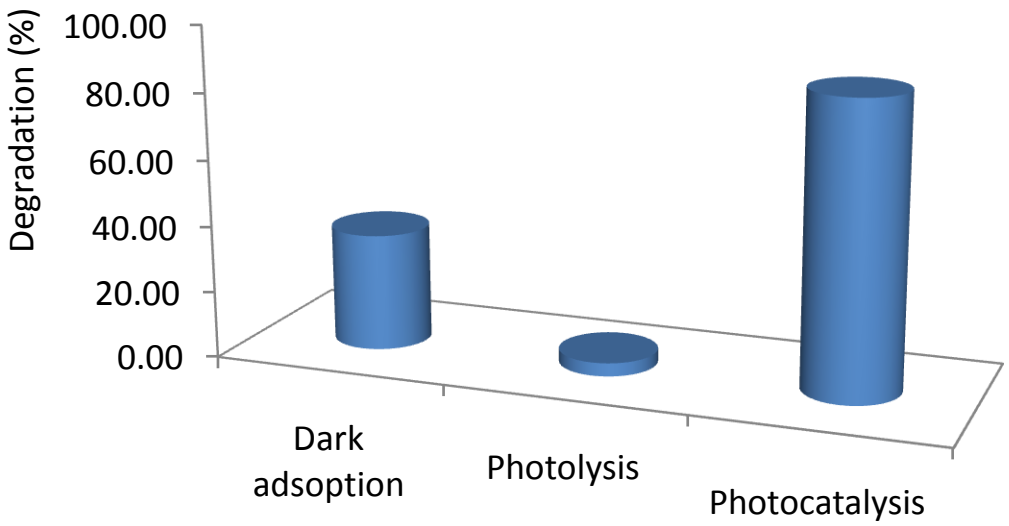

Figure 4.7: Removal of acetaminophen from its aqueous solution via dark adsorption, photolysis and photocatalysis.

4.4 Kinetics of photocatalytic degradation of acetaminophen

The pseudo first order kinetic plots for the photocatalytic degradation of acetaminophen using $ZnFe_2O_4$-TiO_2 composite at 10 mg/L initial concentration of acetaminophen shown in Figure 4.8. The results showed that the reaction kinetics could be fitted acceptably with pseudo first-order reaction kinetics with R^2 of 0.940. The value of the apparent rate constants (k_{app}) derived from Figure 4.10 was 0.023 min^{-1}. Similar kinetic behavior was observed by Gotostos *et al.* (2014) for the photocatalytic degradation of acetaminophen using $K_3[Fe(CN)_6]/TiO_2$ as the photocatalyst under visible light irradiation. For example, k_{app} was found to be 0.00749 min^{-1} for the photocatalytic degradation of acetaminophen using $K_3[Fe(CN)_6]/TiO_2$ under visible light irradiation (Gotostos *et al.*, 2014); this value of k_{app} is much smaller than the k_{app} value obtained in the present work. Therefore, there is

significant potential of $ZnFe_2O_4$-TiO_2 as a photocatalyst for the degradation of acetaminophen.

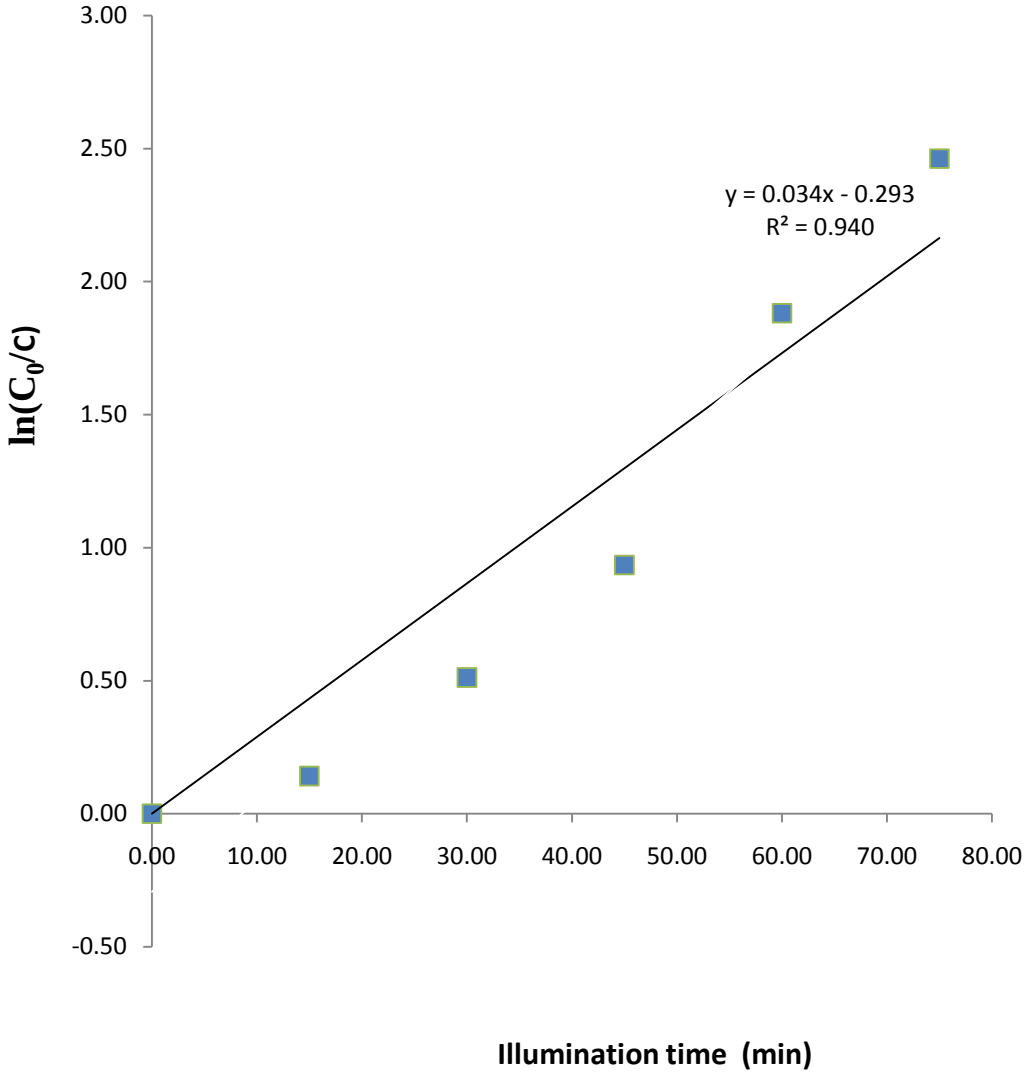

Figure 4.8: Pseudo first order kinetic plot for the photocatalytic degradation of acetaminophen using $ZnFe_2O_4$-TiO_2 at initial concentration of acetaminophen of 10 mg/L

4.5 Modeling of photocatalytic degradation and mineralization of acetaminophen

Photocatalytic degradation and mineralization of acetaminophen were conducted batch wise according to a statistical design of experiments using the central composite design as implemented in Design Expert software package. The designed experiments (Tables 4.4 and 4.5) were used to obtain model equations of the process, and also to obtain optimum process conditions at which photocatalyst consumption was minimal with corresponding high photocatalytic degradation and mineralization of acetaminophen in water. The dependent variables (responses) of the process were: the photocatalytic degradation and the photocatalytic mineralization. The independent variables namely initial concentration of acetaminophen (mg/L), photocatalyst dosage (g/L) and irradiation time (min) were represented by A, B and C, respectively. These variables were studied, their effects on the response analysed and the parameters were estimated by the method of least squares. The developed quadratic model equations in terms of the actual factors are represented by Equations 4.1 and 4.2.

Photocatalytic degradation $= -15.69 + 13.49 \times A + 43.0 \times B + 0.76C - 0.56 \times A^2 - 28.79 \times B^2 - 0.01C^2 - 1.49 \times AB - 0.06 \times AC + 0.31 \times BC$

(4.1)

Photocatalytic Mineralization $= -6.92 + 11.59 \times A + 22.09 \times B + 1.39 \times C - 0.52 \times A^2 - 0.07B^2 - 0.02 \times C^2 - 40 \times AB + 0.02 \times AC - 0.17 \times B$

(4.2)

Proper approximation of the true system can only be achieved with a valid model. Thus,

model adequacy check is necessary to validate the approximations and ensure that none of the least square regression assumptions are violated (Tekin *et al*., 2006).To assert the suitability of the proposed model for navigating the design space in terms of photocatalytic degradation and mineralization, a model adequacy test was conducted. The results of ANOVA for the models for percentage photocatalytic degradation and mineralization are presented in Tables 4.6 and 4.7, respectively.

Table 4.4: Design matrix with values of experimental responses for photocatalytic degradation of acetaminophen

Run	Independent variables			Response
	A	B	C	Photocatalytic degradation (%)
1	11.40	0.55	37.50	91.24
2	0.3	0.55	37.5	47.33
3	4.8	1.0	15	56.79
4	11.40	0.55	-0.34	71.13
5	4.8	0.1	60	40.77
6	18.0	0.1	15	56.36
7	18.0	1.0	15	46.85
8	11.4	0.55	75	83.48
9	4.8	1.0	60	72.84
10	11.4	1.31	37.5	78.18
11	11.4	0.55	37.5	90.14
12	18.0	0.1	60	56.12
13	18	1.0	60	58.76

14	11.4	-0.21	37.5	87.59
15	22.5	0.55	37.5	18.98
16	11.4	0.55	37.5	90.17
17	11.4	0.55	37.5	91.5
18	11.4	0.55	37.5	90.00
19	11.4	0.55	37.5	90.98
20	4.8	0.1	15	48.86

Table 4.5: Design matrix with values of experimental responses for photocatalytic mineralization of acetaminophen

Run	Independent variables			Response
	A	B	C	Photocatalytic mineralization (%)
1	11.40	0.55	37.50	62.96
2	0.3	0.55	37.5	96.29
3	4.8	1.0	15	75.00
4	11.40	0.55	-0.34	92.86
5	4.8	0.1	60	64.58
6	18.0	0.1	15	90.91
7	18.0	1.0	15	73.68
8	11.4	0.55	75	68.42
9	4.8	1.0	60	96.00
10	11.4	1.31	37.5	78.26
11	11.4	0.55	37.5	41.38

12	18.0	0.1	60	49.23
13	18	1.0	60	58.18
14	11.4	-0.21	37.5	23.65
15	22.5	0.55	37.5	95.65
16	11.4	0.55	37.5	58.49
17	11.4	0.55	37.5	33.33
18	11.4	0.55	37.5	65.45
19	11.4	0.55	37.5	93.10
20	4.8	0.1	15	81.82

Table 4.6: Analysis of variance and lack-of-fit test for response surface quadratic model of photocatalytic degradation of acetaminophen using $ZnFe_2O_4$-TiO_2 composite

Source	Sum of Squares	DF	Mean Square	F Value	Prob > F	Remarks
Model	7086.10	9	787.34	1874.74	<	0.0001 significant
A	14.02	1	14.02	33.37	0.0007	
B	34.79	1	34.79	82.83	< 0.0001	
C	139.61	1	139.61	332.43	< 0.0001	
A^2	3704.67	1	3704.67	8821.17	< 0.0001	
B^2	214.92	1	214.92	511.74	< 0.0001	
C^2	288.17	1	288.17	686.16	< 0.0001	
AB	91.93	1	91.93	218.88	< 0.0001	
AC	4.43	1	4.43	10.56	0.0141	

BC	45.18	1	45.18	107.57	< 0.0001	
Residual	2.94	7	0.42			
Lack of Fit	0.85	2	0.43	1.02	0.4260	not significant
Pure Error	2.09	5	0.42			
Cor Total	7089.04	16				

$R^2 = 0.999$; $R^2_{adj} = 0.9741$

Table 4.7: Analysis of variance and lack-of-fit test for response surface quadratic model of photocatalytic mineralization of acetaminophen using $ZnFe_2O_4$-TiO_2 composite

Source	Sum of Squares	DF	Mean Square	F Value	Prob > F	Remark
Model	7150.15	9	794.46	99.80	< 0.0001	significant
A	191.25	1	191.25	24.02	0.0027	
B	125.92	1	125.92	15.82	0.0073	
C	144.91	1	144.91	18.20	0.0053	
A^2	6086.33	1	6086.33	764.54	< 0.0001	
B^2	0.0006	1	0.0002	0.0001	0.9935	
C^2	685.60	1	685.60	86.12	< 0.0001	
AB	7.13	1	7.13	0.90	0.3804	

AC	0.25	1	0.25	0.031	0.8662	
BC	16.14	1	16.14	2.03	0.2043	
Residual	47.76	6	7.96			
Lack of Fit	28.42	2	14.21	2.94	0.1640	not significant
Pure Error	19.34	4	4.84			
Cor Total	7197.91	15				

R^2 = 0.993; R^2_{adj} = 0.984

From the ANOVA results obtained for photocatalytic degradation of acetaminophen presented in Table 4.6, the model obtained was significant for the photocatalytic degradation of the acetaminophen as the percentage degradation has an F-value of 1874.74 implied the model was significant. P-values less than 0.05 indicate that, the model is significant whereas greater than 0.10 indicates model not significant; with a value of 0.001 the model adequacy fit was ascertained. There was only a 0.01% chance that a "Model F-Value" this large (1874.74) could occur due to noise. In this case A, B, C, A^2 and C^2 are significant model terms. The "Lack of Fit F-value" of 1.02 implies the Lack of Fit is not significant relative to the pure error. There is a 42.60% chance that a "Lack of Fit F-value" this large (1.02) could occur due to noise. Non-significant lack of fit is good. The non significant lack of fit indicates good predictability of the model (Sakkas *et al.*, 2009).

The value of 0.999 for the correlation coefficient of the model (R^2) indicated that, there was

a satisfactory quadratic fit as it implied that 99% of the total variation in photocatalytic degradation reported was adequately represented by the model. Although, R^2 reasonably predicts model adequately fairly well but having a high value of R^2 does not necessarily imply a very good prediction. This was associated with the fact that, there exists the possibility of having poor predictions of new observations or estimates of the mean response, thus, a modified form of the R^2 referred to as R^2_{adj} was employed. Values of R^2 are always higher than or equal to R^2_{adj} because the R^2a_{dj} adjusts the number of explanatory terms in a model thus, it can have a negative value. Merit of the former parameter over the latter is that, while addition of variables to the model always results in an increase in R^2 value, it was significantly not affected in R^2_{adj} it is often reported to decrease if unnecessary terms are added. Based on closeness of correlation coefficient values of 0.999 and 0.971 for R^2 and R^2_{adj}, respectively, it showed that the experimental data fitted the model fairly well and signified non-inclusion of insignificant terms. "Adeq Precision" measures the signal to noise ratio.

A ratio greater than 4 is desirable. Ratio of 143.419 indicates an adequate signal. This model can be used to navigate the design space (Montgomery, 2009).

Thus likewise from ANOVA results obtained for photocatalytic mineralization of acetaminophen as shown in Table 4.7 the obtained model was significant for the photocatalytic mineralization of the acetaminophen as the percentage mineralization has an F-value of 99.80 implied the model is significant. There was only a 0.01% chance that a "Model F-Value" this large (99.80) could occur due to noise. In this case A, B, C, A^2 and C^2 are significant model terms which signifies that the P-values were less than 0.05. The value of 0.993 for the correlation coefficient of the model (R^2) indicated that, there was a satisfactory quadratic fit as it implied that 99% of the total variation in Photocatalytic

mineralization reported was adequately represented by the model. Based on closeness of correlation coefficient values of 0.993 and 0.984 for R^2 and R^2_{adj}, respectively, it showed that the experimental data fitted the model fairly well and signified non-inclusion of insignificant terms. "Adeq Precision" of 32.504 indicates an adequate signal, considering the fact that an adequate precision ratio of greater than 4 is desirable.

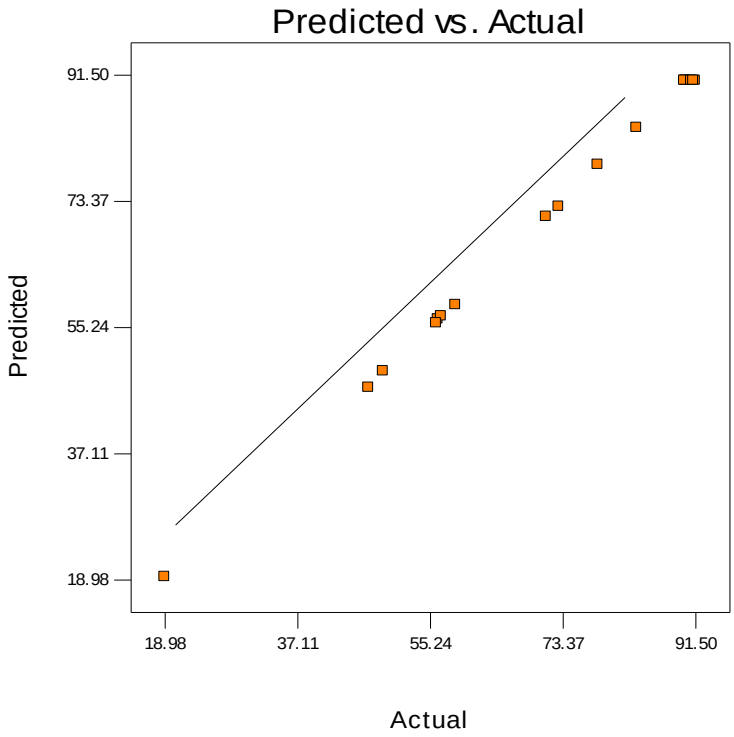

Figure 4.9: Plot of actual vs predicted values of photocatalytic degradation of acetaminophen using $ZnFe_2O_4$-TiO_2 composite

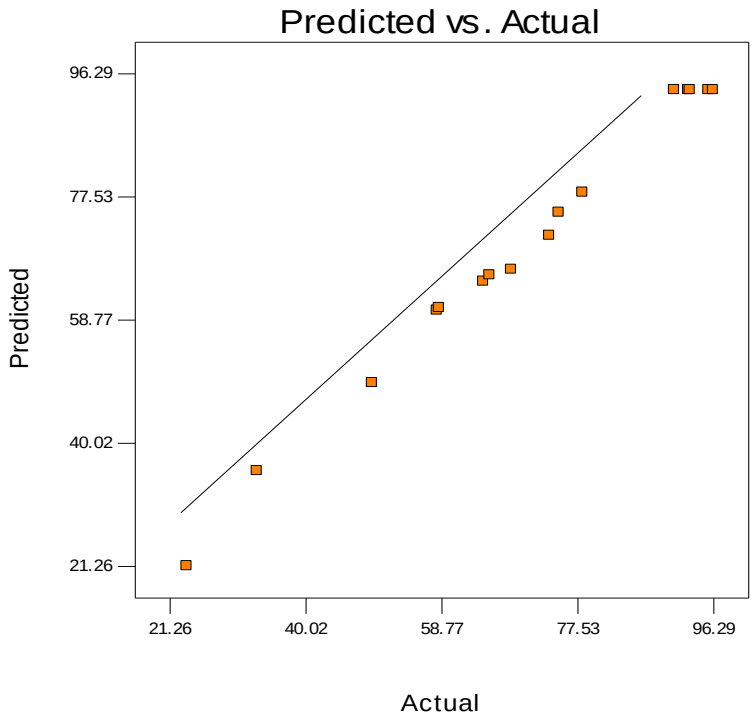

Figure 4.10: Plot of actual vs predicted values of photocatalytic mineralization of acetaminophen using $ZnFe_2O_4$-TiO_2 composite

In Figures 4.9 and 4.10, studentized residuals against predicted photocatalytic degradation and mineralization respectively were depicted and clearly indicate the lack of need for transformation. The random scattering of the points instead of funnel-shaped pattern sometimes observed suggested that, the variance of original observations to be a constant for all values of the response (Myers and Montgomery, 2002; Montgomery, 2009). Experimentally determined responses (actual values) were plotted against responses obtained from the developed approximating function (predicted values). The plot (Figures 4.9 and 4.10) showed that, there was a good agreement between the two set of results thus, validating the model's reliability under the independent variables investigated. Finally, the number of standard deviations of the actual value deviates from the predicted value was determined from the outlier plot (Figures 4.11 and 4.12) for the photocatalytic degradation and mineralization. The outliers (data points that lied far away from the true regression

line) need to be assessed as they can be used to determine data recording error or region of the independent factor variable space where the fitted model is a poor approximation to the true response surface (Montgomery, 2009).

Furthermore, for the photocatalytic degradation and mineralization, the model equation were obtained using the least squares method, the slope and intercept which are sensitive to outliers thus, estimates of regression coefficients can be distorted. From the outlier plot, it was shown that all the standardized residual were within the range of ±3.50 interval. This showed that, the model approximation of the response surface was satisfactory and not associated with data recording error.

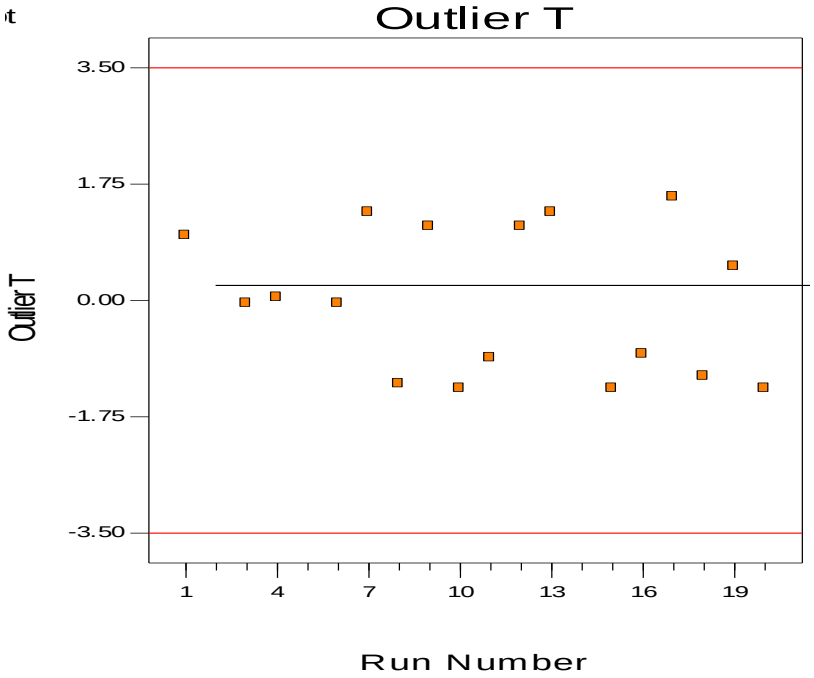

Figure 4.11: The outlier plot of photocatalytic degradation of acetaminophen using $ZnFe_2O_4$-TiO_2 composite

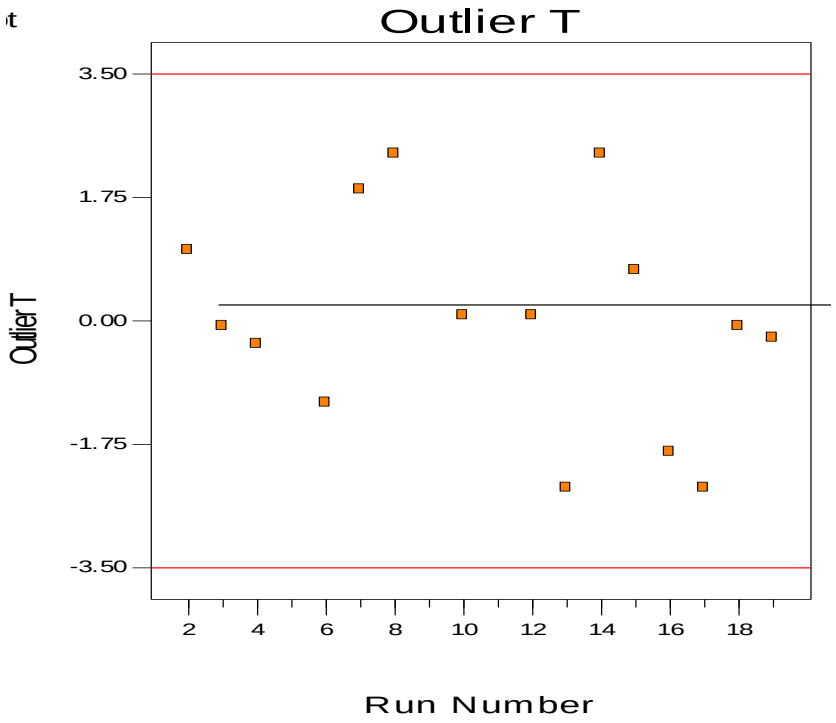

Figure 4.12: The outlier plot of photocatalytic mineralization of acetaminophen using $ZnFe_2O_4$-TiO_2 composite

4.5.1 Effects of photocatalyst dosage and initial concetration of acetaminophen photocatalytic degradation and mineralization of acetaminophen

The 3D interactive effect of catalyst dosage and initial concentration were shown in Figures 4.13 and 4.14 for photocatalytic degradation and mineralization of acetaminophen, respectively. It is seen that the percentage degradation increased with increase in the photocatalyst dosage. The photocatalytic degradation efficiency was found to increase (≥ 86%) with increase in catalyst dosage (0.55 g/L) after which the efficiency decreased (≤ 70%). Figure 4.14 showed that an increase in the concentration of photocatalyst is reflected in the conversion rate to a limit of 0.55 g/L beyond 0.55 g/L, a decrease in degradation was observed. The right amount of photocatalyst is very important in a photocatalytic process (Dalrymple *et al*., 2007). (If a small amount of catalyst is used for

the photocatalytic experiments, there will not be enough generation of •OH radicals on the active sites for degradation and mineralization of the organic pollutant). (On the other hand, if the amount of catalyst is larger than needed, the excess of solid particles does not allow the light to penetrate the solution and activate the surface of the catalyst, thus reducing the generation of active sites and the reaction rate). When the initial concentration of acetaminophen increased from 4.8 to 14.7 mg/L, the degradation and mineralization rate was maintained at a high level. The finding revealed that the degradation and mineralization reaction rate decreased with increasing initial concentration of acetaminophen. This is attributed to the fact that the production of radicals and holes remained constant for a given dosage of photocatalyst. Under the same conditions, the amount of radicals and holes produced by the catalyst is sufficient for the degradation and mineralization of acetaminophen until the concentration of acetaminophen reaches 14.7 mg/L. Thus at higher initial concentration, acetaminophen molecules absorbed additional photons. Consequently, this decreased available photons to activate the catalyst (Chang *et al*., 2015).

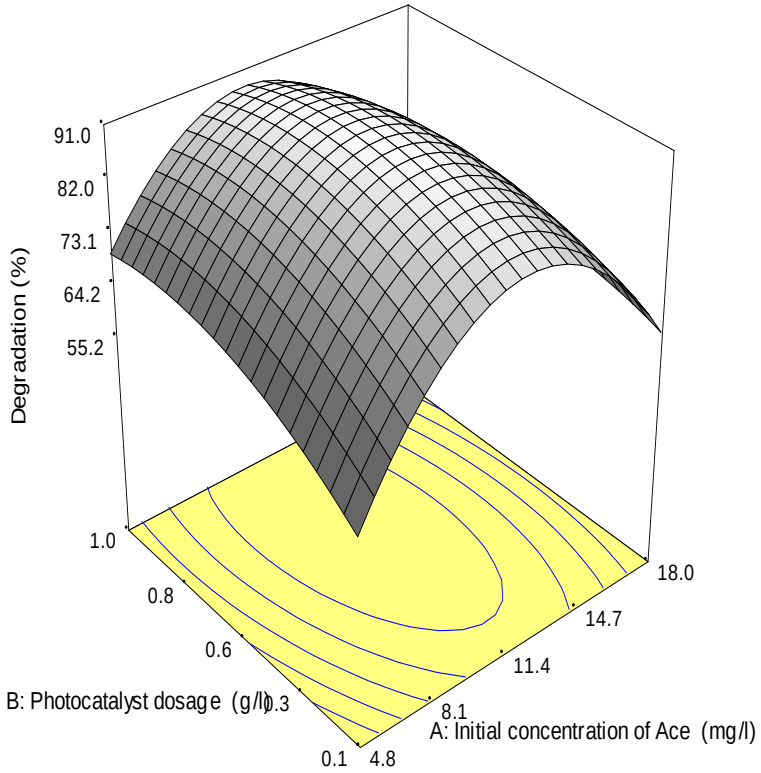

Figure 4.13: 3D response surface plot for photocatalytic degradation of acetaminophen showing the simultaneous influence of photocatalyst dosage and initial concetration of acetaminophen

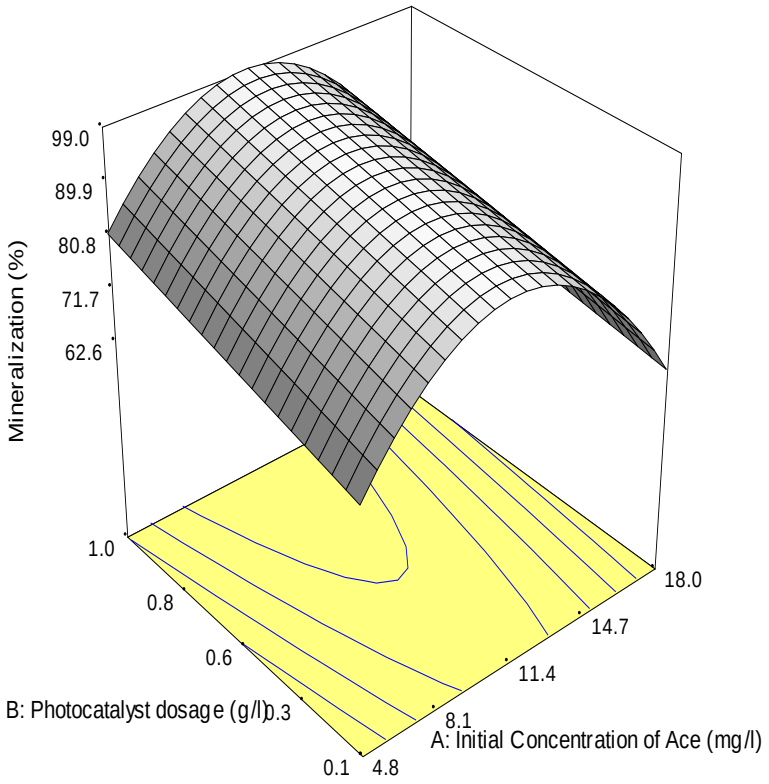

Figure 4.14: 3D response surface plot for photocatalytic mineralization of acetaminophen showing the simultaneous influence of photocatalyst dosage and initial concetration of acetaminophen

4.5.2 Effects of irradiation time and initial concentration photocatalytic degradation and mineralization of acetaminophen

The 3D interactive effects of catalyst dosage and irradiation time were shown in Figures 4.15 and 4.16. The effects of irradiation time of acetaminophen on the photocatalyst degradation and mineralization were studied by varying its irradiation time from 15 to 60 min. Photocatalytic degradation and mineralization of acetaminophen increased with increase in irradiation time. The effect of initial concentration of acetaminophen on the

photocatalyst degradation and mineralization was also studied by varying its initial concentration from 4.8 to 18 mg/L. The finding revealed that the degradation and mineralization reaction rate decreased with increasing initial concentration of acetaminophen. When the initial concentration of acetaminophen was increased from 4.8 to 11.4 mg/L, the degradation and mineralization rate was maintained at a high level (≥ 90.4%). This was attributed to the fact that the production of radicals and holes remained constant for a given dosage of photocatalyst. Under the same optimum conditions, the amount of radicals and holes produced by the catalyst is sufficient for the degradation and mineralization of acetaminophen until the concentration of acetaminophen reaches 14.7 mg/L. Thus at higher initial concentration, acetaminophen molecules absorbed additional photons. Consequently, this decreased available photons to activate the catalyst (Chang *et al*., 2015).

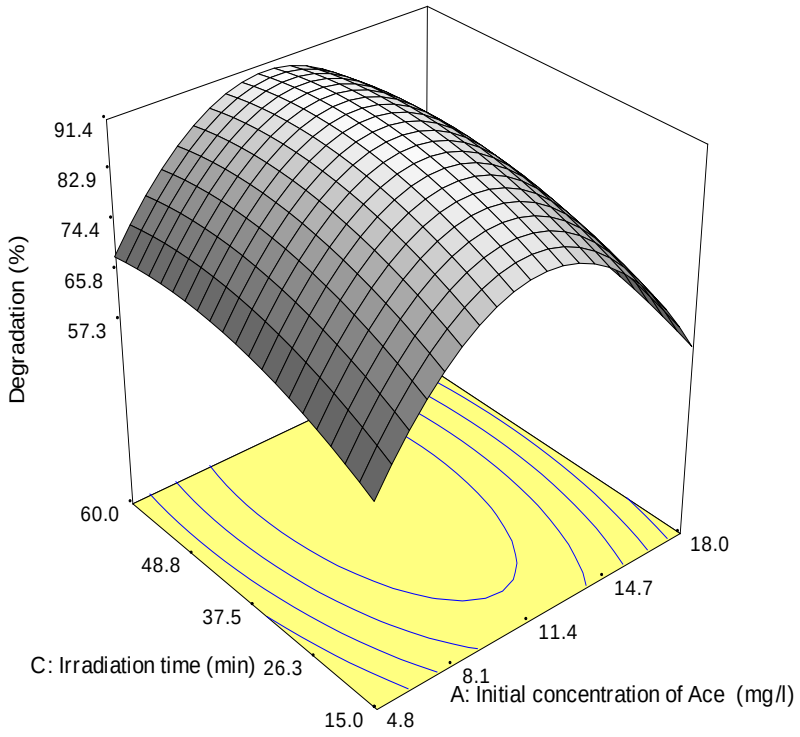

Figure 4.15: 3D response surface plot for photocatalytic degradation of acetaminophen showing the simultaneous influence of irradiation time and initial concetration of acetaminophen

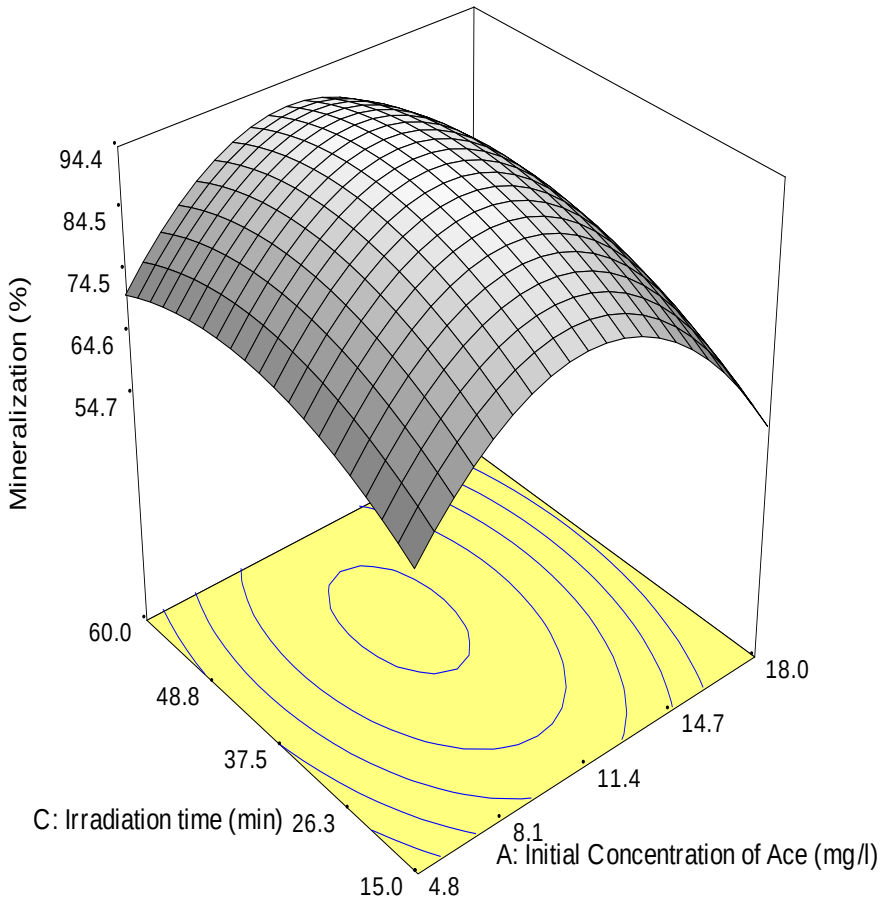

Figure 4.16: 3D response surface plot for photocatalytic mineralization of acetaminophen showing the simultaneous influence of irradiation time and initial concetration of acetaminophen

4.5.3 Effects of photocatalyst dosage and irradiation time on photocatalytic degradation of acetaminophen

The 3D interactive effects of catalyst dosage and irradiation time were shown in Figures 4.17 and 4.18. Different catalyst dosages ranging from 0.1 to 1.0 g/L were used. It was shown that the percentage degradation increased (≥ 90%) with increase in catalyst dosage. The photocatalytic degradation efficiency was found to increase with increase in the

catalyst dosage (0.55 g/L) after which the efficiency decreased (≤ 80%). Figure 4.17 showed that an increase in the catalyst dosage is reflected in the conversion rate to a limit of 0.55 g/L; beyond 0.55 g/L a decrease in the degradation was observed. The right amount of catalysts is very important in a photocatalytic reaction (Dalrymple *et al*., 2007). (If a small amount of catalyst is used for the photocatalytic experiments, there will not be enough generation of •OH radicals on the active sites for degradation and mineralization of the organic pollutant). (On the other hand, if the amount of catalyst is larger than needed, the excess of solid particles does not allow the light to penetrate the solution and activate the surface of the catalyst, thus reducing the generation of active sites and the reaction rate), there will not be enough generation of •OH radicals on the active sites for mineralization of the organic pollutant. In addition the percentage mineralization increases (≥ 79.9%) as the irradiation time increased from 15 min to 60 min. Thus the catalyst dosage had little effect on mineralization of acetaminophen.

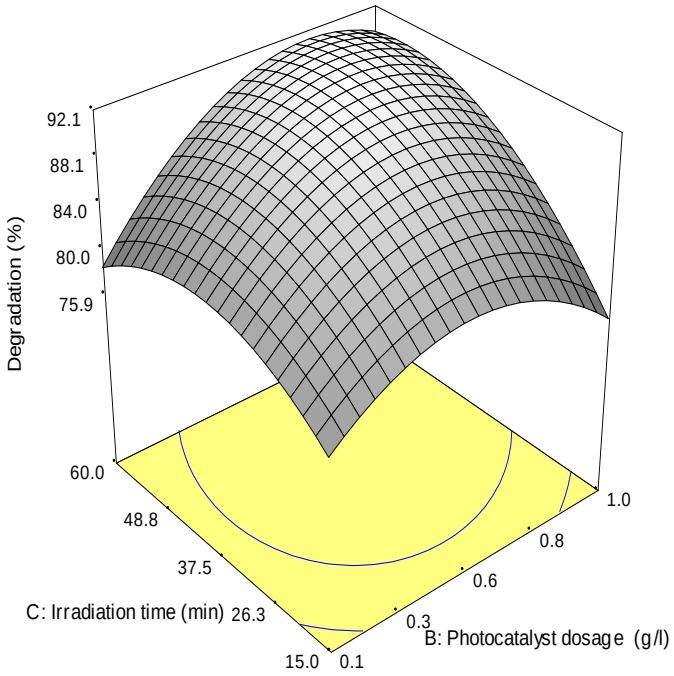

Figure 4.17: 3D response surface plot for photocatalytic degradation of acetaminophen showing the simultaneous influence of photocatalyst dosage and irradiation time

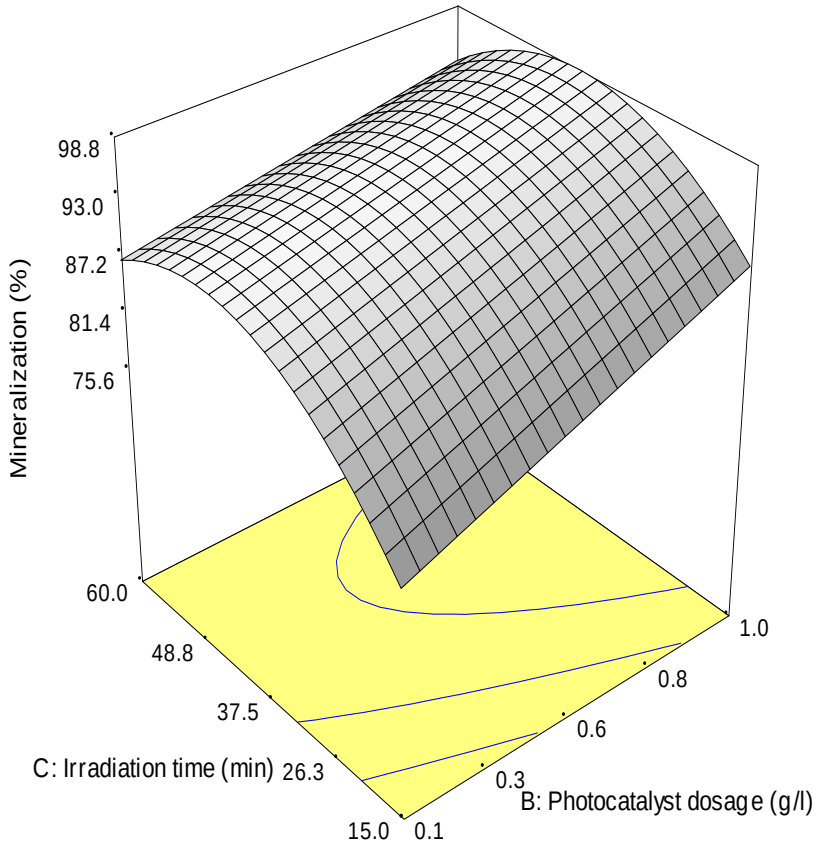

Figure 4.18: 3D response surface plot for photocatalytic mineralization of acetaminophen showing the simultaneous influence of photocatalyst dosage and irradiation time

4.6 Optimization of Photocatalytic Degradation and Mineralization of Acetaminophen

The experimental results were presented in Tables 4.8 and 4.9. From where it was shown that the results were very close with data obtained from optimization analysis using the desirability function, indicating that CCD design in combination with desirability function could be effectively used to optimize photocatalytic degradation and mineralization of acetaminophen using $ZnFe_2O_4$-TiO_2 composite.

Table 4.8: Experimental and predicted values for the photocatalytic degradation of acetaminophen using the $ZnFe_2O_4$-TiO_2 composite under the predicted optimum values of the process variables

Process variables	Predicted optimum conditions	Degradation (%)		% Deviation
		Experimental	Predicted	
Initial concentration of acetaminophen (mg/L)	11.0	90.9	91.5	0.6
Photocatalyst dosage (g/L)	0.60			
Irradiation time (min)	42.0			

Table 4.9: Experimental and predicted values for the photocatalytic mineralization of acetaminophen using the $ZnFe_2O_4$-TiO_2 composite under the predicted optimum values of the process variables

Process variables	Predicted optimum conditions	Degradation (%)		% Deviation
		Experimental	Predicted	

Initial concentration of acetaminophen (mg/L)	11.2	95.9	96.4	0.5
Photocatalyst dosage (g/L)	1.0			
Irradiation time (min)	28.7			

CHAPTER FIVE

CONCLUSIONS AND RECOMMENDATIONS

5.1 Conclusions

The following conclusions could be drawn from the work

1. The prepared $ZnFe_2O_4$-TiO_2 composite is crystalline and exhibits a compact arrangement of particles with roughly irregular shape.
2. Adsorption of acetaminophen in the dark onto the $ZnFe_2O_4$-TiO_2 composite obeys pseudo second-order kinetic model with R^2 of 0.99 and the Langmuir isotherm model with R^2 of 0.979. The maximum adsorption capacity of the $ZnFe_2O_4$-TiO_2 composite is 26.88 mg g^{-1}.
3. The percentage removal of acetaminophen via adsorption in the dark, photolysis (irradiation with visible light) and photocatalysis are 35%, 4% and 88%, respectively.
4. The kinetics of photocatalytic degradation of acetaminophen under visible light irradiation using the $ZnFe_2O_4$-TiO_2 composite follows pseudo-first order with R^2 of 0.94 approximation of the Langmuir-Hinshelwood kinetic model.
5. Quadratic model equations that adequately describe photocatalytic degradation and mineralization of acetaminophen were developed. The significant photocatalytic

process parameters are: initial concentration of acetaminophen, dosage of $ZnFe_2O_4$-TiO_2 composite and irradiation time.

6. The predicted optimum conditions for photocatalytic degradation of acetaminophen are initial acetaminophen concentration of 11.0 mg/L, photocatalyst dosage of 0.6 g/L and irradiation time of 42.0 min. The predicted optimum conditions for photocatalytic mineralization of acetaminophen are initial acetaminophen concentration of 11.2 mg/L, photocatalyst dosage of 1.0 g/L and irradiation time of 28.7 min. Under the predicted optimum conditions, photocatalytic degradation and mineralization of acetaminophen are 91.5% and 96.29% respectively. The experimental photocatalytic degradation and mineralization of acetaminophen are 90.9% and 95.9 %, respectively.

5.2 Recommendations

1. Optimization of the $ZnFe_2O_4$ to TiO_2 ratio in the composite.
2. Reusability of the composite should be studied.
3. Further research work should be carried out to design a pilot plant for the photocatalytic mineralization of acetaminophen using $ZnFe_2O_4$-TiO_2 composite.
4. Economic analyses for the photocatalytic degradation of organic pollutants using $ZnFe_2O_4$-TiO_2 composite should be carried out.

REFERENCES

Aguilar, C.A., Montalvo, C., Ceron, J.G., and Moctezuma, E**.** (2011). Photocatalytic Degradation of Acetaminophen. *International Journal of Environmental Resource,* 5(4):1071-1078.

Ahmed, S., Rasul, M.G., Martens, W.N., Brown, R., and Hashib, M.A. (2010). Heterogeneous Photocatalytic Degradation of Phenol in Wastewater: A review on current status and developments. *Desalination*, 26(1): 3-18.

Alfano, O. M., Bahnemann, D., Cassano, A. E., Dilert, R., and Goslich, R. (2000). Photocatalysis in Water Environments Using Artificial and Solar Light. *Catalyst Today,* 58(2): 199-230.

Andreozzi, R., Canterino, M., Giudice, R., Marotta, R., Pinto, G., and Pollio, A. (2006). Lincomycin Solar Photo Degradation, Algal Toxicity and Removal from Wastewaters by Means of Ozonation. *Water Resource,* 40(3): 630-638.

Andreozzi, R., Canterino, M., Marotta, R., and Paxeus, N. (2005). Antibiotic Removal from Wastewaters: The Ozonation of Amoxicillin. *Journal of Hazard Material*, 122(3):

243-250.

Annesini, M., Gironi, F., Ruzzi, M., and Tomei, C. (1987). Adsorption of organic Compounds onto Activated Carbon. *Water Resource*, 21(5): 567-571.

Araña, J., Herrera Melián, J., Doña Rodríguez, J., González Díaz, O., Viera, A., Pérez Peña, J., Marrero Sosa, P., Espino Jiménez, V. (2002). TiO_2-Photocatalysis as a Tertiary Treatment of Naturally Treated Wastewater. *Catalyst Today*: 76 (2-4): 279-289

Arcand-Hoy, L.D., Nimrod, A.C., Benson, W.H. (1998) Endocrine Modulating Substances in the Environment Estrogenic Effects of Pharmaceutical Products. *Internetional Journal of Toxicology*, 17(2): 139–158.

Balcioglu, I, Ötker, M., (2003). Treatment of Pharmaceutical Wastewater Containing Antibiotics by O_3 and O_3/H_2O_2 Processes. *Chemosphere*, 50 (1): 85-95.

Bellona, C. and Drewes, J. (2007). Viability of a Low-Pressure Nanofliter in Treating Recycled Water for Water Reuse Applications: A Pilot-Scale Study. *Water Resource*, 41 (17): 3948–3958.

Braeken, L., Ramaekers, R., Zhang, Y., Maes, G., Van Der Bruggen, B., and Vandecasteele, C. (2005). Influence of Hydrophobicity on Retention in Nanofiltration of Aqueous Solutions Containing Organic Compounds. *Journal of Membrane. Science*, 252 (1–2):

195–203.

Brahimi, R., Bessekhouad, Y., Bouguelia, A., Trari, M. (2007). Photo-Fenton Degradation of

Diclofenac: Identification of Main Intermediates and Degradation Pathway. *Catalysis Today* 122 62.

Bräuer, G. (2009). Technology Guide, H.-J. Bullinger. (Ed.) *Surface and coating*

technologies Springer.

Bruce.G.M., Pleus R.C. and Snyder, S.A. (2010). Kinetic Study of Acetaminophen Degradation by visible light Photocatalysis. *Environment Science Technology*, 44: 56-19.

Burdett, J. K., Hughbanks, T., Miller, G. J., Richardson J. W., and Smith J. V. Photo-Dechlorination of PCBs in presence of Titanium-Dioxide in Aqueous Suspensions. *B. Environmental Contamination Toxicity,* 16 (6): 697-701

Carballa, M., Omil, F., Lema, J.M., Llompart, M., Garcia-Jares, C., Rodriguez, I., Gomez, M.,Carp, O., Huisman, C.L., Reller, A. (2004). Photoinduced Reactivity of Titanium Dioxide. *Progress Solid State Chemistry,* 32 (1–2): 33–177.

Carp.O., Huisman, C., and Reller, A. (2004) The Photocatalytic process as a tool to identify metabolitic products formed from dopant substances. *Progress in Solid State Chemistry* 32(1–2):33–177.

Castiglioni, S., Bagnati, R., Fanelli, R., Pomati, F., Calamari, D., Zuccato, E. (2006). Removal of Pharmaceuticals in Sewage Treatment Plants in Italy. *Environmental Science Technology,* 40 (1): 357- 363.

Chang, C., Chang, J., Vigneswaran, S., Kandasamy, J. (2008). Pharmaceutical wastewater treatment by membrane bioreactor process: A Case Study in Southern Taiwan. *Desalination*, 234 (1-3): 386-392.

Chelliapan, S., Wilby, T., Sallis, P. (2006). Performance of an up-flow anaerobic stage reactor (UASR) in the treatment of pharmaceutical wastewater containing macrolide
antibiotics. *Water Resources,* 40 (3): 507-516.

Chen , Z., Nanqi, R., Wang, A., Zang, Z., Shi, Y. (2008). A novel application of TPAD-MBR system to the pilot treatment of chemical synthesis based wastewater. *Water*

Resources, 42 (13): 3385-3392.

Cheng, P., Li, W., Liu, H., Gu, M., and Shangguah, W. (2004). Influence of zinc ferrite doping on the optical properties and phase transformation of titania powders prepared by sol–gel method, *Materials Science and Engineering: A*, 386: 43-47.

Chien, S.H., and Clayton W.R. (1980). Application of Elovich equation to the kinetics of phosphate release and sorption in soils. *Soil Science Society Journal*, 44: 265-268.

Choi, W., Termin A., Hoffmann M.R. (1994). Evaluation of a novel Carberry type photoreactor for the degradation of organic pollutants in water. *Journal of Physical Chemistry*, 98:13669-13679.

Chong, M.N., Jin, B., Chow, C.W.K., Saint, C. (2010). Recent developments in photocatalytic water treatment technology: a review, *Water Resources*. 44: 2997–3027.

Chun, H., Yizhong, W. (1999). Decolorization and biodegradability of photocatalytic treated azo dyes and wool textile wastewater. *Chemosphere* 39: 2107.

Corey, E.J., Czakó, B., Kürti, L.(2007). Molecules and Medicine, John Wiley & Sons, NewJersey, USA.

Crane.M,, Watts, C., and Boucard, T. (2006). Large scale studies in solar catalytic wastewater treatment. *Science of the Total Environment*, 367: 23

Dantes, R., Contreras, S., Sans, C., Esplugas, S. (2008). Sulfamethoxazole abatement by means of ozonation. *Journal of Hazardous Material*, 150 (3): 790–794.

El Gohary, F., Abou-Elea, S. (1995). Evaluation of biological technologies for wastewater

treatment in the pharmaceutical industry. *Water Science Technology*, 32(11): 13-20 (8
pages).

Enright, A., McHugh, S., Collins, G., O'Flaherty, V. (2005). Low-temperature anaerobic biological treatment of solvent containing pharmaceutical wastewater. *Water Resources*, 39 (19): 4587-4596.

Feng,J., Wang, Y., Zou, L., Li, B., He, X., Ren, Y., Lv, Y., Fan, Z. (2014). Synthesis of Magnetic ZnO/$ZnFe_2O_4$ by a Microwave Combustion Method, and Its High Rate of Adsorption of Methylene Blue. *Journal of Colloid and Interface Science* S0021-9797(14)00762-0, doi: http://dx.doi.org/10.1016/j.jcis.2014.10.009

Fountoulakis, M., Stamatelatou, K., Lyberatos, G. (2008). The effect of pharmaceuticals on the kinetics of methanogenesis and acetogenesis. *Bioresource Technology*, 99 (15): 7083-7090.

Fujishima, A. and Honda, K. (1972)."Electrochemical Photolysis of Water at a Semiconductor Electrode." *Nature*, 238: 37-38.

Fujishima, A. and Rao, T. (1997). "Recent advances in heterogeneous TiO_2 photocatalysis." *Journal of Chemical Sciences*, 109: 471-486.

Fujishima, A., Rao, T. N. and Tryk, D. A. (2000). Titanium dioxide photocatalysis. *Journal of Photochemical Chemistry*, 1 (1):1- 21.

Gangagni Rao, A., Venkata Naidu, G., Krishna Prasad, K., Chandrasekhar Rao, N., Venkata Mohan, S., Jetty, A., Sarma P. (2005). Anaerobic treatment of wastewater with high suspended solids from a bulk drug industry using fixed film reactor (AFFR). *Bioresource Technology*, 96(1): 87-93.

Gotostos Mary Jane N., Chia-Chi Su, Mark Daniel G. De luna & Ming-chun Lu (2014) Kinetic study of acetaminophen degradation by visible light photocatalysis. *Journal of Environmental Science and Health, Part A: Toxic/ Hazardous Substances and Environmental Engineering*, 49(8): 892-899, DOI: 10.1080/10934529.2014.894310

Halling-Sorensen.B., .Nielson.S.N., Lanzky P.F., Ingerslev.F., Holten Lutzhoft, S.E.Jorgensen. (2002). Heterogeneous photocatalysis: fundamentals and applications to the removal of various types of aqueous pollutants. *Chemosphere*, 35, 357.

Han, W.Y., Zhu, W.P., Zhang, P.Y., Zhang,Y. and Li, L.S. (2004). Photocatalytic degradation of phenols in aqueous solution under irradiation of 254 and 185 nm UV light. *Catalyst Today*, 90 (3-4): 319-324

Hanaor D.A., C. C. Sorrell., (2011) Removal of selected persistent organic pollutants by heterogeneous photocatalysis in water. *Journal of Materials Science*, 46: 855–874. Doi: http://dx.doi.org/10.1007/ 10853 -010-5113-0.

He, H.Y. (2008). Photo-catalytic Degradation of Methyl Orange in Water on CuS-Cu2S powders. *International Journal of Environmental Resources*, 2 (1): 23-26.

Ho.Y.S., and McKay, G. (1998). Kinetic models for the sorption of dye from aqueous solution by wood. *Process Safety Environmental Protection*, 76 (B2): 183-191.

Hrubec, J., Vankreijl, C., Orra, C. (1983). Treatment of Municipal Wastewater by Reverse-Osmosis and Activated- Carbon-Removal of Organic Micropollutants and Reduction of Toxicity. *Science Total Environment*, 27 (1): 71-88.

Ikehata, K., Naghashkar, N., El-Din, M. (2006). Degradation of Aqueous Pharmaceuticals

by Ozonation and Advanced Oxidation Processes: *A Review "Ozone-Science Engineering"* 28(6): 353-414.

Ileri, R., Sengil, I., Kulac, S., Damar, Y. (2003). Treatment of mixed pharmaceutical industry and domestic wastewater by sequencing batch reactor. *Journal Environmental Science Health*, 38 (10): 2101-2111.

Irie.H, Y., Watanabe, K., Hashimoto. (2003) Heterogeneous photoatalysis: state of the art and present applications. *Chemistry Letters* 32.

Stanley, J.K., Ramirez, A.J., Chambliss, C.K., Brooks, B.W. (2007). Efficacy of ultraviolet radiation and hydrogen peroxide oxidation to eliminate large number of pharmaceutical compounds in mixed solution, *Chemosphere*, 69, 9.

Jina, Choi. (2010). *Development of visible-light-active photocatalyst for hydrogen production and environmental application.* Doctoral dissertation, California Institute of Technology, Pasadena, California.

Kabra, K., Chaudhary, R. and Sawhney, R. L. (2004). Treatment of hazardous organic and inorganic compounds through aqueous-phase photocatalysis: A review "Industrial Engineering". *Chemical Resource*, 43 (24): 7683-7696.

Khetan, S., Collins, T., (2007). Human Pharmaceuticals in the Aquatic Environment: A Challenge to Green Chemistry. *Chemistry Revised*, 107 (6), 2319-2364.

Kiril M.B., Yonar, T., Yalili Kiliç, M., Kestioglu, K. (2010). Pre-treatment studies on olive oil mill effluent using physicochemical Fenton and Fenton-like oxidations processes. *Journal of Hazardous Material*, 174: 122-128.

Konstantinou, I.K., Albanis, T.A., (2004). TiO_2-assisted photocatalytic degradation of azo dyes in aqueous solution: kinetic and mechanistic investigations. A review:

"Applied Catalysis". *B: Environment,* 49 (1): 1–14.

Kummerer, K.,(2004). Resistance in the environment. *Journal of Antimicrobial. Chemotheraphy,* 54 (2): 311– 320.

Langmuir.I. (1918). The adsorption of gases on plane surfaces of glass, mica and platinum. *Journal of Chemical Society,* 40: 1361-1403.

Laokul.P., Amornkitbamrung, V., Seraphin, S., Maensiri, S. (2011). *Current Applied Physics,* 11:101–108.

LaPara, T., Nakatsu, C., Pantea, L., Alleman, J. (2002). Stability of the bacterial communities supported by a seven-stage biological process treating pharmaceutical wastewater as revealed by PCR-DGGE. *Water Resources,* 36 (3): 638-646.

Largergren.S. (1898). Zur theorie der sogennanten adsorption geloster stoffe Kungliga Svenka Vetenskapsakademies, Handglingar 24: 1-39.

Larsson D.G.J., P.C.De, N.Paxéus. (2007). Transparency throughout the production chain-a way to reduce pollution from the manufacturing of pharmaceuticals. *Journal Hazardous Materials,* 148, 751

Li, X., Lu, G., and Li, S. (1996). Synthesis and characterization of fine particle $ZnFe_2O_4$ powder by a low temperature method. *Journal of Alloys and Compounds*, vol.235, pp. 150-155.

Li.X.Y., Hou ,Y., Zhao, Q.D., Teng, W., Hu, X.J., Chen, G.H. (2011). Photocatalytic degradation of methyl orange in a sparged tube reactor with TiO2-coated activated carbon composites. *Chemosphere,* 82: 581–586.

Marci.G., Augugliaro, V., Lopez-Mu˜noz, M.J., Martin, C., Palmisano, L., Rives, V., Schiavello, M., Tilley, R.J.D., Venezia, A.M. (2001). Decomposition of nonionic surfactant in a labyrinth flow photoreactor with immobilised TiO_2 bed. *Journal of Physical Chemistry,* 105 1026.

Monal, D., Uttiya, D., Saurav, M., Suparna B., Remanisha, K., and Ratan, B. (2015). Adsorption of acetaminophen by using tea waste derived activated carbon. *International journal of environmental sciences,* 6(2): 0976 – 4402.

Montgomery DC (2009). Design and Analysis of Experiments. 7th edition, John Wiley and Sons, New York.

Morikawa.T., Asahi, R., Ohwaki, T., Aoki, K., Taga, Y.(2011). Adsorption and desorption of atrazine on carbon nanotube. *Japanese Journal of Applied Catalysis*, 101: 382–387.

Myers R.H., Montgomery D.C. (2002). Response Surface Methodology: Process and Product Optimization Using Designed Experiments. 2nd ed., Wiley, New York.

Muir, N., Nichols, J.D., Clifford, J.M., Sykes, J. 13 (1997). Combined chemical treatment of pharmaceutical effluents from medical ointment production. *Current Medical Resource Opinion,* 491–500.

Nakada, H., Shinohara, A., Murata, K., Kiri, S., Managaki, N., Sato, N., Takada, H. (2007). Removal of selected pharmaceuticals and personal care products (PPCPs) and endocrine-disrupting chemicals (EDCs) during sand filtration and ozonation at a municipal sewage treatment plant. *Water Resources*, 41 (19): 4372–4382.

Nguyen.T.V., Wu, J.C., Chiou. C.H. (2008). Photodegradation of famotodine by integrated photocatalytic adsorbent. *Catalysis Communications*, 9(10): 2073–2076. doi: http://dx.doi .org /10.1016/j. catcom.2008.04.004.

Nikolaou, A., Meric, S., Fatta, D. (2007). Occurrence patterns of pharmaceuticals in water and wastewater environments. *Analysis of Biochemistry,* 387 (4): 1225–1234.

Noble, J. (2006). GE ZeeWeed MBR technology for pharmaceutical wastewater treatment. *Membrane Technology*, (9): 7-9.

Ohtani B. (2011). *PhotocatalysisA to Z —What We Know and What We Don't Know in A Scientific Sense.* Catalysis Research Center, Hokkaido University, Sapporo 001-0021, Japan.

Oktem, Y., Ince, O., Sallis, P., Donnelly, T., Ince, B. (2007). Anaerobic treatment of a chemical synthesis-based Pharmaceutical wastewater effluent. *Bioresource. Technology*, 99 (5): 1089-1096.

Oladoja, N.A., Aboluwoye, C.O., Oladimeji, Y.B. (2008). Kinetics and Isotherm Studies on Methylene Blue Adsorption onto Ground Palm Kernel Coat. *Turkish Journal of Engineering and Environmental Science*, 32: 303–312.

Oz, N., Ince, O., Ince, B. (2004). Effect of wastewater composition on methanogenic activity in an anaerobic reactor. *Journal Environtal Science. Health*. 39 (11-12): 2029-2042.

Ozaki, H., Li, H. (2002). Rejection of organic compounds by ultralow pressure reverse osmosis membrane. *Water Resource*, 36 (1): 123–130.

Pelaez, M., Nolan N. T, Pillai S. C, Seery M. K, Falaras K. P, Kontos A. G, Dunlop P. M, Hamilton J. W, Byrne J, O'Shea K, Entezari M. H, Dionysiou D. D (2012). *A*

Review on the Visible Light Active Titanium Dioxide Photocatalysts for Environmental Applications. Applied Catalysis B 125: 331– 349 Physics (JJAP) 40 (2001).

Qamar, M., Munner, M. and Bahnemann, D. (2006). Heterogeneous photocatalysed degradation of two selected pesticide derivatives, triclopyr and daminozid in aqueos suspensions of titanium dioxide. *Journal of Environmental Management,* 80 (2): 99-106.

Quinn.B,,.Gagne, F., Blaise, C. (2008). Photocatalytic degradation of phenols in wastewater *Science of the Total Environment,* 389 306.

Rabiet, M., Togola, A., Brissaud, F., Seidel, J.-L., Budzinski, H., Elbaz-Poulichet, F. (2006). Consequences of treated water recycling as regards pharmaceuticals and drugs in surface and ground waters of a medium-sized Mediterranean catchment. *Environmental Science Technology,* 40 (17): 5282–5288.

Glassmeyer, S.T., Furlong, E.T., Kolpin, D.W., Cahill, J.D., Zaugg, S.D., Werner, S.L. (2005). Heterogeneous photocatalytic degradation of organic contaminants over Titanium dioxide. *Environmental Science Technology,* 36, 5157.

Sakkas.V.A., Calza, P., Medana, C. (2007). Heterageneous photocatalytic degradation of pharmaceutical agent salbutamol in aqeous Titanium Dioxide suspensions. *Applied Catalysis. B: Environment,* 77: 135-144.

Sanderson.H., Johnson, D.J., Reitsma, T., Brain, R.A., Wilson, C.J., Solomon, K.R. (2004). Treatment of mixed pharmaceutical industry and domestic wastewater by sequencing batch reactor. *Regulatory Toxicology and Pharmacology*, 39(2): 158.

Snyder, S., Adham, S., Redding, A., Cannon, F., DeCarolis, J., Oppenheimer, J., Wert, E., Yoon, Y. (2007). Role of membranes and activated carbon in the removal of

endocrine disruptors and pharmaceuticals. *Desalination*, 202 (1-3): 156- 181.

Sreekanth, D., Sivaramakrishna, D., Himabindu, V., Anjaneyulu, Y. (2009). Thermophilic treatment of bulk drug pharmaceutical industrial wastewaters by using hybrid up flow anaerobic sludge blanket reactor. *Bioresource Technology*, 100 (9): 2534-2539.

Stackelberg, P.E., Furlong, E.T., Meyer, M.T., Zaugg, S.D., Henderson, A.K., Reissman, D.B. (2004). Persistence of pharmaceutical compounds and other organic wastewater contaminants in a conventional drinking-water treatment plant. *Science Total Environment*, 329 (1–3): 99–113.

Suman Raj, D., and Anjaneyulu, Y. (2005). Evaluation of biokinetic parameters for pharmaceutical wastewaters using aerobic oxidation integrated with chemical treatment. *Process Biochemistry*, 40 (1): 165-175.

Suppan, P (1994). Photocatalysis: Fundamentals and Applications. *Chemistry and Light Royal Society of Chemistry*, Cambridge. 33-35.

Suresh P., Micahel S., Nicholas N., Miguel, Athanassios G. K., Patrick S.M., Jeremy W.J., J.Anthony B, Kevin O., Mohammad H. E, and Dionysios D.D. (2012). *A Review on the Visible Light Active Titanium Dioxide Photocatalysts for Environmental Applications. Chemosphere*, 125: 331-349

Tarley, C.R.T., Silveira, G., dos Santos, W.N.L., Matos, G.D., da Silva, E.G.P,, Bezerra, M.A., Miró, M., Ferreira, S.L.C. (2009). Chemometric tools in electro analytical chemistry: Methods for optimization based on factorial design and response surface methodology. *Microchemical Journal*, 39 (12): 2029-2042

Tekin, H., Bilkay, O., Ataberk, S.S., Balta, T.H., Ceribasi, I.H., Sanin, F.D., Dilek, F.B., Yetis. U. (2006). Use of Fenton oxidation to improve the biodegradability of a pharmaceutical wastewater. *Journal of Hazardous Material*, 136: 258-265.

Ternes, T. (1998). Behavior of pharmaceuticals, cosmetics and hormones in a sewage treatment plant. *Water Resource*. 38 (12): 2918–2926.

Ternes, T., Stüber, J., Herrmann, N., McDowell, D., Ried, A., Kampmann, M., Teiser, B. (2003). Ozonation: a tool for removal of pharmaceuticals, contrast media and musk fragrances from wastewater. *Water Resource*, 37(8): 1976-1982.

Tristão.J.C., F. Magalhães, P. Corio, M.T.C. Sansiviero. (2006). Electronic characterization and photocatalytic properties of CdS/TiO2 semiconductor composite. *Journal of Photochemical Photobiology*. A. 181: 152–157.

Shapovalov, V.I. (2010). Nanopowders and films of titanium oxide for photocatalysis. *Physical Chemistry,* 36: 121–157.

Virkutyte, J., Rokhina, E., Jegatheesan, V. (2010). Optimisation of Electro- Fenton denitrification of a model wastewater using a response surface methodology. *Bioresource Technology*, 101: 1440-1446**.**

Watkinson, A., Murby, E., Costanzo, S. (2007). Removal of antibiotics in conventional and advanced wastewater treatment: Implications for environmental discharge and wastewater recycling. *Water Resource*, 41 (18): 4164-4176.

Weber.W.J., Morriss, J.C. (1963). Kinetics of adsorption on the carbon from solution, Sanitary. *Journal of Engineering Diverse Society,* 89: 31-60.

WHO(2013):http://www.who.int/water_sanitation_health/emerging/info_sheet_ pharmaceuticals/en/index.html accessed on 5 June, 2013.

Wu, M,, Atchley, D., Greer, L., Janssen, S., Rosenberg, D., and Sass. (2009). Journal of Natural Resources Defense Council White Paper, 60.

Xu.S.H., D.L. Feng, W.F., Shangguan. (2009). Transformation of Aromatic Ether and Amine

Containing Pharmaceuticals during Chlorine Disinfection. *Journal of Physical chemistry C*, 113: 2463–2467.

Yang, W., Cicek, N., Ilg, J. (2006). State-of-the-art of membrane bioreactors: Worldwide research and commercial applications in North America, *Journal of Membrane Science*, 270 (1-2): 201-211

Yang.L., Yu, L.E., Ray, M.B.(2008). Evaluation of biokinetic parameters for pharmaceutical wastewaters using aerobic oxidation integrated with chemical treatment.*Water Resource,* 42: 3480–3488.[5].

Yao, Y., Qin, J., Chen, H., Wei, F., Liu, X., Wang, J. and Wang, S. (2015). One-pot approach

for synthesis of N-doped $TiO_2/ZnFe_2O_4$ hybrid as an efficient photocatalyst for degradation of aqueous organic pollutants. *Journal of hazardous materials*, *291*, pp.28-37

Yurdakal.S,. Loddo, Augugliaro.V, H. Berber, G. Palmisano, L. Palmisano. (2007).

Optimisation of the heterogeneous Fenton-oxidation of the model pollutant 2,4-xylidine using the optimal experimental design methodology. *Catalysis Today,* 129(1– 2): 9–15. Doi: http: //dx.doi.org/10.1016/j.cattod.2007.06.044.

Zhang, Y., Zhou, J. (2005). Removal of estrone and 17 âestradiol from water by adsorption. *Water Resource*, 39 (16): 3991–4003.

Zhang.G., Qu, J., Liu, H., Cooper, A.T., Wu, R. (2007) CuFe2O4/activated carboncomposite:

a novel magnetic adsorbent for the removal of acid orange II andcatalytic regeneration. *Chemosphere*, 68:1058–1066.

Zwiener, C., Frimmel, F.H. (2000). Oxidative treatment of pharmaceuticals in water. *Water Resource,* 34 (6): 1881–1885.

Zwiener, C., Frimmel, F., (2003). Short-term tests with a pilot sewage plant and biofilm reactors for the biological degradation of the pharmaceutical compounds clofibric acid, ibuprofen, and diclofenac. *Science Total Environment,* 309 (1-3): 201-211.

APPENDIX A

ADSORPTION TEST

To evaluate the adsorption capacity of $ZnFe_2O_4$ photocatalyst, it was necessary to determine the adsorption isotherm of Acetaminophen using Freundlich and Langmuir

adsorption isotherms. In order to convert the absorbance to concentration, absorbance of Acetaminophen was taken at various concentrations as shown in Table A1. A plot of absorbance against concentration as shown in Figure A gave the equation A=kC in which A= absorbance, C= concentration (mg/L), k= constant (0.0677). this equation was used to convert all absorption to concentration

Table A1: Adsorption of acetaminophen at various concentrations

CONCENTRATION (mg/L)	Absorbance
5	0.33385
10	0.677
15	1.0155
20	1.345
25	1.6925

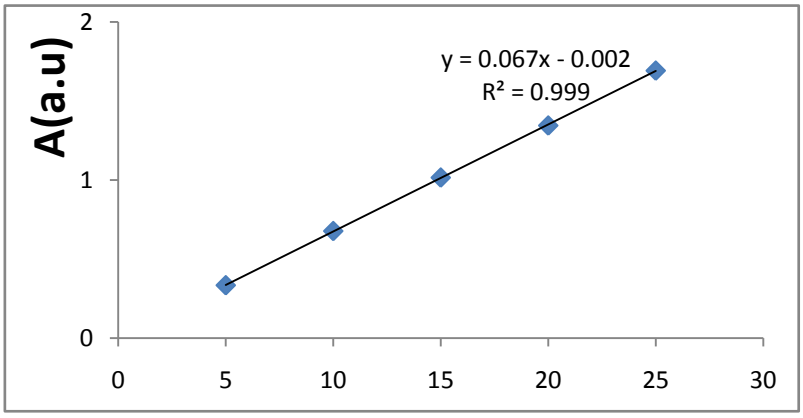

Figure A: A plot of absorption against concentration

Maximum wavelength (λmax) for ACE absorption = 242nm

Catalyst dosage= 1.0g/L of solution

Source of light = 500W halogen lamp

Dark absorption= 60 minutes

Table A2: Absorbance test for adsorption of acetaminophen unto $ZnFe_2O_4$-TiO_2 composite

ABSORBANCE

Time(t)	5 mg/L	10 mg/L	15 mg/L	20 mg/L	25 mg/L
0	0.17	0.411	0.705	1.01	1.315
10	0.16	0.385	0.651	0.922	1.10
20	0.12	0.267	0.501	0.715	0.851
30	0.113	0.256	0.461	0.63	0.791
40	0.112	0.252	0.413	0.591	0.78
50	0.11	0.209	0.387	0.542	0.761
60	0.11	0.208	0.387	0.541	0.761

CONCENTRATION

Time(t)	5 mg/L	10 mg/L	15 mg/L	20 mg/L	25 mg/L
0	2.511	6.071	10.419	14.918	19.424
10	2.399	5.687	9.616	13.619	16.248
20	1.799	3.944	7.400	10.561	12.570
30	1.694	3.781	6.809	9.3057	11.684
40	1.679	3.722	6.100	8.729	11.521
50	1.649	3.087	5.716	8.006	11.240
60	1.649	3.072	5.716	7.991	11.240

TableA3: Parameters for plotting Langmuir Adsorption Isotherm

$1/c_e$	$1/q_e$
0.606364	0.149217
0.325481	0.072175
0.174935	0.053858
0.125139	0.041636
0.088962	0.036339

Langmuir Isotherm

To determine the value of R_L for $ZnFe_2O_4$-TiO_2 composite from equation (2)

$$\boldsymbol{R_L = \frac{1}{1+bC_o}} \quad \ldots\ldots\ldots\ldots\ldots\ldots\ldots\ldots\ldots\ldots\ldots\ldots \quad (2)$$

Also from equation (3) we have;

$$\frac{1}{q_e} = \frac{1}{q_{max}} + \left(\frac{1}{q_{max}k_L}\right)\frac{1}{C_e} \quad \ldots\ldots\ldots\ldots\ldots\ldots \quad (3)$$

Thus slope = $\frac{1}{q_{max}}$ = 0.0372, q_{max} = 26.8817

$\left(\frac{1}{q_{max}k_L}\right) = 0.3862$, therefore K_L = 0.0963

Hence R_L = 0.41

Table A4: Parameters for plotting Freundlich Adsorption Isotherm

$\ln c_e$	$\ln q_e$
0.500275	1.902354
1.122452	2.628664
1.743339	2.921397
2.078333	3.178792

2.419547	3.314857

Freundlich Isotherm

Slope = n = 0.7169

Therefore,

1/n =1/0.7169 = 1.3949

ADSORPTION KINETICS

Table A5: Absorbance test for adsorption kinetics of ACE using $ZnFe_2O_4$-TiO_2 composite

ABSORBANCE

Time(min)	**5 mg/L**	**10 mg/L**	**15 mg/L**	**20 mg/L**
15	0.1	0.181	0.336	0.519
30	0.076	0.127	0.232	0.411
45	0.055	0.089	0.152	0.345
60	0.033	0.044	0.059	0.279
75	0.021	0.031	0.033	0.273

CONCENTRATION

Time(min)	**5 mg/L**	**10 mg/L**	**15 mg/L**	**20 mg/L**
15	1.477	2.673	4.963	7.666
30	1.122	1.876	3.426	6.071
45	0.812	1.314	2.246	5.096
60	0.487	0.649	0.871	4.121
75	0.310	0.458	0.487	4.032

Table A6: Parameters for plotting Pseudo-Second Order Kinetics (t/Qt Vs t)

Time(min)	5 mg/L	10 mg/L	15 mg/L	20 mg/L
0	0	0	0	0
10	3.844	2.318	1.857	1.567
20	6.248	3.302	2.631	2.119
30	9.075	4.824	3.662	2.805
40	12.045	6.371	4.494	3.549
50	14.921	7.232	5.385	4.168
60	17.906	8.661	6.463	4.996

Table A7: Parameters for plotting Lagergren First Order Kinetics (Log (Qe-Qt) Vs t)

Time(min)	5 mg/L	10 mg/L	15 mg/L	20 mg/L
0	0	0	0	0
10	0.613	0.979	1.120	1.246
20	0.544	0.892	1.040	1.163
30	0.531	0.883	1.016	1.124
40	0.529	0.879	0.985	1.105
50	0.525	0.841	0.967	1.080
60	0.525	0.840	0.967	1.079

Table A8: Parameters for plotting ELOVICH Kinetics (t/Qt Vs t)

lnT(time)	5 mg/L	10 mg/L	15 mg/L	20 mg/L
0	0	0	0	0
2.302	2.601	4.313	5.384	6.381
2.995	3.201	6.056	7.599	9.438
3.401	3.305	6.218	8.190	10.694
3.688	3.320	6.277	8.899	11.270
3.912	3.350	6.912	9.283	11.994
4.094	3.350	6.927	9.283	12.008

Table A9: Parameters for plotting Intra-Particle diffusion (Qt Vs $t^{1/2}$)

$t^{1/2}$(time)	5 mg/L	10 mg/L	15 mg/L	20 mg/L
0	0	0	0	0
3.162	2.601	4.313	5.384	6.381
4.472	3.201	6.056	7.599	9.438
5.477	3.305	6.218	8.190	10.694

6.324	3.320	6.277	8.899	11.270
7.071	3.350	6.912	9.283	11.994
7.745	3.350	6.927	9.283	12.008

APPENDIX B

PHOTOCATALYTIC ACTIVITY TEST

To evaluate the photocatalytic degradation of Acetaminophen at various initial concentrations using $ZnFe_2O_4$-TiO_2 photocatalyst, it was necessary to determine the plot of change in concentration(C/Co) against time (t). Also to determine the photocatalytic oxidation kinetics of Ace it was modelled using the Langmuir–Hinshelwood (L–H) equation by plotting degradation rate constants (1/kapp) against initial Ace concentrations (Daneshvar *et al*., 2004).

Table B1: Absorbance test for photocatalytic degradation of acetaminophen using $ZnFe_2O_4$-TiO_2 composite at various initial concentrations

ABSORBANCE

Time(min)	**5 mg/L**	**10 mg/L**	**15 mg/L**	**20 mg/L**
0	0.11	0.208	0.387	0.541
15	0.1	0.181	0.336	0.519
30	0.076	0.127	0.232	0.411

45	0.055	0.089	0.152	0.345
60	0.033	0.044	0.059	0.279
75	0.021	0.031	0.033	0.273

CONCENTRATION

TIME(min)	5 mg/L	10 mg/L	15 mg/L	20 mg/L
0	1.649	3.073	5.716	7.991
15	1.477	2.673	4.963	7.666
30	1.122	1.876	3.426	6.070
45	0.812	1.314	2.245	5.096
60	0.487	0.649	0.871	4.121
75	0.310	0.458	0.487	4.032

Table B2: Parameters for plotting photocatalytic degradation of Acetaminophen (C/Co Vs Time)

Time(min)	5 mg/L	10 mg/L	15 mg/L	20 mg/L
0	1	1	1	1
15	0.895	0.870	0.868	0.959
30	0.680	0.610	0.599	0.759
45	0.492	0.427	0.392	0.637
60	0.295	0.211	0.152	0.515
75	0.188	0.149	0.0852	0.504

Table B3: Parameters for plotting pseudo-first order kinetics (lnC/Co Vs Time)

Time(min)	5 mg/L	10 mg/L	15 mg/L	20 mg/L
0	0	0	0	0
15	0.110	0.139	0.141	0.041
30	0.384	0.493	0.511	0.274
45	0.708	0.849	0.934	0.449

60	1.218	1.553	1.880	0.662
75	1.670	1.903	2.462	0.683

Table B4: Apparent rate constant, *k* values for the photocatalytic degradation of Acetaminophen using $ZnFe_2O_4$-TiO_2 composite at various concentrations.

Initial Concentration (mg/L)	1/kapp
5	43.668
10	59.171
15	70.422
20	96.153